

Copyright © 1984, by the author(s).
All rights reserved.

Permission to make digital or hard copies of all or part of this work for personal or classroom use is granted without fee provided that copies are not made or distributed for profit or commercial advantage and that copies bear this notice and the full citation on the first page. To copy otherwise, to republish, to post on servers or to redistribute to lists, requires prior specific permission.

CANONICAL PIECEWISE-LINEAR ANALYSIS
PART II: TRACING DRIVING-POINT AND TRANSFER CHARACTERISTICS

by

L. O. Chua and A. C. Deng

Memorandum No. UCB/ERL M84/12

30 January 1984

ELECTRONICS RESEARCH LABORATORY

College of Engineering
University of California, Berkeley
94720

CANONICAL PIECEWISE-LINEAR ANALYSIS
PART II: TRACING DRIVING-POINT AND TRANSFER CHARACTERISTICS[†]

L. O. Chua and A. C. Deng

Department of Electrical Engineering and Computer Sciences
and the Electronics Research Laboratory
University of California, Berkeley, CA 94720

Abstract

An extremely efficient breakpoint-hopping algorithm is presented for tracing the driving-point and transfer characteristics of any nonlinear circuit made of linear (possibly multi-terminal) resistors, dc independent sources, linear controlled sources (all 4 types) and 2-terminal nonlinear resistors described by piecewise-linear v-i characteristics. Most resistive nonlinear electronic circuits can be realistically modeled by such circuits. The algorithm can trace not only violently nonlinear (with sharp turning points) and multivalued characteristics, but also characteristics composed of several disconnected branches, provided one point in each branch is given.

The remarkable computational efficiency of the breakpoint-hopping algorithm is due to two key properties built into the algorithm:

- 1) the circuit equation is formulated into a special form; namely, a canonical piecewise-linear equation with a lattice structure.
- 2) the algorithm finds only the breakpoints and possibly one point on each end (unbounded) segment via explicit formulas (hence no convergence problem). These data points represent the minimal amount of information needed to specify a piecewise-linear characteristic uniquely.

[†]This research is supported in part by the Air Force Office of Scientific Research (AFSC) United States Air Force Contract F49620-79-C-0178.

1. INTRODUCTION

This paper is a sequel to [1], where we have proved that for a very large class of resistive piecewise-linear circuits--most electronic circuits can be modeled by such a circuit--the algebraic equations resulting from various analysis methods (node, cut set, loop, hybrid and tableau analysis) can always be cast into an explicit analytical form where the only nonlinearities are absolute-value functions; namely,

$$f(x) = a + Bx + \sum_{i=1}^P c_i |\langle \alpha_i, x \rangle - \beta_i| = 0 \quad (1.1)$$

where β_i is a scalar, x , a , c_i , and α_i are n -vectors, B is an $n \times n$ matrix, and $\langle \cdot, \cdot \rangle$ denotes vector dot product. For circuits having a unique solution, the canonical Katzenelson algorithm given in [1] can be used to find this solution in a finite number of iterations. For circuits having multiple solutions, the general (necessarily less efficient) algorithm given in [2] can be used to find all of the solutions.

With the operating-point problem essentially solved in [1,2] for the canonical piecewise-linear equation (1.1), we now turn to the equally important problem of finding the v -vs- i (or i -vs- v) driving-point characteristic of the one-port N shown in Fig. 1, or the v_0 (or i_0)-vs- y_{in} (either v_{in} or i_{in}) transfer characteristic (4 types) of the two-port N shown in Fig. 2. The one-port N in Fig. 1 and the two-port N in Fig. 2 may contain an arbitrary interconnection of the circuit elements listed in Table 1.

Since the low-frequency behavior of most multi-terminal devices can be realistically modeled by a circuit made only of elements from Table 1, it is clear that the class of resistive nonlinear circuits considered in this paper is extremely broad.

A common method for finding the driving-point or transfer characteristic is to solve for the operating point using a computer simulation program as the input source y_{in} is varied by increments over the dynamic range of interest. This "brute force" method unfortunately suffers from two major shortcomings: 1) it is extremely time consuming, and 2) it is valid only if the driving point or transfer characteristic is a single-valued function, and therefore excludes many circuits of practical interest [5,6], including the examples given in the following Figs.: 19, 20, 22, 23 and 25.

The above objections can be overcome by several recent algorithms [7-10] for tracing solution curves of general (not necessarily piecewise-linear)

Table 1. Repertoire of allowed circuit elements

1. linear (positive or negative) 2-terminal resistors
2. dc voltage and current sources
3. linear controlled sources (all 4 types)
4. any linear multi-terminal resistors (e.g., ideal transformers, gyrators, circulators, etc.)
5. nonlinear 2-terminal resistors described by a voltage-controlled canonical piecewise-linear representation

$$i_k = \hat{i}_k(v_k) = a_k + b_k v_k + \sum_{m=1}^{\sigma_k} c_{km} |v_k - E_{km}| \quad (1.2)$$

or by a current-controlled canonical piecewise-linear representation

$$v_k = \hat{v}_k(i_k) = a_k + b_k i_k + \sum_{m=1}^{\sigma_k} c_{km} |i_k - I_{km}| \quad (1.3)$$

$k = 1, 2, \dots, n$, where a_k , b_k , and c_{km} are determined from explicit formulas given in [1,3] for an arbitrary continuous piecewise-linear function having (σ_k+1) -segments. Here E_{km} (resp.; I_{km}) denotes the voltage (resp.; current) coordinate at the m -th breakpoint, and the subscript k denotes the k -th resistor.

In fact, these 2-terminal resistors may be coupled to each other via the generalized representation defined in (2.8) and (2.9), thereby including any multi-terminal elements (e.g., see the piecewise-linear equation (2.37) for bipolar transistors) described in the form of (2.8)-(2.9).[†]

nonlinear equations with respect to a parameter ρ , which in the present context represents y_{in} . These algorithms essentially trace the characteristic from one point to a "nearby" point via a homotopic approach. For piecewise-linear circuits, however, this approach does not take advantage of the piecewise-linear nature of the characteristics (where only 2 breakpoints are needed to specify any segment of the characteristic) and proceed to calculate even the points between the breakpoints, completely oblivious of the fact that the segment is a straight line! Other algorithms which do exploit the piecewise-linear characteristic exist [11,12], but they do not exploit the canonical piecewise-linear representation considered in this paper and are therefore computationally inefficient.

[†]Alternately, a multi-terminal device may be modeled by a circuit using only uncoupled piecewise-linear 2-terminal resistors and linear controlled sources [4]. In which case, (2.8) and (2.9) reduce to (1.2) or (1.3).

In this paper, we develop a highly efficient breakpoint-hopping algorithm which systematically finds all breakpoints of the characteristic (plus possibly one point on each "unbounded" segment tending to $+\infty$ or $-\infty$) within the specified dynamic range. If the driving-point or transfer characteristic consists of several "unicursal" [13] (i.e.; contiguous) branches, our algorithm will find all branches where one point on each branch is given. In other words, the problem of finding all branches reduces to that of locating one point on each branch. For simple circuits, this information can be obtained by using the algorithm in [2].

Since only the minimal number of points needed to specify a piecewise-linear characteristic uniquely is sought by our algorithm, it is the most efficient algorithm possible, assuming of course that the breakpoints can be found efficiently. Since our algorithm uses one breakpoint to find the next nearest breakpoint, it is called a breakpoint-hopping algorithm.

The key idea responsible for the remarkable computational efficiency of our algorithm is the choice of a particular equation formulation (a generalized form of hybrid analysis [14, 2]) which gives rise to a canonical piecewise-linear equation with a lattice structure; namely,

$$\underline{B}\underline{x} + \sum_{j=1}^n \sum_{i=1}^{\sigma_j} \underline{c}_{ji} |x_j - \beta_{ji}| = \underline{a} + \rho \underline{r} \quad (1.4)$$

where x_j and β_{ji} are scalars, and \underline{x} , \underline{c}_{ji} , \underline{a} and \underline{r} are $(n+1)$ -vectors, \underline{B} is an $(n+1) \times (n+1)$ matrix, where n is the number of nonlinear resistors, σ_j is the number of breakpoints in the piecewise-linear v_j - i_j curve of the j -th resistor, $j = 1, 2, \dots, n$, and ρ is a scalar equal to the value of the input variable, i.e., $\rho = v_{in}$ or $\rho = i_{in}$.

Observe that the canonical equation (1.4) is a special case of (1.1) because, here, the argument inside each absolute-value function contains only one variable, namely, $x_j - \beta_{ji}$, $1 \leq i \leq \sigma_j$. This implies that the "hyperplane" boundaries in the n -dimensional $x_1 - x_2 - \dots - x_n$ space which separates the various piecewise-linear regions are all parallel to the respective coordinate axis, as illustrated in Fig. 3 for a circuit containing 2 piecewise-linear resistors characterized by the $v_1 - i_1$ curve in Fig. 3(a) and the $i_2 - v_2$ curve in Fig. 3(b). Here, we identify the parameters in (1.4) as follows: $x_1 \triangleq v_1$,

$x_2 \triangleq i_2$, $n = 2$, $\sigma_1 = 2$, $\sigma_2 = 1$, $\beta_{11} = -1$, $\beta_{12} = 2$, and $\beta_{21} = 3$. Equation (1.4) partitions the x_1 - x_2 plane into exactly 6 "rectangular" regions via the 2 vertical lines (one-dimensional hyperplanes $x_1 = -1$ and $x_1 = 2$) and the horizontal line $x_2 = 3$, as shown in Fig. 3(c). Such a "parallel" boundary structure as defined by (1.4) is called a lattice structure in [2]. We will see shortly that this parallel structure is crucial to the computational efficiency of our breakpoint-hopping algorithm.

Since not all equation formulation methods (e.g., node analysis, loop analysis, cut set analysis [1]) give rise to a canonical piecewise-linear equation with a lattice structure, Section 2 is devoted to a general formulation method which guarantees such a structure.

The breakpoint-hopping algorithm for solving (1.4) is derived in Section 3. Several validating examples illustrating this algorithm are collected in Section 4. For completeness, various degenerate (ill-conditioned) cases which could invalidate our algorithm are analyzed in Section 5.

2. FORMULATION OF CANONICAL PIECEWISE-LINEAR EQUATIONS WITH LATTICE STRUCTURE

Consider the circuit configurations in Figs. 1 and 2 where N contains only elements listed in Table 1. Let us extract all nonlinear resistors in N and redraw the circuit as an $(n+1)$ -port \hat{N} terminated by " ℓ " voltage-controlled resistors on the left, " $n-\ell$ " current-controlled resistors on the right, and the input source v_{in} (which for convenience is assumed to be a voltage source) at the bottom, as shown in Fig. 4(a). The $(n+1)$ -port \hat{N} is linear and time-invariant and can be described by various standard representations, depending on the choice of independent variables. For our present purpose, the independent variables must be chosen to be the same as those of the terminating nonlinear resistors, as shown in Fig. 4(b).

Except for the rare and degenerate cases \hat{N} can be represented by an affine equation

$$\underline{P}\underline{x} = \underline{Q}\underline{y} + \underline{s} \quad (2.1)$$

where

$$\underline{x} \triangleq [v_1, v_2, \dots, v_\ell, i_{\ell+1}, i_{\ell+2}, \dots, i_n, i_{in}]^T, \quad (2.2)$$

$$\underline{y} \triangleq [i_1, i_2, \dots, i_\ell, v_{\ell+1}, v_{\ell+2}, \dots, v_n, v_{in}]^T \quad (2.3)$$

\underline{s} is a constant $(n+1)$ -vector which accounts for the dc independent sources inside \hat{N} , \underline{P} and \underline{Q} are constant $(n+1) \times (n+1)$ matrices which depend only on the

parameters of the linear elements inside \hat{N} . Note that if \underline{Q} is nonsingular, then (2.1) reduces to the usual hybrid representation [1,2]:

$$\underline{y} = \underline{H}\underline{x} + \underline{s}_0 \quad (2.4)$$

where $\underline{H} \triangleq \underline{Q}^{-1}\underline{P}$ and $\underline{s}_0 \triangleq -\underline{Q}^{-1}\underline{s}$. Consequently, we call (2.1) the generalized hybrid representation (since both \underline{x} and \underline{y} are hybrid vectors). Given any non-degenerate circuit (Fig. 4(b)), (2.1) can be derived manually by standard circuit analysis methods for simple circuits ($n \leq 3$), or by the systematic elimination algorithm given in [4] for larger circuits. For the few degenerate cases where \hat{N} can not be represented by (2.1), we can always extract a linear resistor from one or more nonlinear resistors to remove the degeneracy.[†] Hence, there is no loss of generality in assuming that \hat{N} has a generalized hybrid representation (2.1) Once (2.1) is found, the circuit elements and topology inside \hat{N} become irrelevant as the canonical piecewise-linear equation that we are about to formulate for the circuit in Fig. 4(a) depends only on \underline{P} , \underline{Q} , \underline{s} and the external terminating elements.

Since v_{in} in the vector \underline{y} is the input source, let us separate it from the remaining dependent variables by rewriting

$$\underline{y} = \underline{y}' + \rho \underline{e}_{n+1} \quad (2.5)$$

where

$$\underline{y}' \triangleq [i_1, i_2, \dots, i_\ell, v_{\ell+1}, v_{\ell+2}, \dots, v_n, 0]^T \quad (2.6)$$

$$\underline{e}_{n+1} \triangleq [0, 0, \dots, 0, 0, 0, \dots, 0, 1]^T \quad (2.7)$$

and $\rho \triangleq v_{in}$ is the value of the driving voltage source, where ρ can vary between the specified dynamic range $[\rho_{min}, \rho_{max}]$ of interest.

Our next step is to express \underline{y}' in terms of the "unknown" independent variables \underline{x} . This can be easily achieved by substituting the voltage-controlled piecewise-linear representation (1.2) in place of i_1, i_2, \dots, i_ℓ , and the current-controlled piecewise-linear representation (1.3) in place of $v_{\ell+1}, v_{\ell+2}, \dots, v_n$ in (2.5). Without any extra work, however, we can allow the 2-terminal nonlinear resistors to be coupled to each other in accordance with the following much more general "coupled" representation:

[†]Of course, the v_k-i_k characteristic of each nonlinear resistor so extracted will have to be modified by subtracting a linear term equal to the extracted series or parallel linear resistor.

$$i_k = a_k + \underset{\sim}{b}_k^T \underset{\sim}{x} + \sum_{j=1}^n \sum_{i=1}^{\sigma_j} c_{jik} |x_j - \beta_{ji}|, \quad (2.8)$$

$$k = 1, 2, \dots, \ell,$$

$$v_k = a_k + \underset{\sim}{b}_k^T \underset{\sim}{x} + \sum_{j=1}^n \sum_{i=1}^{\sigma_j} c_{jik} |x_j - \beta_{ji}|, \quad (2.9)$$

$$k = \ell+1, \ell+2, \dots, n$$

where a_k , c_{jik} , and β_{ji} are scalars, $\underset{\sim}{b}_k$ and $\underset{\sim}{x}$ are $(n+1)$ -vectors with $\underset{\sim}{x}$ defined in (2.2). Here, we assume, without loss of generality, that

$$\beta_{ji} < \beta_{jk} \quad \text{iff} \quad i < k \quad \text{for each } j = 1, 2, \dots, n.$$

Note that if the k -th resistor is uncoupled to the other elements, we have

$$\underset{\sim}{b}_k = [0 \dots 0 \ 1 \ 0 \dots 0]^T$$

where the k -th entry in $\underset{\sim}{b}_k$ is 1 and $c_{jik} = 0$ for all $j \neq k$. In this case, (2.8) (resp.; (2.9)) reduces to (1.2) (resp.; (1.3)) with $c_{jik} = c_{ki}$ for $j = k$.

Substituting (2.8)-(2.9) in place of i_k and v_k in (2.5), we obtain

$$\underset{\sim}{y} = \underset{\sim}{\hat{a}} + \underset{\sim}{\hat{B}} \underset{\sim}{x} + \sum_{j=1}^n \sum_{i=1}^{\sigma_j} \underset{\sim}{\hat{c}}_{ji} |x_j - \beta_{ji}| + \rho e_{n+1} \quad (2.10)$$

where

$$\underset{\sim}{\hat{a}} \triangleq \begin{bmatrix} a_1 \\ a_2 \\ \vdots \\ a_n \\ 0 \end{bmatrix} \quad \underset{\sim}{\hat{B}} \triangleq \begin{bmatrix} \underset{\sim}{b}_1^T \\ \underset{\sim}{b}_2^T \\ \vdots \\ \underset{\sim}{b}_n^T \\ 0 \end{bmatrix} \quad \underset{\sim}{c}_{ji} \triangleq \begin{bmatrix} c_{ji1} \\ c_{ji2} \\ \vdots \\ c_{jin} \\ 0 \end{bmatrix} \quad (2.11)$$

for $i = 1, 2, \dots, \sigma_j$ and $j = 1, 2, \dots, n$. Substituting (2.10) for $\underset{\sim}{y}$ in (2.1), we obtain (1.4); namely,

canonical piecewise-linear equation with lattice structure:

$$\underset{\sim}{B} \underset{\sim}{x} + \sum_{j=1}^n \sum_{i=1}^{\sigma_j} c_{ji} |x_j - \beta_{ji}| = \underset{\sim}{a} + \rho \underset{\sim}{r} \quad (2.12)$$

where

$$\underline{B} \triangleq \underline{Q}\hat{B} - \underline{P} \quad (2.13a)$$

$$\underline{c}_{ji} \triangleq \underline{Q}\hat{c}_{ji} \quad (2.13b)$$

$$\underline{a} \triangleq -\underline{s} - \underline{Q}\hat{a} \quad (2.13c)$$

$$\underline{r} \triangleq -\underline{Q}\underline{e}_{n+1} \quad (2.13d)$$

Observe that (2.12) is a special case of the general canonical piecewise-linear equation (1.1) with

$$\underline{\alpha}_j = [0 \ 0 \ \dots \ 0 \ 1 \ 0 \ \dots \ 0]^T$$

where the j -th entry in $\underline{\alpha}_j$ is 1 for some $j \in \{1, 2, \dots, n\}$. In other words, the argument inside each absolute-value function in (2.12) contains only one variable x_j , $j = 1, 2, \dots, n$. It is indeed remarkable that the rather general piecewise-linear circuit in Fig. 4(a) can be described analytically by equation with such a highly specialized structure.

Remarks

1. If the nonlinear resistors in Fig. 4(a) are not coupled to each other, then (2.8)-(2.9) reduce to (1.2)-(1.3) and \hat{B} in (2.11) reduces to a diagonal matrix (see (2.16), (2.20), (2.25) and (2.33) in Examples 2.1-2.4). In this case, \underline{c}_{ji} reduces to $c_{jij}\underline{e}_j$ where

$$\underline{e}_j = [0 \ 0 \ \dots \ 0 \ 1 \ 0 \ \dots \ 0]^T$$

and 1 is located in the j -th entry (see (2.16), (2.20), (2.25), and (2.33) in Examples 2.1-2.4).

2. Although both the hybrid and the tableau equations in [1] also give rise to an equation with a lattice structure, we choose the generalized hybrid representation in this paper because 1) the hybrid representation for \hat{N} does not exist in many circuits and 2) the tableau representation would have resulted in a much larger system of equations. This is especially objectionable if the number of linear elements inside \hat{N} is relatively large compared to the number of nonlinear elements.

We close this section with several examples whose driving-point or transfer characteristic is to be found in Section 4.

Example 2.1 (Fig. 5)

Consider the circuit in Fig. 5(a) where nonlinear resistors R_1 and R_2 are described by the piecewise-linear characteristics shown in Figs. 5(c) and

(d). Although these two characteristics are strictly increasing and are therefore both voltage-controlled and current-controlled, we have chosen v_1 and i_2 to be the independent variables for illustration purposes. Using the explicit formulas in [1], we obtain the following canonical piecewise-linear equations for R_1 and R_2 :

$$R_1: \hat{i}_1 = i_1(v_1) = 9/8 v_1 + 7/8 |v_1| \quad (2.14a)$$

$$R_2: v_2 = \hat{v}_2(i_2) = 9/4 i_2 + 7/4 |i_2-1| - 9/4 \quad (2.14b)$$

Extracting the two nonlinear resistors, we obtain the linear 3-port \hat{N} shown in Fig. 5(b). By straightforward analysis, we obtain the following generalized hybrid representation for \hat{N} :

$$\underbrace{\begin{bmatrix} 1 & 0 & 0 \\ 0 & 0 & 1 \\ 0 & 1 & -1 \end{bmatrix}}_{\underline{P}} \underbrace{\begin{bmatrix} v_1 \\ i_2 \\ i_{in} \end{bmatrix}}_{\underline{x}} = \underbrace{\begin{bmatrix} 0 & -1 & 1 \\ 1 & 1 & 0 \\ 0 & 0 & 0 \end{bmatrix}}_{\underline{Q}} \underbrace{\begin{bmatrix} i_1 \\ v_2 \\ v_{in} \end{bmatrix}}_{\underline{y}} + \underbrace{\begin{bmatrix} 0 \\ 0 \\ 0 \end{bmatrix}}_{\underline{s}} \quad (2.15)$$

Note that \underline{s} in (2.1) is always equal to $\underline{0}$ if \hat{N} contains no dc sources.

Substituting (2.14) into (2.10) and (2.11), we obtain

$$\beta_{11} = 0, \beta_{21} = 1, \hat{\underline{a}} = \begin{bmatrix} 0 \\ -9/4 \\ 0 \end{bmatrix}, \hat{\underline{B}} = \begin{bmatrix} 9/8 & 0 & 0 \\ 0 & 9/4 & 0 \\ 0 & 0 & 0 \end{bmatrix}, \hat{\underline{c}}_{11} = \begin{bmatrix} 7/8 \\ 0 \\ 0 \end{bmatrix}, \hat{\underline{c}}_{21} = \begin{bmatrix} 0 \\ 7/4 \\ 0 \end{bmatrix} \quad (2.16)$$

Substituting (2.15) and (2.16) into (2.13), we obtain

$$\underline{B} = \begin{bmatrix} -1 & -9/4 & 0 \\ 9/8 & 9/4 & -1 \\ 0 & -1 & 1 \end{bmatrix}, \underline{a} = \begin{bmatrix} -9/4 \\ 9/4 \\ 0 \end{bmatrix}, \underline{r} = \begin{bmatrix} -1 \\ 0 \\ 0 \end{bmatrix}, \underline{c}_{11} = \begin{bmatrix} 0 \\ 7/8 \\ 0 \end{bmatrix}, \underline{c}_{21} = \begin{bmatrix} -7/4 \\ 7/4 \\ 0 \end{bmatrix} \quad (2.17a)$$

Substituting (2.17a) into (2.12), we obtain the following canonical piecewise-linear equation for the circuit in Fig. 5(a)

$$\underbrace{\begin{bmatrix} -1 & -9/4 & 0 \\ 9/8 & 9/4 & -1 \\ 0 & -1 & 1 \end{bmatrix}}_{\underline{B}} \underbrace{\begin{bmatrix} v_1 \\ i_2 \\ i_{in} \end{bmatrix}}_{\underline{x}} + \underbrace{\begin{bmatrix} 0 \\ 7/8 \\ 0 \end{bmatrix}}_{\underline{c}_{11}} |x_1 - \beta_{11}| + \underbrace{\begin{bmatrix} -7/4 \\ 7/4 \\ 0 \end{bmatrix}}_{\underline{c}_{21}} |x_2 - \beta_{21}| = \underbrace{\begin{bmatrix} -9/4 \\ 9/4 \\ 0 \end{bmatrix}}_{\underline{a}} + \rho \underbrace{\begin{bmatrix} -1 \\ 0 \\ 0 \end{bmatrix}}_{\underline{r}} \quad (2.17b)$$

Note that the parameters β_{ji} in (2.12) always correspond to the breakpoint coordinate (ordered from left to right) for resistor R_j . In this case $n = 2$, $\sigma_1 = 1$, $\sigma_2 = 1$ and hence we could have obtained $\beta_{11} = 0$ and $\beta_{21} = 1$ by inspection of Figs. 5(c) and (d) directly.

Example 2.2 (Fig. 6)

Consider the circuit in Fig. 6(a) where nonlinear resistors R_1 and R_2 are described in Figs. 6(c) and (d) respectively. Since R_1 and R_2 are both non-monotonic and voltage-controlled, it is necessary to choose v_1 and v_2 as the independent variables in this example. Their canonical piecewise-linear equations are found as follow:

$$R_1 : i_1 = \hat{i}_1(v_1) = -7/4 + 7/4 v_1 - 25/18 |v_1 - 1.2| + 41/36 |v_1 - 3| \quad (2.18a)$$

$$R_2 : i_2 = \hat{i}_2(v_2) = -2.2 + 4v_2 - 7/2 |v_2 - 0.8| + 5/2 |v_2 - 2| \quad (2.18b)$$

The associated linear 3-port \hat{N} in Fig. 6(b) is described by the following generalized hybrid representation:

$$\underbrace{\begin{bmatrix} 0 & 0 & 1 \\ 0 & 0 & 1 \\ 1 & 1 & 3.2 \end{bmatrix}}_{\underline{P}} \underbrace{\begin{bmatrix} v_1 \\ v_2 \\ i_{in} \end{bmatrix}}_{\underline{x}} = \underbrace{\begin{bmatrix} 1 & 0 & 0 \\ 0 & 1 & 0 \\ 0 & 0 & 1 \end{bmatrix}}_{\underline{Q}} \underbrace{\begin{bmatrix} i_1 \\ i_2 \\ v_{in} \end{bmatrix}}_{\underline{y}} + \underbrace{\begin{bmatrix} 0 \\ 0 \\ 0 \end{bmatrix}}_{\underline{s}} \quad (2.19)$$

Substituting (2.18) into (2.10) and (2.11), we obtain (here $n = 2$, $\sigma_1 = 2$, and $\sigma_2 = 2$)

$$\beta_{11} = 1.2, \beta_{12} = 3, \beta_{21} = 0.8, \beta_{22} = 2 \quad (2.20a)$$

$$\hat{\underline{a}} = \begin{bmatrix} -7/4 \\ -2.2 \\ 0 \end{bmatrix}, \hat{\underline{B}} = \begin{bmatrix} 7/4 & 0 & 0 \\ 0 & 4 & 0 \\ 0 & 0 & 0 \end{bmatrix}, \hat{\underline{c}}_{11} = \begin{bmatrix} -25/18 \\ 0 \\ 0 \end{bmatrix}, \hat{\underline{c}}_{12} = \begin{bmatrix} 41/36 \\ 0 \\ 0 \end{bmatrix}, \hat{\underline{c}}_{21} = \begin{bmatrix} 0 \\ -7/2 \\ 0 \end{bmatrix}, \hat{\underline{c}}_{22} = \begin{bmatrix} 0 \\ 5/2 \\ 0 \end{bmatrix} \quad (2.20b)$$

Substituting (2.19) and (2.20) into (2.13), we obtain

$$\underline{B} = \begin{bmatrix} 7/4 & 0 & -1 \\ 0 & 4 & -1 \\ -1 & -1 & -3.2 \end{bmatrix}, \underline{a} = \begin{bmatrix} 7/4 \\ 2.2 \\ 0 \end{bmatrix}, \underline{r} = \begin{bmatrix} 0 \\ 0 \\ -1 \end{bmatrix},$$

$$\xi_{11} = \begin{bmatrix} -25/18 \\ 0 \\ 0 \end{bmatrix}, \xi_{12} = \begin{bmatrix} 41/36 \\ 0 \\ 0 \end{bmatrix}, \xi_{21} = \begin{bmatrix} 0 \\ -7/2 \\ 0 \end{bmatrix}, \xi_{22} = \begin{bmatrix} 0 \\ 5/2 \\ 0 \end{bmatrix} \quad (2.21)$$

Substituting (2.21) into (2.12), we obtain the following canonical piecewise-linear equation for the circuit in Fig. 6(a):

$$\underbrace{\begin{bmatrix} 7/4 & 0 & 1 \\ 0 & 4 & -1 \\ -1 & -1 & -3.2 \end{bmatrix}}_{\tilde{B}} \underbrace{\begin{bmatrix} v_1 \\ v_2 \\ i_{in} \end{bmatrix}}_{\tilde{x}} + \underbrace{\begin{bmatrix} -25/18 \\ 0 \\ 0 \end{bmatrix}}_{\xi_{11}} \underbrace{|v_1 - 1.2|}_{|x_1 - \beta_{11}|} + \underbrace{\begin{bmatrix} 41/36 \\ 0 \\ 0 \end{bmatrix}}_{\xi_{12}} \underbrace{|v_1 - 3|}_{|x_1 - \beta_{12}|} + \underbrace{\begin{bmatrix} 0 \\ -7/2 \\ 0 \end{bmatrix}}_{\xi_{21}} \underbrace{|v_2 - 0.8|}_{|x_2 - \beta_{21}|} + \underbrace{\begin{bmatrix} 0 \\ 5/2 \\ 0 \end{bmatrix}}_{\xi_{22}} \underbrace{|v_2 - 2|}_{|x_2 - \beta_{22}|} = \underbrace{\begin{bmatrix} 7/4 \\ 2.2 \\ 0 \end{bmatrix}}_{\tilde{a}} + \rho \underbrace{\begin{bmatrix} 0 \\ 0 \\ -1 \end{bmatrix}}_{\tilde{r}} \quad (2.22)$$

Example 2.3 (Fig. 7)

Consider the circuit in Fig. 7(a) where nonlinear resistors R_1 and R_2 are described in Figs. 7(c) and (d). Since R_1 and R_2 are both non-monotonic and current-controlled, it is necessary to choose i_1 and i_2 as the independent variables in this example. Their canonical piecewise-linear equations are found as follow:

$$R_1 : v_1 = \hat{v}_1(i_1) = -1 + i_1 - |i_1 - 2| + |i_1 - 3| \quad (2.23a)$$

$$R_2 : v_2 = \hat{v}_2(i_2) = -2 + i_2 - 2|i_2 - 4| + 2|i_2 - 5| \quad (2.23b)$$

The associated linear 3-port \hat{N} in Fig. 7(b) is described by the following generalized hybrid representation:

$$\underbrace{\begin{bmatrix} 0 & 0 & 0 \\ 1 & -1 & 0 \\ 1 & 0 & -1 \end{bmatrix}}_{\tilde{P}} \underbrace{\begin{bmatrix} i_1 \\ i_2 \\ i_{in} \end{bmatrix}}_{\tilde{x}} = \underbrace{\begin{bmatrix} 1 & 1 & -1 \\ 0 & 0 & 0 \\ 0 & 0 & 0 \end{bmatrix}}_{\tilde{Q}} \underbrace{\begin{bmatrix} v_1 \\ v_2 \\ v_{in} \end{bmatrix}}_{\tilde{y}} + \underbrace{\begin{bmatrix} 0 \\ 0 \\ 0 \end{bmatrix}}_{\tilde{s}} \quad (2.24)$$

Substituting (2.23) into (2.10) and (2.11), we obtain (here $n = 2$, $\sigma_1 = 2$ and $\sigma_2 = 2$):

$$\beta_{11} = 2, \beta_{12} = 3, \beta_{21} = 4, \beta_{22} = 5 \quad (2.25a)$$

$$\hat{\underline{a}} = \begin{bmatrix} -1 \\ -2 \\ 0 \end{bmatrix}, \hat{\underline{B}} = \begin{bmatrix} 1 & 0 & 0 \\ 0 & 1 & 0 \\ 0 & 0 & 0 \end{bmatrix}, \hat{\underline{c}}_{11} = \begin{bmatrix} -1 \\ 0 \\ 0 \end{bmatrix}, \hat{\underline{c}}_{12} = \begin{bmatrix} 1 \\ 0 \\ 0 \end{bmatrix}, \hat{\underline{c}}_{21} = \begin{bmatrix} 0 \\ -2 \\ 0 \end{bmatrix}, \hat{\underline{c}}_{22} = \begin{bmatrix} 0 \\ 2 \\ 0 \end{bmatrix} \quad (2.25b)$$

Substituting (2.24) and (2.25) into (2.13), we obtain

$$\underline{B} = \begin{bmatrix} 1 & 1 & 0 \\ -1 & 1 & 0 \\ -1 & 0 & 1 \end{bmatrix}, \underline{a} = \begin{bmatrix} 3 \\ 0 \\ 0 \end{bmatrix}, \underline{r} = \begin{bmatrix} 1 \\ 0 \\ 0 \end{bmatrix}$$

$$\underline{c}_{11} = \begin{bmatrix} -1 \\ 0 \\ 0 \end{bmatrix}, \underline{c}_{12} = \begin{bmatrix} 1 \\ 0 \\ 0 \end{bmatrix}, \underline{c}_{21} = \begin{bmatrix} -2 \\ 0 \\ 0 \end{bmatrix}, \underline{c}_{22} = \begin{bmatrix} 2 \\ 0 \\ 0 \end{bmatrix} \quad (2.26)$$

Substituting (2.26) into (2.12), we obtain the following canonical piecewise-linear equation for the circuit in Fig. 7(a):

$$\underbrace{\begin{bmatrix} 1 & 1 & 0 \\ -1 & 1 & 0 \\ -1 & 0 & 1 \end{bmatrix}}_{\underline{B}} \underbrace{\begin{bmatrix} i_1 \\ i_2 \\ i_{in} \end{bmatrix}}_{\underline{x}} + \underbrace{\begin{bmatrix} -1 \\ 0 \\ 0 \end{bmatrix}}_{\underline{c}_{11}} \underbrace{|i_1 - 2|}_{|x_1 - \beta_{11}|} + \underbrace{\begin{bmatrix} 1 \\ 0 \\ 0 \end{bmatrix}}_{\underline{c}_{12}} \underbrace{|i_1 - 3|}_{|x_1 - \beta_{12}|}$$

$$+ \underbrace{\begin{bmatrix} -2 \\ 0 \\ 0 \end{bmatrix}}_{\underline{c}_{21}} \underbrace{|i_2 - 4|}_{|x_2 - \beta_{21}|} + \underbrace{\begin{bmatrix} 2 \\ 0 \\ 0 \end{bmatrix}}_{\underline{c}_{22}} \underbrace{|i_2 - 5|}_{|x_2 - \beta_{22}|} = \underbrace{\begin{bmatrix} 3 \\ 0 \\ 0 \end{bmatrix}}_{\underline{a}} + \rho \underbrace{\begin{bmatrix} 1 \\ 0 \\ 0 \end{bmatrix}}_{\underline{r}} \quad (2.27)$$

Example 2.4 (Fig. 8)

Consider the one-transistor circuit shown in Fig. 8(a) containing 3 linear resistors and an ideal transformer with a turns-ratio $n = 10$. Let us model the transistor by the usual Ebers-Moll circuit model [4] as shown in Fig.

8(c), except that instead of using pn-junction diodes for R_1 and R_2 , we approximate the diode exponential law by a piecewise-linear function. Let

$$f(x) \triangleq I_S (e^{x/V_T} - 1) \quad (2.28)$$

where V_T is the thermal voltage which is 26 mV at room temperature and

$$I_S = \alpha_f I_{ES} = \alpha_r I_{CS} \quad (2.29)$$

where I_{ES} (resp.; I_{CS}) is the reverse saturation current in the base-emitter (resp.; base-collector) junction. For $V_T = 26$ mV and $I_S = 10^{-14}$ A, we approximate $f(x)$ by a 3-segment piecewise-linear function

$$\hat{f}(x) = -3.6374 \times 10^{-3} + 6.15 \times 10^{-3} x + 2.63 \times 10^{-4} |x-0.4| + 5.887 \times 10^{-3} |x-0.6| \quad (2.30)$$

as shown in Fig. 8(d). From (2.29) and choosing $\alpha_f = 0.995$ and $\alpha_r = 0.5$, the canonical piecewise-linear equation for R_1 and R_2 , which model the base-emitter and base-collector junction diodes respectively, are found as follow:

$$R_1: i_1 = \hat{i}_1(v_1) = -3.6557 \times 10^{-3} + 6.18 \times 10^{-3} v_1 + 2.643 \times 10^{-4} |v_1 - 0.4| + 5.916 \times 10^{-3} |v_1 - 0.6| \quad (2.31a)$$

$$R_2: i_2 = \hat{i}_2(v_2) = -7.2748 \times 10^{-3} + 1.23 \times 10^{-2} v_2 + 5.26 \times 10^{-4} |v_2 - 0.4| + 1.1774 \times 10^{-2} |v_2 - 0.6| \quad (2.31b)$$

The associated linear 3-port \hat{N} in Fig. 8(b) is described by the following generalized hybrid representation:

$$\underbrace{\begin{bmatrix} -0.25 & -1 & 0 \\ -20 & -1 & 0 \\ -1 & 0 & 8 \times 10^3 \end{bmatrix}}_{\underline{P}} \underbrace{\begin{bmatrix} v_1 \\ v_2 \\ i_{in} \end{bmatrix}}_{\underline{x}} = \underbrace{\begin{bmatrix} -945 & 6 \times 10^3 & 1 \\ -1.0145 \times 10^4 & 9.1 \times 10^4 & 0 \\ 8 \times 10^3 & -4 \times 10^3 & 0 \end{bmatrix}}_{\underline{Q}} \underbrace{\begin{bmatrix} i_1 \\ i_2 \\ v_{in} \end{bmatrix}}_{\underline{y}} + \underbrace{\begin{bmatrix} 0 \\ 0 \\ 0 \end{bmatrix}}_{\underline{s}} \quad (2.32)$$

Substituting (2.31) into (2.10) and (2.11), we obtain (here $n=2$, $\sigma_1=2$ and $\sigma_2=2$):

$$\beta_{11} = \beta_{21} = 0.4, \quad \beta_{12} = \beta_{22} = 0.6 \quad (2.33a)$$

$$\begin{aligned}
\hat{\underline{a}} &= \begin{bmatrix} -3.6557 \times 10^{-3} \\ -7.2748 \times 10^{-3} \\ 0 \end{bmatrix}, \quad \hat{\underline{B}} = \begin{bmatrix} 6.18 \times 10^{-3} & 0 & 0 \\ 0 & 1.23 \times 10^{-2} & 0 \\ 0 & 0 & 0 \end{bmatrix} \\
\hat{\underline{c}}_{11} &= \begin{bmatrix} 2.643 \times 10^{-4} \\ 0 \\ 0 \end{bmatrix}, \quad \hat{\underline{c}}_{12} = \begin{bmatrix} 5.916 \times 10^{-3} \\ 0 \\ 0 \end{bmatrix}, \quad \hat{\underline{c}}_{21} = \begin{bmatrix} 0 \\ 5.26 \times 10^{-4} \\ 0 \end{bmatrix}, \\
\hat{\underline{c}}_{22} &= \begin{bmatrix} 0 \\ 1.774 \times 10^{-2} \\ 0 \end{bmatrix}
\end{aligned} \tag{2.33b}$$

Substituting (2.32) and (2.33) into (2.13), we obtain

$$\begin{aligned}
\underline{B} &= \begin{bmatrix} -5.59 & 74.8 & 0 \\ -42.7 & 1120 & 0 \\ 50.4 & -49.2 & -8000 \end{bmatrix}, \quad \underline{a} = \begin{bmatrix} 40.2 \\ 625 \\ 0.146 \end{bmatrix}, \quad \underline{r} = \begin{bmatrix} -1 \\ 0 \\ 0 \end{bmatrix} \\
\underline{c}_{11} &= \begin{bmatrix} -0.25 \\ -2.68 \\ 2.11 \end{bmatrix}, \quad \underline{c}_{12} = \begin{bmatrix} -5.59 \\ -60 \\ 47.3 \end{bmatrix}, \quad \underline{c}_{21} = \begin{bmatrix} 3.16 \\ 47.9 \\ -2.10 \end{bmatrix}, \quad \underline{c}_{22} = \begin{bmatrix} 70.6 \\ 1071 \\ -47.1 \end{bmatrix}
\end{aligned} \tag{2.34}$$

Substituting (2.34) into (2.12), we obtain the following piecewise-linear equation for the circuit in Fig. 8(a):

$$\begin{aligned}
\underbrace{\begin{bmatrix} -5.59 & 74.8 & 0 \\ -42.7 & 1120 & 0 \\ 50.4 & -49.2 & -8000 \end{bmatrix}}_{\underline{B}} \underbrace{\begin{bmatrix} v_1 \\ v_2 \\ i_{in} \end{bmatrix}}_{\underline{x}} + \underbrace{\begin{bmatrix} -0.25 \\ -2.68 \\ 2.11 \end{bmatrix}}_{\underline{c}_{11}} \underbrace{|v_1 - 0.4|}_{|x_1 - \beta_{11}|} + \underbrace{\begin{bmatrix} -5.59 \\ -60 \\ 47.3 \end{bmatrix}}_{\underline{c}_{12}} \underbrace{|v_1 - 0.6|}_{|x_1 - \beta_{12}|} \\
+ \underbrace{\begin{bmatrix} 3.16 \\ 47.9 \\ -2.10 \end{bmatrix}}_{\underline{c}_{21}} \underbrace{|v_2 - 0.4|}_{|x_2 - \beta_{21}|} + \underbrace{\begin{bmatrix} 70.6 \\ 1071 \\ -47.1 \end{bmatrix}}_{\underline{c}_{22}} \underbrace{|v_2 - 0.6|}_{|x_2 - \beta_{22}|} = \underbrace{\begin{bmatrix} 40.2 \\ 625 \\ 0.146 \end{bmatrix}}_{\underline{a}} + \rho \underbrace{\begin{bmatrix} -1 \\ 0 \\ 0 \end{bmatrix}}_{\underline{r}}
\end{aligned} \tag{2.35}$$

Example 2.5 (Figs. 8(a) and 9)

Consider the same circuit in Fig. 8(a) again, but redraw as shown in Fig. 9(a). Instead of replacing the transistor by a circuit model (made of uncoupled 2-terminal piecewise-linear resistors and controlled sources) as in Fig. 8(b), let us describe the transistor by an equivalent version of Ebers-Moll equation; namely,

$$i_1 = \hat{i}_1(v_1, v_2) = -f(v_2) + \frac{1}{\alpha_f} f(v_1) \quad (2.36a)$$

$$i_2 = \hat{i}_2(v_1, v_2) = -f(v_1) + \frac{1}{\alpha_r} f(v_2) \quad (2.36b)$$

where the function $f(\cdot)$ is as defined in (2.28). Approximating the function $f(\cdot)$ by the 3-segment piecewise-linear function $\hat{f}(\cdot)$ as defined in (2.30) and choosing $\alpha_f = 0.995$ and $\alpha_r = 0.5$, we obtain the following pair of coupled piecewise-linear equation describing the npn transistor:

3-segment piecewise-linear Ebers-Moll equation:

$$\begin{aligned} i_1 = \hat{i}_1(v_1, v_2) &= -1.8187 \times 10^{-5} + 6.18 \times 10^{-3} v_1 - 6.15 \times 10^{-3} v_2 + 2.643 \times 10^{-4} |v_1 - 0.4| \\ &\quad + 5.916 \times 10^{-3} |v_1 - 0.6| - 2.63 \times 10^{-4} |v_2 - 0.4| - 5.887 \times 10^{-3} |v_2 - 0.6| \\ i_2 = \hat{i}_2(v_1, v_2) &= -3.6374 \times 10^{-3} - 6.15 \times 10^{-3} v_1 + 1.23 \times 10^{-2} v_2 - 2.63 \times 10^{-4} |v_1 - 0.4| \\ &\quad - 5.887 \times 10^{-3} |v_1 - 0.6| + 5.26 \times 10^{-4} |v_2 - 0.4| + 1.1774 \times 10^{-2} |v_2 - 0.6| \end{aligned} \quad (2.37)$$

Observe that (2.37) can be interpreted as the equations of two coupled 2-terminal resistors as shown in Fig. 9(b). Note that \hat{N} in Fig. 9 is identical to that of Fig. 8(b) except that the two controlled sources have been removed: their role in the circuit model in Fig. 8(c) is now assumed directly by an explicit coupling term in the corresponding equation model (2.37). Indeed if we extract the two controlled sources in Fig. 8(b) and connect them externally in parallel with R_1 and R_2 , then the "composite" equation describing the resulting parallel combination is precisely given by (2.37). In other words, our present formulation is exactly equivalent to that of Example 2.4 and we should expect to obtain the same canonical piecewise-linear equation in the end, even though the intermediate calculations are different. Let us verify

this observation as follows:

The new 3-port \hat{N} in Fig. 9(b) is described by the following generalized hybrid representation:

$$\begin{array}{c} \begin{bmatrix} -0.25 & -1 & 0 \\ -20 & -1 & 0 \\ -1 & 0 & 8000 \end{bmatrix} \begin{bmatrix} v_1 \\ v_2 \\ i_{in} \end{bmatrix} = \begin{bmatrix} 10^4 & 1.1 \times 10^4 & 1 \\ 1.6 \times 10^5 & 1.71 \times 10^5 & 0 \\ 8000 & 0 & 0 \end{bmatrix} \begin{bmatrix} i_1 \\ i_2 \\ v_{in} \end{bmatrix} + \begin{bmatrix} 0 \\ 0 \\ 0 \end{bmatrix} \quad (2.38) \\ \tilde{P} \quad \quad \tilde{x} \quad \quad \quad \tilde{Q} \quad \quad \quad \tilde{y} \quad \quad \quad \tilde{s} \end{array}$$

Substituting (2.37) into (2.10) and (2.11), we obtain (here $n=2$, $\sigma_1=2$ and $\sigma_2=2$):

$$\beta_{11} = \beta_{12} = 0.4, \beta_{21} = \beta_{22} = 0.6 \quad (2.39a)$$

$$\begin{array}{c} \tilde{\hat{a}} = \begin{bmatrix} -1.8187 \times 10^{-5} \\ -3.6374 \times 10^{-3} \\ 0 \end{bmatrix}, \tilde{\hat{B}} = \begin{bmatrix} 6.18 \times 10^{-3} & -6.15 \times 10^{-3} & 0 \\ -6.15 \times 10^{-3} & 1.23 \times 10^{-2} & 0 \\ 0 & 0 & 0 \end{bmatrix} \\ \tilde{\hat{c}}_{11} = \begin{bmatrix} 2.643 \times 10^{-4} \\ -2.63 \times 10^{-4} \\ 0 \end{bmatrix}, \tilde{\hat{c}}_{12} = \begin{bmatrix} 5.916 \times 10^{-3} \\ -5.887 \times 10^{-3} \\ 0 \end{bmatrix}, \tilde{\hat{c}}_{21} = \begin{bmatrix} -2.63 \times 10^{-4} \\ 5.26 \times 10^{-4} \\ 0 \end{bmatrix}, \\ \tilde{\hat{c}}_{22} = \begin{bmatrix} -5.887 \times 10^{-3} \\ 1.1774 \times 10^{-2} \\ 0 \end{bmatrix} \quad (2.39b) \end{array}$$

Observe that unlike (2.16), (2.20), (2.25) and (2.33) in the previous examples where \hat{B} is a diagonal matrix, $\tilde{\hat{B}}$ is not a diagonal matrix in (2.39) in view of the additional coupling terms in (2.37). Likewise, observe that whereas \hat{c}_{ji} in (2.16), (2.20), (2.25) and (2.33) has only one nonzero entry, $\tilde{\hat{c}}_{ji}$ has more than one nonzero entry in (2.39).

Substituting (2.38) and (2.39) into (2.13), we obtain the same equation as (2.34) and consequently the canonical piecewise-linear equation should be the same as (2.35).

3. THE BREAKPOINT-HOPPING ALGORITHM

A. Assumptions

To exclude pathological and degenerate cases, the algorithm to be developed in this section makes the following assumptions:

1. The driving-point or transfer characteristic is made of one or more unicursal (i.e.; contiguous 1-dimensional) curves. Hence, degenerate characteristics containing points forming nonzero areas, such as the characteristic of a norator, are excluded.

In terms of the algorithm, this assumption is satisfied (see Section 5C) if

- a) the Jacobian matrix corresponding to the starting point of each solution curve[†] has a nullity at most equal to one;
 - b)^{††} the solution curve never hits a corner point.^{†††}
2. The output variable y_0 (either v_0 or i_0 in Fig. 2) of the desired transfer characteristic is a linear combination of at most $n+1$ port variables z_j , $j = 1, 2, \dots, n+1$, where $z_j \in \{x_1, x_2, \dots, x_{n+1}; y_1, y_2, \dots, y_{n+1}\}$; namely,

$$y_0 = \alpha_0 + \alpha_1 z_1 + \alpha_2 z_2 + \dots + \alpha_{n+1} z_{n+1} \quad (3.1)$$

where $\alpha_0, \alpha_1, \dots, \alpha_{n+1}$ are real constants. This assumption is satisfied except in rare degenerate circuits. Indeed, in most cases, the output variable will be a linear combination of only the independent variables x_1, x_2, \dots, x_n in (2.2) and v_{in} ; namely,

$$y_0 = \alpha_0 + \alpha_1 x_1 + \alpha_2 x_2 + \dots + \alpha_n x_n + \alpha_{n+1} v_{in} \quad (3.2)$$

In terms of the circuit in Fig. 4(b), (3.2) implies that \hat{N} has a unique solution for y_0 when the ports are driven as shown in Fig. 4(b).^{††††}

[†]See Section 3B.

^{††}See Assumption 4 below.

^{†††}A corner is a closed connected set determined by the intersection of at least two boundary hyperplanes, or determined by the union of regions with Jacobian matrices of nullity at least two [16].

^{††††}For example, if we choose $y_0 \triangleq i_{in}$ in Figs. 5(a), 6(a) and 7(a), then the last row of the corresponding piecewise-linear equations (2.17), (2.22) and (2.27) is of the form (3.2). On the other hand, $y_0 \triangleq i_{in}$ in Fig. 8(a) can not be expressed in the form of (3.2). By inspection of Fig. 9(b), we find $i_{in} = -v_1/8k - i_1$ is of the form (3.1). Note that i_{in} is a linear function of both v_1 and i_1 of port 1, and is independent of v_2 and i_2 .

3. The canonical piecewise-linear equation (2.12) is derived for the case when the input variable is a voltage source v_{in} . This involves no loss of generality for driving-point characteristics because our algorithm is capable of tracing multivalued characteristics and hence it does not matter whether v_{in} or i_{in} is chosen as the independent variable. However, for transfer characteristics driven by a current source, it is necessary to interchange i_{in} in (2.2) with v_{in} in (2.3). The form of the resulting canonical piecewise-linear equation remains unchanged, however.
4. The solution curve to be defined below never hits a corner in the sense that as we sweep the input variable ρ , no two (or more) nonlinear resistors arrive at a breakpoint in their v - i curves simultaneously, i.e., for the same value $\rho = \rho^*$. Since this assumption can only be violated by a precise (usually contrived) choice of circuit parameter values, we can avoid the corner problem (if it occurs) by an arbitrarily small perturbation of some circuit parameters.

B. Basic Ideas Behind the Algorithm

If we choose the output variable y_0 to coincide with each variable x_1, x_2, \dots, x_{n+1} in (2.2), then Assumption 1 guarantees that each $x_j - v_s - v_{in}$ transfer characteristic is made of one or more one-dimensional unicursal branches for $j = 1, 2, \dots, n+1$. Note that $x_{n+1} - v_s - v_{in}$ is just the driving-point characteristic. For other choices of output variable y_0 , Assumption 2 allows us to calculate easily the corresponding transfer characteristic by substituting each $x_j - v_s - v_{in}$ transfer characteristic in place of x_j in (3.2), or (3.1) in which case the corresponding relationships for y_j 's are obtained from (1.2)-(1.3) (for the uncoupled case) or (2.8)-(2.9) (for the coupled case). Consequently our basic problem is to solve for x_1, x_2, \dots, x_{n+1} in the canonical piecewise-linear equation (2.12) for each value of the input $v_{in} = \rho$, where $\rho_{min} \leq \rho \leq \rho_{max}$.

Since the circuit is piecewise-linear, the solution of (2.12) will trace out a one-dimensional piecewise-linear space curve $\hat{\Gamma}$ in the $x_1 - x_2 \dots - x_{n+1}$ space \mathbb{R}^{n+1} , as we sweep the input from $v_{in} = \rho_{min}$ to $v_{in} = \rho_{max}$. Each (straight-line) segment of $\hat{\Gamma}$ corresponds to a particular combination of segments of the n piecewise-linear resistors R_1, R_2, \dots, R_n . Since the boundaries of each linear region are determined by the breakpoints of the nonlinear resistors, and not on $x_{n+1} \triangleq i_{in}$, it is convenient to project $\hat{\Gamma}$ onto the first n relevant coordinates $x_1 - x_2 - \dots - x_n$. This projection gives a one-dimensional

piecewise-linear curve in \mathbb{R}^n , henceforth called a solution curve Γ . Each breakpoint of Γ must clearly fall on a particular hyperplane boundary.

For example, consider the three boundaries $v_1 = -1$, $v_1 = 2$, and $i_2 = 3$ in the $v_1 - i_2$ plane in Fig. 3(c) corresponding to a hypothetical circuit containing only two piecewise-linear resistors, as described in Figs. 3(a) and (b). Suppose that at $v_{in} = \rho_{min} \triangleq \rho^{(0)}$, the solution of (2.12) gives the operating point $\tilde{x}^{(0)}$. As we vary ρ from ρ_{min} , the solution of (2.12) traces out a piecewise linear solution curve Γ such as that shown in Fig. 10. Note that each segment of Γ terminates on a boundary (at $\tilde{x}^{(1)}(\rho^{(1)})$, $\tilde{x}^{(2)}(\rho^{(2)})$, $\tilde{x}^{(3)}(\rho^{(3)})$, and $\tilde{x}^{(4)}(\rho^{(4)})$) before changing slopes. These breakpoints are parametrized by the input voltages $\rho^{(1)}$, $\rho^{(2)}$, $\rho^{(3)}$, and $\rho^{(4)}$ corresponding to the input voltages where the operating point arrives at a breakpoint in Figs. 3(a) or (b). Note that Assumption 4 guarantees that these breakpoints do not occur at a "corner," which in Fig. 10 represents the intersection between any two of the three boundary straight lines; namely, points A and B. Note also that the solution curve Γ in general does not have to cover all regions. Here, region (1,2) is bypassed.

The goal of our algorithm is to calculate the locations of all breakpoints $\tilde{x}^{(j)}(\rho^{(j)})$ of the solution curve Γ over the specified dynamic range $\rho_{min} \leq \rho \leq \rho_{max}$. Because (2.12) reduces to a linear equation in each region, it is a trivial matter to calculate this direction vector (slope in this example) of each segment of Γ from any initial point. Because the boundaries all possess a lattice structure, it is also relatively easy to identify which boundary will be crossed first and hence a formula for calculating the corresponding breakpoint can be derived. Consequently, we can devise a highly efficient algorithm to calculate each breakpoint $\tilde{x}^{(k)}(\rho^{(k)})$, given the location of the preceding breakpoint $\tilde{x}^{(k-1)}(\rho^{(k-1)})$, henceforth called the breakpoint-hopping algorithm. The various assumptions in Section 3A merely guarantees that this algorithm does not get stuck in various degenerate (ill-conditioned) situations to be analyzed in Section 5.

C. Derivation of the Algorithm

Let us begin by finding an operating point $\tilde{x}^{(0)}$ of the circuit when[†] $v_{in} = \rho_{min} \triangleq \rho^{(0)}$ using any method (e.g., algorithm in [1] or [2]). If the circuit has several operating points, pick one point arbitrarily and denote it

[†]See Section 3D for other choices of the initial parameter $\rho^{(0)}$.

as $\tilde{x}^{(0)}$. Some if not all of the remaining operating points may also fall on the solution curve Γ through $\tilde{x}^{(0)}$. The remaining operating points which do not fall on Γ must therefore belong to one or more additional branches and our algorithm below is simply repeated recursively with one of these remaining operating points as the initial point. If the original set X of operating points happen to contain a subset consisting of one point on each distinct branch, then our recursive algorithm would find all such branches.

Our algorithm consists of two main steps:

Step I. Initialization:

From the coordinates of the initial operating point $\tilde{x}^{(0)}$, we can identify the region $R^{(0)}$ containing $\tilde{x}^{(0)}$ by comparing each coordinate $x_j^{(0)}$ with (1.2)-(1.3) (for the uncoupled case) or (2.8)-(2.9) (for the coupled case); namely, identify segment " i_j " such that

$$\beta_j(i_{j-1}) \leq x_j^{(0)} \leq \beta_j(i_j) \quad j = 1, 2, \dots, n \quad (3.3a)$$

For the two end segments tending to $-\infty$ and $+\infty$, respectively, we define

$$\beta_j 0 = -\infty \text{ and } \beta_j(\sigma_j+1) = +\infty \quad (3.3b)$$

We assume $\tilde{x}^{(0)}$ is an interior point of $R^{(0)}$, i.e., there exists $\delta > 0$ such that all points satisfying $\|\tilde{x} - \tilde{x}^{(0)}\| < \delta$ also lie within $R^{(0)}$. If this assumption fails, then $\tilde{x}^{(0)}$ must lie on a boundary hyperplane of $R^{(0)}$ and we simply proceed directly to Step II of the algorithm which deals with such "boundary" points as starting points.

Choose next another value of $\rho = \rho^{(0)} + \Delta\rho \triangleq \hat{\rho}^{(0)}$ near $\rho^{(0)}$ (i.e., $\Delta\rho > 0$ is sufficiently small) such that the corresponding operating point $\hat{\tilde{x}}^{(0)}$ still lies within $R^{(0)}$. This is always possible if $\tilde{x}^{(0)}$ is an interior point.

It follows that for both $\rho = \rho^{(0)}$ and $\rho = \hat{\rho}^{(0)}$, (2.12) reduces to a linear equation obtained by substituting all parameters in (2.12) corresponding to $R^{(0)}$; namely,

$$\tilde{B}^{(0)} \tilde{x}^{(0)} = \tilde{a}^{(0)} + \rho^{(0)} \tilde{r} \quad (3.4)$$

$$\tilde{B}^{(0)} \hat{\tilde{x}}^{(0)} = \tilde{a}^{(0)} + \hat{\rho}^{(0)} \tilde{r} \quad (3.5)$$

where

$$\tilde{B}^{(0)} \triangleq \tilde{B} + \sum_{j=1}^n \left[- \sum_{i=1}^{i_j-1} c_{ji} e_{i-j}^T + \sum_{i=i_j}^{\sigma_j} c_{ji} e_{i-j}^T \right] \quad (3.6)$$

(Here, e_j^T denotes the unit row vector with zero entries except at the j -th position, $j = 1, 2, \dots, n$).

$$\tilde{a}^{(0)} \triangleq \tilde{a} + \sum_{j=1}^n \left[- \sum_{i=1}^{i_j-1} c_{ji} \beta_{ji} + \sum_{i=i_j}^{\sigma_j} c_{ji} \beta_{ji} \right] \quad (3.7)$$

$$\tilde{x}^{(0)} - \tilde{x}^{(0)} = (\hat{\rho}^{(0)} - \rho^{(0)}) [\tilde{B}^{(0)}]^{-1} \tilde{r} = (\hat{\rho}^{(0)} - \rho^{(0)}) \tilde{d}^{(0)} \quad (3.8)$$

where $\tilde{d}^{(0)} \triangleq [\tilde{B}^{(0)}]^{-1} \tilde{r}$ denotes the direction vector which falls on the straight line $\tilde{x}^{(0)}$ to $\hat{x}^{(0)}$. As we increase ρ from $\rho = \rho^{(0)}$, the solution curve Γ starting from $\tilde{x}^{(0)}$ will grow along the direction $\tilde{d}^{(0)}$ until it crosses the nearest boundary hyperplane of $R^{(0)}$. This boundary as well as the intersecting breakpoint $\tilde{x}^{(1)}$ can be identified as follows:

Let $d_j^{(0)}$ denote the j -th component of $\tilde{d}^{(0)}$. If $d_j^{(0)} > 0$ (resp.; $d_j^{(0)} < 0$), then Γ is increasing (resp.; decreasing) along the direction of the j -th coordinate axis, and Γ will reach the j -th boundary hyperplane $x_j = \beta_{ji_j}$ (resp.; $x_j = \beta_{j(i_j-1)}$) at $\rho^{(1)} = \rho^{(0)} + \Delta\rho_j^{(0)}$, where

$$\Delta\rho_j^{(0)} \triangleq (\beta_{ji_j} - x_j^{(0)}) / |d_j^{(0)}| \quad (3.9a)$$

$$\text{(resp.; } \Delta\rho_j^{(0)} \triangleq (x_j^{(0)} - \beta_{j(i_j-1)}) / |d_j^{(0)}|) \quad (3.9b)$$

Choose the index j_0 such that $\Delta\rho_{j_0}^{(0)}$ is minimal compared to the other $\Delta\rho_j^{(0)}$ with $d_j^{(0)} \neq 0$, $j = 1, 2, \dots, j_0-1, j_0+1, \dots, n$. Then $x_{j_0} = \beta_{j_0 i_{j_0}}$ (resp.; $x_{j_0} = \beta_{j_0(i_{j_0}-1)}$) is the first (hence nearest) boundary hyperplane intersected by the solution curve Γ from $\tilde{x}^{(0)}$. Hence, the breakpoint $\tilde{x}^{(1)}$ which is located on the boundary hyperplane $x_{j_0} = \beta_{j_0 i_{j_0}}$ (resp.; $x_{j_0} = \beta_{j_0(i_{j_0}-1)}$) is given by

$$\tilde{x}^{(1)} = \tilde{x}^{(0)} + \Delta\rho^{(0)} \tilde{d}^{(0)} \quad (3.10)$$

where

$$\rho = \rho^{(0)} + \Delta\rho^{(0)} \triangleq \rho^{(1)} \quad (3.11)$$

Note that $\Delta\rho^{(0)} \neq 0$ if $B^{(0)}$ is nonsingular because $\tilde{x}^{(0)}$ is an interior point within $R^{(0)}$. Also $\Delta\rho^{(0)} > 0$ because $\rho^{(0)} = \rho_{\min}$ and the direction vector $\tilde{d}^{(0)}$ is chosen for the solution curve.

The above initialization algorithm for locating the first breakpoint $\tilde{x}^{(1)}$

of the solution curve Γ from $\tilde{x}^{(0)}$ is illustrated in Fig. 11(a) for a typical 2-dimensional region $R^{(0)}$, and in Fig. 11(b) for a typical 3-dimensional region $R^{(0)}$. Note that in Fig. 11(a), the boundary line $x_1 = \beta_1 i_1$ is penetrated by the direction vector $\tilde{d}^{(0)}$ at $\tilde{x}^{(1)}$ ($\rho = \rho^{(1)}$) before its extension intersects the second boundary line $x_2 = \beta_2 i_2$ at $\tilde{x}_1^{(1)'}$ ($\rho = \rho^{(1)'}$). Hence $\tilde{x}^{(1)}$ is the "nearest" breakpoint where the solution curve first hits a boundary of $R^{(0)}$. In Fig. 11(b), the boundary plane $x_2 = \beta_2 i_2$ is penetrated by the direction vector $\tilde{d}^{(0)}$ at $\tilde{x}^{(1)}$ ($\rho = \rho^{(1)}$) before its extension intersects the next two boundary planes, first at $x_1 = \beta_1 (i_1 - 1)$ (back side of the "cube" $R^{(0)}$) at $\tilde{x}^{(1)'}$ and then at $x_3 = \beta_3 i_3$ (top side of $R^{(0)}$) at $\tilde{x}^{(1)''}$. Here, the "nearest" breakpoint is located at $\tilde{x}^{(1)}$ (right side of $R^{(0)}$).

Note also that for the direction vector $\tilde{d}^{(0)}$ drawn in Fig. 11(a), its components $d_1^{(0)} > 0$ and $d_2^{(0)} > 0$ are both positive. However, for the direction vector $\tilde{d}^{(0)}$ drawn in Fig. 11(b), we have $d_1^{(0)} < 0$, $d_2^{(0)} > 0$ and $d_3^{(0)} > 0$. In other words, the components of the direction vector $\tilde{d}^{(0)}$ in general have different signs.

Since only one boundary is crossed for any $v_{j_0} = \rho$ (by Assumption 4), the boundary hyperplanes of the next (adjacent to $R^{(0)}$) region $R^{(1)}$ are identical to those of $R^{(0)}$ except that the index i_{j_0} of $R^{(1)}$ is greater (resp.; less) than that of $R^{(0)}$ by one. More specifically, if $R^{(0)}$ is bounded by $\beta_j (i_j - 1) \leq x_j \leq \beta_j i_j$, then $R^{(1)}$ is bounded by $\beta_j (i_j - 1) \leq x_j \leq \beta_j i_j$ for $j \neq j_0$ and $\beta_{j_0} i_{j_0} \leq x_{j_0} \leq \beta_{j_0} (i_{j_0} + 1)$ (resp.; $\beta_{j_0} (i_{j_0} - 2) \leq x_{j_0} \leq \beta_{j_0} (i_{j_0} - 1)$).

Step II. Breakpoint Hopping:

Step I identifies a breakpoint $\tilde{x}^{(1)}$ lying at the boundary hyperplane separating region $R^{(0)}$ from region $R^{(1)}$. It follows from Assumption 1 that the solution curve Γ in region $R^{(1)}$ from $\tilde{x}^{(1)}$ will be a straight-line segment which either intersects another boundary hyperplane as shown in Fig. 12(a) or tends to infinity as shown in Fig. 12(b). The latter situation corresponds to the case where $R^{(1)}$ is an unbounded region (i.e., one of the piecewise-linear resistors is operating in its end segment) and we are done.

Consequently, it suffices for us to consider the general situation where the solution curve Γ starting from some breakpoint $\tilde{x}^{(k-1)}$ (at $\rho = \rho^{(k-1)}$) in region $R^{(k-1)}$ intersects another boundary hyperplane separating regions $R^{(k-1)}$

and $R^{(k)}$ at a new breakpoint $\tilde{x}^{(k)}$ (at $\rho = \rho^{(k)}$). In other words, given breakpoint $\tilde{x}^{(k-1)}$, find the adjacent breakpoint $\tilde{x}^{(k)}$.

The basic ideas behind the initialization algorithm in Step I is still applicable here. However, there is a new complication which we must overcome; namely, the direction vector $\tilde{d}^{(k)}$ which lies along the solution curve Γ in region $R^{(k)}$ may point in the wrong direction, as illustrated in Fig. 13. Here, the portion of the solution curve Γ in the two adjacent regions $R^{(k-1)}$ and $R^{(k)}$ (drawn for the 2-dimensional case) is shown connecting breakpoints $\tilde{x}^{(k-1)}$, $\tilde{x}^{(k)}$ and $\tilde{x}^{(k+1)}$. If the two direction vectors $\tilde{d}^{(k-1)}$ (along Γ in $R^{(k-1)}$) and $\tilde{d}^{(k)}$ (along the extension of Γ in $R^{(k)}$) are as indicated in Fig. 13, then we would traverse from $\tilde{x}^{(k-1)}$ (corresponding to $\rho = \rho^{(k-1)}$) to $\tilde{x}^{(k)}$ in the direction of $\tilde{d}^{(k-1)}$ as we increase ρ from $\rho^{(k-1)}$ to $\rho^{(k)} \triangleq \rho^{(k-1)} + \Delta\rho^{(k-1)}$, where $\Delta\rho^{(k-1)} > 0$. However, any further increase in ρ from $\rho^{(k)}$ to $\rho^{(k)} + \Delta\rho$ would take us back into region $R^{(k-1)}$ along the direction $\tilde{d}^{(k)}$ if $\Delta\rho > 0$. Clearly, in this case, we should proceed in a direction exactly opposite to that of $\tilde{d}^{(k)}$ in order to arrive at breakpoint $\tilde{x}^{(k+1)}$ at $\rho^{(k+1)} \triangleq \rho^{(k)} + \Delta\rho^{(k)}$, where $\Delta\rho^{(k)} < 0$.

The situation depicted in Fig. 13 actually is not pathological but actually occurs whenever the solution curve Γ is not a single-valued function of $v_{in} = \rho$. For example, consider the driving-point characteristics shown in Figs. 14(a), (b) and (c). Note that in all three cases, we traverse from breakpoint ① to breakpoint ② by increasing the value of v_{in} from $\rho^{(1)}$ to $\rho^{(1)} + \Delta\rho^{(1)}$, where $\Delta\rho^{(1)} > 0$. However, in order to continue from breakpoint ② to breakpoint ③, we must decrease the value of v_{in} from $\rho^{(2)}$ to $\rho^{(2)} + \Delta\rho^{(2)}$ where $\Delta\rho^{(2)} < 0$ in Figs. 14(a) and (b), or hold constant at $v_{in} = \rho^*$ in Fig. 14(c). Observe that this would trace out a different segment even though the values of ρ overlaps those of the preceding segment because the parameters of the canonical equation (2.12) must be updated to those corresponding to the new region.

It follows from the above observations that it is necessary to develop an algorithm for determining which direction we should proceed (i.e., $\tilde{d}^{(k)}$ or $-\tilde{d}^{(k)}$) upon reaching a breakpoint $\tilde{x}^{(k)}$ in order that the solution curve Γ can be traced in a continuous manner; i.e., hopping from one breakpoint $\tilde{x}^{(k)}$ to the "next neighboring" breakpoint $\tilde{x}^{(k+1)}$. In view of the lattice structure of the boundary hyperplanes, a highly efficient algorithm can be devised with the help of Fig. 13.

For the moment,[†] let us assume that the previous direction vector $\underline{d}^{(k-1)}$ is (correctly) directed towards breakpoint $\underline{x}^{(k)}$; i.e., $\Delta\rho^{(k-1)} > 0$. Assume that the breakpoint $\underline{x}^{(k)}$ lies at the boundary hyperplane defined by the j_{k-1} -th coordinate; namely, at $x_{j_{k-1}} = \beta_{j_{k-1}}(i_{j_{k-1}} - 1)$. It follows from the above assumption ($\Delta\rho^{(k-1)} > 0$) that

$$\underline{d}_{j_{k-1}}^{(k-1)} \cdot \underline{d}_{j_{k-1}}^{(k)} < 0 \quad (3.12)$$

if and only if $\underline{d}^{(k)}$ is directed away from $R^{(k)}$; i.e., returning back to region $R^{(k-1)}$. Hence, if (3.12) holds, then we must follow the opposite direction $-\underline{d}^{(k)}$. This is equivalent to choosing $\Delta\rho^{(k)} < 0$. By a similar derivation, (3.8) now takes the following form in $R^{(k)}$:

$$\underline{x}^{(k+1)} - \underline{x}^{(k)} = [\rho^{(k+1)} - \rho^{(k)}] \underline{d}^{(k)} \quad (3.13)$$

where

$$\underline{d}^{(k)} \triangleq [\underline{B}^{(k)}]^{-1} \underline{r} \quad (3.14a)$$

and

$$\Delta\rho^{(k)} \triangleq \rho^{(k+1)} - \rho^{(k)} < 0 \quad (3.14b)$$

Here $\underline{B}^{(k)}$ is the Jacobian matrix of (2.12) in region $R^{(k)}$ and is given by

$$\underline{B}^{(k)} \triangleq \underline{B} + \sum_{j=1}^n \left[- \sum_{i=1}^{i_j-1} c_{ji} e_j^T + \sum_{i=i_j}^{\sigma_j} c_{ji} e_j^T \right] \quad (3.15)$$

The above formulas which cover the two typical cases depicted in Figs. 14(a) and (b) are valid if and only if $\underline{B}^{(k)}$ is nonsingular. However, the case depicted in Fig. 14(c) has singular Jacobian matrix $\underline{B}^{(k)}$ and $\Delta\rho^{(k)} \triangleq \rho^{(k+1)} - \rho^{(k)} = 0$. This degenerate case will be analyzed in Section 5. Meanwhile, let us summarize the above properties as follows:

strict-monotone parameter variation property:

If $\underline{B}^{(k)}$ is nonsingular and $\Delta\rho^{(k)} \triangleq \rho^{(k+1)} - \rho^{(k)}$, then $\Delta\rho^{(k)} > 0$ (resp.; $\Delta\rho^{(k)} < 0$) in $R^{(k)}$ if and only if the solution curve Γ in $R^{(k)}$ follows the direction of $\underline{d}^{(k)}$ (resp.; $-\underline{d}^{(k)}$) from $\underline{x}^{(k)}$ to $\underline{x}^{(k+1)}$.

It follows from the preceding property that if $\underline{B}^{(j)}$ is nonsingular, then

[†]This assumption is not necessary and will be lifted shortly.

the solution curve Γ will traverse the region $R^{(j)}$ along the direction of $\text{sgn}(\Delta\rho^{(j)})\underline{d}^{(j)}$. Hence, we can now remove the earlier assumption that $\underline{d}^{(k-1)}$ in $R^{(k-1)}$ is directed towards $\underline{x}^{(k)}$, and replace (3.12) by the more general criterion:

$$\underline{d}_{j_{k-1}}^{(k)} \cdot \underline{d}_{j_{k-1}}^{(k-1)} \cdot \text{sgn}(\Delta\rho^{(k-1)}) > 0 \quad (3.16a)$$

$$(\text{resp.}; \underline{d}_{j_{k-1}}^{(k)} \cdot \underline{d}_{j_{k-1}}^{(k-1)} \cdot \text{sgn}(\Delta\rho^{(k-1)}) < 0) \quad (3.16b)$$

if and only if $\underline{d}^{(k)}$ is directed towards (resp.; away from) $R^{(k)}$.

Observe that (3.16) uses only data from the j_{k-1} -th entry of $\underline{d}^{(k)}$ and $\underline{d}^{(k-1)}$, where j_{k-1} corresponds to the piecewise-linear resistor $R_{j_{k-1}}$ (where one of its breakpoints had just been reached).

Equation (3.16a) (resp.; (3.16b)) implies that we should choose $\Delta\rho^{(k)} > 0$ (resp.; $\Delta\rho^{(k)} < 0$) in the next region $R^{(k)}$. Observe also that we can replace $\text{sgn}(\Delta\rho^{(k-1)})$ by $\Delta\rho^{(k-1)}$ in (3.16) without changing the validity of the preceding property.

Having thus identified the correct direction to proceed in $R^{(k)}$, our next objective is to determine the first boundary hyperplane of $R^{(k)}$ penetrated by the solution curve Γ . To do this, we need to find the direction (identical or opposite) traversed by each component of Γ along the j -th coordinate axis (i.e., the projection of Γ onto x_j within $R^{(k)}$), $j = 1, 2, \dots, n$. This information can be determined with the help of (3.16) as follows:

component direction criterion:

The component of Γ along the x_j coordinate axis traverses towards the positive (resp.; negative) direction of x_j as Γ moves from $\underline{x}^{(k)}$ to $\underline{x}^{(k+1)}$ in $R^{(k)}$ if, and only if,

$$\underline{d}_j^{(k)} \cdot \underline{d}_{j_{k-1}}^{(k)} \cdot \underline{d}_{j_{k-1}}^{(k-1)} \cdot \Delta\rho^{(k-1)} > 0 \quad (3.17a)$$

$$(\text{resp.}; \underline{d}_j^{(k)} \cdot \underline{d}_{j_{k-1}}^{(k)} \cdot \underline{d}_{j_{k-1}}^{(k-1)} \cdot \Delta\rho^{(k-1)} < 0) \quad (3.17b)$$

In view of the lattice structure, the boundary hyperplanes of $R^{(k)}$ can be described trivially as follows:

$$\beta_j(i_{j-1}) \leq x_j \leq \beta_j i_j, \quad j = 1, 2, \dots, n \quad (3.18)$$

If (3.17a) (resp.; (3.17b)) holds, then the right (resp.; left) boundary $x_j = \beta_j i_j$ (resp.; $x_j = \beta_j(i_{j-1})$) will be reached at

$$\rho^{(k+1)} = \rho^{(k)} \pm \Delta\rho_j^{(k)} \quad (3.19)$$

where

$$\Delta\rho_j^{(k)} \triangleq (\beta_j i_j - x_j^{(k)}) / |d_j^{(k)}| > 0 \quad (3.20a)$$

$$\text{(resp.; } \Delta\rho_j^{(k)} \triangleq (x_j^{(k)} - \beta_j(i_{j-1})) / |d_j^{(k)}| > 0) \quad (3.20b)$$

provided $d_j^{(k)} \neq 0$, and the plus sign (resp.; minus sign) in (3.19) is chosen if $d_j^{(k)}$ is directed towards (resp.; away from) $R^{(k)}$, i.e., if (3.16a) (resp.; (3.16b)) applies.

Equation (3.20) gives the corresponding (positive) increment $\Delta\rho_j^{(k)}$ in ρ needed to reach the boundary along each coordinate axis x_j , $j = 1, 2, \dots, n$. To determine the first boundary crossed by the solution curve Γ , pick the index j_k such that $\Delta\rho_{j_k}^{(k)}$ is minimal; i.e.,

$$\Delta\rho_{j_k}^{(k)} = \text{Min}_{1 \leq j \leq n} \Delta\rho_j^{(k)} \quad (3.21)$$

It follows that the breakpoint $\tilde{x}^{(k+1)}$ is reached when

$$\rho = \rho^{(k)} + \Delta\rho_{j_k}^{(k)} \quad (3.22a)$$

$$\text{(resp.; } \rho = \rho^{(k)} - \Delta\rho_{j_k}^{(k)}) \quad (3.22b)$$

provided that (3.16a) (resp.; (3.16b)) holds. In this case, the first boundary hyperplane is given by

$$x_{j_k} = \beta_{j_k} i_{j_k} \quad (3.23a)$$

$$\text{(resp.; } x_{j_k} = \beta_{j_k}(i_{j_k} - 1)) \quad (3.23b)$$

if (3.17a) (resp.; (3.17b)) holds for $j = j_k$.

It follows from the above analysis that

$$\underline{x}^{(k+1)} = \underline{x}^{(k)} + \Delta\rho^{(k)} \cdot \underline{d}^{(k)} \quad (3.24)$$

where

$$\Delta\rho^{(k)} \triangleq \begin{cases} \Delta\rho_{j_k}^{(k)}, & \text{if } d_{j_{k-1}}^{(k)} \cdot d_{j_{k-1}}^{(k-1)} \cdot \Delta\rho^{(k-1)} > 0 \end{cases} \quad (3.25a)$$

$$\begin{cases} -\Delta\rho_{j_k}^{(k)}, & \text{if } d_{j_{k-1}}^{(k)} \cdot d_{j_{k-1}}^{(k-1)} \cdot \Delta\rho^{(k-1)} < 0 \end{cases} \quad (3.25b)$$

Assuming region $R^{(k)}$ is bounded by (3.18), the next region can be trivially identified: $R^{(k+1)}$ is bounded by the following boundary hyperplanes:

$$\beta_{j_k}(i_{j_k}-1) \leq x_{j_k} \leq \beta_{j_k} i_{j_k} \quad j \neq j_k \quad (3.26)$$

and

$$\beta_{j_k} i_{j_k} \leq x_{j_k} \leq \beta_{j_k}(i_{j_k}+1), \quad \text{if } d_{j_k}^{(k)} \cdot \Delta\rho^{(k)} > 0 \quad (3.27a)$$

$$\text{(resp.; } \beta_{j_k}(i_{j_k}-2) \leq x_{j_k} \leq \beta_{j_k}(i_{j_k}-1), \quad \text{if } d_{j_k}^{(k)} \cdot \Delta\rho^{(k)} < 0) \quad (3.27b)$$

We can iterate (3.24) until all breakpoints within the user-prescribed dynamic range $\rho_{\min} \leq v_{in} \leq \rho_{\max}$ had been found. If $\rho_{\max} < \infty$, then the solution curve Γ will terminate at some "bounded" point in \mathbb{R}^n provided the corresponding Jacobian matrix is nonsingular and $\rho = \rho_{\max}$ can be reached.

D. Adding Bells and Whistles

The preceding algorithm (Section 3C) should be adequate for tracing the driving-point and transfer characteristics of most garden-variety electronic circuits. It may, however, occasionally get stuck in some contrived but not degenerate circuits. We will now describe these situations so that additional checks and refinements can be built into the algorithm.

a) Choice of initial point: For simplicity, the preceding algorithm in Section 3C is initiated by finding one operating point when $\rho_{in} = \rho_{\min}$, where ρ_{\min} is the user prescribed lower limit of the input voltage. There are several situations, however, where the prescribed ρ_{\min} may not be the best choice for a starting point. One situation is when the circuit is made of passive elements with no internal power supply, such as the class of two-

transistor negative resistance circuits described in [5,6]. In this case, $v_{in} = \rho = 0$ would be a better choice because the origin in this case is guaranteed to be an operating point. For such circuits, the user should simply specify the origin as the starting point instead of wasting computer time to find another operating point due to some (often arbitrarily) chosen value $v_{in} = \rho_{min}$.

In fact, there are other occasions where a nonzero operating point (different from that at ρ_{min}) is known from some previous analysis and should be used instead.

In both cases, the algorithm in Section 3C would find only the part of the solution curve Γ for $0 \leq \rho \leq \rho_{max}$. To find the remaining portion corresponding to $\rho_{min} \leq \rho \leq 0$, we simply repeat Step I along the opposite direction of $\underline{d}^{(0)}$; i.e., choose $\Delta\rho^{(0)} < 0$ in Step I and then repeat Step II until the solution curve Γ is beyond the range $\rho_{min} \leq \rho \leq \rho_{max}$.

b) The user specified ρ_{min} may be poorly chosen such as in Fig. 15(a), where the driving-point characteristic is a closed loop located to the right of ρ_{min} , or in Fig. 15(b) where ρ_{min} gives rise to 3 operating points. In the first case, another ρ_{min} such that $\rho_2 > \rho_{min} > \rho_1$ must be chosen. In the second case, assuming the operating point P is specified, then only the portion of the driving-point characteristic below point P would be found by the algorithm in Section 3C, and the same modification described in a) above must be used to find the remaining portion.

c) The user specified ρ_{max} may be poorly chosen, such as in Figs. 15(a), 16(a), or 16(b). In all three cases, the solution curve Γ does not exist at $v_{in} = \rho_{max}$. For such situations, the complete solution curve Γ will be either a loop with a finite perimeter (e.g., Fig. 15(a)), or a multivalued curve with two unbounded end segments (e.g., Figs. 16(a) and 16(b)).

d) Even if an algorithm capable of finding all operating points such as that described in [2], is used to find the initial points corresponding to $v_{in} = \rho_{min}$, there is no guarantee that one and only one point on each separate branch of the solution curve will be found. For example, consider the hypothetical driving-point characteristic in Fig. 17 which is made of two distinct branches. Note that although the algorithm in [2] will find all three operating points corresponding to $v_{in} = \rho_{min}$ in Fig. 17, only one of these three points should be used in the algorithm in Section 3C. On the other hand, since no operating point on the second "bow-tie" shaped branch has been found, our

algorithm will fail to uncover this branch.

e) The algorithm in Section 3C fails whenever $\tilde{B}^{(k)}$ in (3.8) or (3.14) is singular. In this case, $\tilde{B}^{(k)}$ has a nullity equal to one (by Assumption 1) and the solution curve Γ is well defined as a straight-line segment in region $R^{(k)}$. The vertical segment in Fig. 14(c) is a case in point.[†] This situation is analyzed in Section 5 and appropriate modifications to the algorithm in Section 3C will be presented there.

Let us now incorporate the preceding modifications into the algorithm in Section 3C as follows:

Refined Breakpoint-Hopping Algorithm

Step 0. (Searching the starting points)

Find a set of operating points $X = \{x_a, x_b, \dots, x_m\}$ corresponding to one or more input voltages $v_{in} = \rho$. Include any user-furnished operating point X .

In general, the operating points in X are found by letting $\rho_{in} = \rho_{min} \Delta \rho^{(0)}$ and then using either [1] (if the circuit is known a priori to have a unique solution branch, or if only one branch is sought) or [2] to find the corresponding operating points.

The following steps are iterated for each operating point x_k in X , and the corresponding solution curve Γ_k passing through x_k will be found over the user-specified dynamic range $\rho_{min} \leq v_{in} \leq \rho_{max}$ in the usual case, or over some modified range $\rho_1 < \rho < \rho_2$ (where ρ_1 may be $-\infty$ and ρ_2 may be $+\infty$) where the solution curve Γ_k is defined (e.g., Figs. 15(a), 15(b), 16(a), and 16(b)). Since two or more solution curves may turn out to be identical even though they pass through distinct operating points in X (e.g., see Fig. 15(b)), the following algorithm will detect this situation by comparing their breakpoints: any two branches Γ_j and Γ_k having an identical breakpoint are identified as the same branch.

If X contains at least one point in each branch, in addition to possible extraneous points falling on the same branch, then the following algorithm will find all distinct solution curves.

[†]The algorithm for the ill-conditioned case in [2] must be modified as described in Appendix B.

(i) if $\Delta\rho^{(0)} = +\infty$ then compute $\tilde{x}^{(1)} = \tilde{x}^{(0)} + (\rho_{\max} - \rho^{(0)}) \tilde{d}^{(0)}$ and set $\rho^{(1)} = \rho_{\max}$; (ii) go to Step 11.

Remark 1: j_0 can be uniquely determined due to Assumption 4 in Section 3A, where we assume the solution curve never hits a corner point.

Remark 2: In the case when $\Delta\rho^{(0)} = +\infty$, the solution curve is a straight line over the range $[\rho_{\min}, \rho_{\max}]$.

$$(i) \text{ Compute } \rho^{(1)} = \rho^{(0)} + \Delta\rho^{(0)} \quad (3.32)$$

$$\tilde{x}^{(1)} = \tilde{x}^{(0)} + \omega \cdot \Delta\rho^{(0)} \tilde{d}^{(0)} \quad (3.33)$$

(j) Set $k = 1$.

(k) Go to Step 2.

Step 2. (Characterization of the new region)

$$i_j = \begin{cases} i_j + 1, & \text{if } j = j_{k-1} \text{ and } d_{j_{k-1}}^{(k-1)} \cdot \Delta\rho^{(k-1)} > 0 \\ i_j - 1, & \text{if } j = j_{k-1} \text{ and } d_{j_{k-1}}^{(k-1)} \cdot \Delta\rho^{(k-1)} < 0 \\ i_j, & \text{if } j \neq j_{k-1} \end{cases} \quad (3.34a)$$

$$i_j = \begin{cases} i_j + 1, & \text{if } j = j_{k-1} \text{ and } d_{j_{k-1}}^{(k-1)} \cdot \Delta\rho^{(k-1)} > 0 \\ i_j - 1, & \text{if } j = j_{k-1} \text{ and } d_{j_{k-1}}^{(k-1)} \cdot \Delta\rho^{(k-1)} < 0 \\ i_j, & \text{if } j \neq j_{k-1} \end{cases} \quad (3.34b)$$

$$i_j = \begin{cases} i_j + 1, & \text{if } j = j_{k-1} \text{ and } d_{j_{k-1}}^{(k-1)} \cdot \Delta\rho^{(k-1)} > 0 \\ i_j - 1, & \text{if } j = j_{k-1} \text{ and } d_{j_{k-1}}^{(k-1)} \cdot \Delta\rho^{(k-1)} < 0 \\ i_j, & \text{if } j \neq j_{k-1} \end{cases} \quad (3.34c)$$

Go to Step 3.

Remark: If $d_{j_{k-1}}^{(k-1)} \cdot \Delta\rho^{(k-1)} > 0$ (resp.; $d_{j_{k-1}}^{(k-1)} \cdot \Delta\rho^{(k-1)} < 0$), then the solution curve is in the direction of positive (resp.; negative) j_{k-1} -th coordinate axis.

Step 3. Compute

$$F = \begin{cases} 1 + 2e_{j_{k-1}}^T [B^{(k-1)}]^{-1} c_{j_{k-1}} (i_{j_{k-1}} - 1), & \text{if } d_{j_{k-1}}^{(k-1)} \cdot \Delta\rho^{(k-1)} > 0 \\ 1 - 2e_{j_{k-1}}^T [B^{(k-1)}]^{-1} c_{j_{k-1}} i_{j_{k-1}}, & \text{if } d_{j_{k-1}}^{(k-1)} \cdot \Delta\rho^{(k-1)} < 0 \end{cases} \quad (3.35a)$$

$$F = \begin{cases} 1 + 2e_{j_{k-1}}^T [B^{(k-1)}]^{-1} c_{j_{k-1}} (i_{j_{k-1}} - 1), & \text{if } d_{j_{k-1}}^{(k-1)} \cdot \Delta\rho^{(k-1)} > 0 \\ 1 - 2e_{j_{k-1}}^T [B^{(k-1)}]^{-1} c_{j_{k-1}} i_{j_{k-1}}, & \text{if } d_{j_{k-1}}^{(k-1)} \cdot \Delta\rho^{(k-1)} < 0 \end{cases} \quad (3.35b)$$

Go to Step 4.

Step 4. Compute

$$[B^{(k)}]^{-1} = \begin{cases} [B^{(k-1)}]^{-1} \left\{ I - \frac{2}{F} c_{j_{k-1}} (i_{j_{k-1}} - 1) e_{j_{k-1}}^T [B^{(k-1)}]^{-1} \right\}, & \text{if } d_{j_{k-1}}^{(k-1)} \cdot \Delta\rho^{(k-1)} > 0 \\ [B^{(k-1)}]^{-1} \left\{ I + \frac{2}{F} c_{j_{k-1}} i_{j_{k-1}} e_{j_{k-1}}^T [B^{(k-1)}]^{-1} \right\}, & \text{if } d_{j_{k-1}}^{(k-1)} \cdot \Delta\rho^{(k-1)} < 0 \end{cases} \quad (3.36a)$$

$$[B^{(k)}]^{-1} = \begin{cases} [B^{(k-1)}]^{-1} \left\{ I - \frac{2}{F} c_{j_{k-1}} (i_{j_{k-1}} - 1) e_{j_{k-1}}^T [B^{(k-1)}]^{-1} \right\}, & \text{if } d_{j_{k-1}}^{(k-1)} \cdot \Delta\rho^{(k-1)} > 0 \\ [B^{(k-1)}]^{-1} \left\{ I + \frac{2}{F} c_{j_{k-1}} i_{j_{k-1}} e_{j_{k-1}}^T [B^{(k-1)}]^{-1} \right\}, & \text{if } d_{j_{k-1}}^{(k-1)} \cdot \Delta\rho^{(k-1)} < 0 \end{cases} \quad (3.36b)$$

Go to Step 5.

Remark: Regions $R^{(k)}$ and $R^{(k-1)}$ are separated by a boundary hyperplane $x_{j_{k-1}} = \beta_{j_{k-1}} (i_{j_{k-1}} - 1)$ (resp.; $x_{j_{k-1}} = \beta_{j_{k-1}} i_{j_{k-1}}$) if $d_{j_{k-1}}^{(k-1)} \cdot \Delta \rho^{(k-1)} > 0$ (resp.; $d_{j_{k-1}}^{(k-1)} \cdot \Delta \rho^{(k-1)} < 0$). (Note that $i_{j_{k-1}}$ has been renewed in Step 2).

Hence,

$$\underline{\underline{B}}^{(k)} = \underline{\underline{B}}^{(k-1)} + 2c_{j_{k-1}} (i_{j_{k-1}} - 1) \cdot \underline{\underline{e}}_{j_{k-1}}^T \quad (3.37a)$$

$$\text{(resp.; } \underline{\underline{B}}^{(k)} = \underline{\underline{B}}^{(k-1)} - 2c_{j_{k-1}} i_{j_{k-1}} \cdot \underline{\underline{e}}_{j_{k-1}}^T \text{)} \quad (3.37b)$$

Steps 3 and 4 use Householder's formula

$$(\underline{\underline{H}} + \underline{\underline{G}}\underline{\underline{L}}\underline{\underline{M}})^{-1} = \underline{\underline{H}}^{-1} \{ \underline{\underline{I}} - \underline{\underline{G}}(\underline{\underline{M}}\underline{\underline{H}}^{-1}\underline{\underline{G}} + \underline{\underline{L}}^{-1})^{-1}\underline{\underline{M}}\underline{\underline{H}}^{-1} \} \quad (3.38)$$

to compute $[\underline{\underline{B}}^{(k)}]^{-1}$ via $[\underline{\underline{B}}^{(k-1)}]^{-1}$. The number of multiplication operations in this formula for finding the matrix inverse is of the order of n^2 while that for LU decomposition is of the order of n^3 . Unfortunately, there is one drawback in using this formula; namely, the round-off error may propagate and accumulate sequentially, and hence the computed inverse will exponentially deviate from the correct result especially when the matrix is ill-conditioned.

Since the computational efficiency of this formula is quite attractive especially when n is large, we choose a tradeoff between it and the LU decomposition as follows: after using the formula for several steps (depending on the matrix condition), we re-evaluate the Jacobian matrix $\underline{\underline{B}}^{(k)}$ by (3.15) and use LU decomposition to compute the inverse, and then continue to use the formula for several steps and so forth.

Step 5. Compute $\underline{\underline{d}}^{(k)} \triangleq [\underline{\underline{B}}^{(k)}]^{-1} \underline{\underline{r}}$. (3.39)

Go to Step 6.

Step 6. Let $S^{(k)} \triangleq \{j | d_j^{(k)} \neq 0, j = 1, 2, \dots, n\}$, and for $j \in S^{(k)}$, let

$$g_j = \text{sgn}\{d_j^{(k)} \cdot d_{j_{k-1}}^{(k)} \cdot d_{j_{k-1}}^{(k-1)} \cdot \Delta \rho^{(k-1)}\}. \quad (3.40)$$

Go to Step 7.

Step 7. For $j \in S^{(k)}$ compute

$$\Delta\rho_j^{(k)} = \begin{cases} (x_j^{(k)} - \beta_j(i_{j-1})) / |d_j^{(k)}|, & \text{if } g_j = -1 \\ (\beta_j i_j - x_j^{(k)}) / |d_j^{(k)}|, & \text{if } g_j = 1 \end{cases} \quad (3.41a)$$

$$(3.41b)$$

Go to Step 8.

Step 8. Let $\Delta\rho^{(k)} \triangleq \text{Min}_{j \in S^{(k)}} \{\Delta\rho_j^{(k)}\}$ and if $\Delta\rho^{(k)}$ is finite, let j_k be the unique (see Remark 1 under Step 1(g)) index in $S^{(k)}$ such that $\Delta\rho^{(k)} = \Delta\rho_{j_k}^{(k)}$.
Go to Step 9.

Step 9.

$$\Delta\rho^{(k)} = \begin{cases} \Delta\rho^{(k)}, & \text{if } d_{j_{k-1}}^{(k)} \cdot d_{j_{k-1}}^{(k-1)} \cdot \Delta\rho^{(k-1)} > 0 \\ -\Delta\rho^{(k)}, & \text{if } d_{j_{k-1}}^{(k)} \cdot d_{j_{k-1}}^{(k-1)} \cdot \Delta\rho^{(k-1)} < 0 \end{cases} \quad (3.42a)$$

$$(3.42b)$$

Go to Step 10.

Step 10. (a) If $\Delta\rho^{(k)} = -\infty$ and $\rho^{(k)} < \rho^{(0)}$ then go to Step 11.
(b) If $\Delta\rho^{(k)} = -\infty$ and $\rho^{(k)} > \rho^{(0)}$ or $\Delta\rho^{(k)} = +\infty$ and $\rho^{(k)} < \rho^{(0)}$, then
(i) set $\rho^{(k+1)} = \rho^{(0)}$ and compute $\underline{x}^{(k+1)} = \underline{x}^{(k)} + (\rho^{(0)} - \rho^{(k)}) \underline{d}^{(k)}$;
(ii) if $\underline{x}^{(k+1)} \in X$ then delete it from X ; (iii) go to Step 11.
(c) If $\Delta\rho^{(k)} = +\infty$ and $\rho^{(k)} > \rho^{(0)}$ then (i) if $\rho_{\max} > \rho^{(k)}$ then set

$$\rho^{(k+1)} = \rho_{\max} \quad (3.43a)$$

and compute

$$\underline{x}^{(k+1)} = \underline{x}^{(k)} + (\rho_{\max} - \rho^{(k)}) \underline{d}^{(k)} \quad (3.43b)$$

(ii) go to Step 11.

(d) If $\Delta\rho^{(k)}$ is finite then compute

$$\rho^{(k+1)} = \rho^{(k)} + \Delta\rho^{(k)} \quad (3.44)$$

$$\underline{x}^{(k+1)} = \underline{x}^{(k)} + \Delta\rho^{(k)} \cdot \underline{d}^{(k)} \quad (3.45)$$

If $(\rho^{(k+1)} - \rho^{(0)}) \cdot (\rho^{(k)} - \rho^{(0)}) < 0$ or $\rho^{(k+1)} = \rho^{(0)}$ then (i) compute $\underline{x}_0 = \underline{x}^{(k)} + (\rho^{(0)} - \rho^{(k)}) \underline{d}^{(k)}$ and if $\underline{x}_0 \in X$ then delete it from X ; (ii) if $\underline{x}_0 = \underline{x}^{(0)}$ then go to Step 1(a).

- (e) Set $k = k + 1$.
- (f) Go to Step 2.

Remark 1: Steps 10(b)(ii) and (d)(i) are to delete those operating points of X which can be reached by the same branch of solution curve.

Remark 2: In the case of Step 10(d)(ii) when $\underline{x}_0 = \underline{x}^{(0)}$, the solution curve Γ becomes cyclic since Γ returns to the initial point $\underline{x}^{(0)}$ and it will be shown in Section 5 that there is at most one branch of solution curve to pass any point \underline{x} in the domain space under Assumption (5.55).

- Step 11. (a) If $\omega = -1$ then go to Step 1(a).
 (b) If $\omega = 1$ then set $\omega = -1$ and go to Step 1(c).

Remark: In Step 1, for $\omega = 1$, if we don't destroy the information on $[\underline{B}^{(0)}]^{-1}$, $\underline{d}^{(0)}$, and the characterization on $R^{(0)}$ during the breakpoint-hopping procedures, then when re-entering Step 1 in Step 11(b), we can go to Step 1(f) directly and skip the redundant calculations in Steps 1(c), (d), and (e).

E. Illustrative Examples

We close this section with two simple examples chosen so that their driving-point characteristics can be readily obtained by standard graphical methods [15] for checking purposes. Several nontrivial validating examples are given in Section 4 not only to demonstrate the generality of our algorithm, but also for validating future algorithms.

Example 3.1 (Fig. 18)

Consider the circuit shown in Fig. 18(a), where nonlinear resistors R_1 and R_2 are described by the piecewise-linear characteristics shown in Figs. 18(b) and (c). Using the graphical method in [15], the driving-point characteristic for this circuit is easily obtained as shown in Fig. 18(d).

To derive this driving-point characteristic using the breakpoint-hopping algorithm, we choose $\underline{x} = [v_1, i_2, i_{in}]^T$ and $\underline{y} = [i_1, v_2, v_{in}]^T$ and write the following associated canonical piecewise-linear equation (detailed calculation is given in Appendix D-1):

$$\begin{bmatrix} -1 & -9/4 & 0 \\ 17/8 & -1 & 0 \\ 0 & 1 & -1 \end{bmatrix} \begin{bmatrix} x_1 \\ x_2 \\ x_3 \end{bmatrix} + \begin{bmatrix} 0 \\ 7/8 \\ 0 \end{bmatrix} |x_1| + \begin{bmatrix} -7/4 \\ 0 \\ 0 \end{bmatrix} |x_2 - 1| = \begin{bmatrix} -9/4 \\ 0 \\ 0 \end{bmatrix} + \rho \begin{bmatrix} -1 \\ 0 \\ 0 \end{bmatrix} \quad (3.46)$$

Suppose it is desired to trace the driving-point characteristic over the dynamic range $-7 \leq v_{in} \leq 7$. Hence, $\rho_{\min} = -7$ and $\rho_{\max} = 7$.

Step 1. Starting from $v_{in} = -7 \triangleq \rho^{(0)}$, we find by inspection of Fig. 18(d) that $i_{in} = -5$ and hence, $i_2 = -5$, $v_2 = -3$, $v_1 = -4$ and $i_1 = -1$. It follows from Figs. 18(b), (c) and (3.28) that the circuit is initially operating in segment (1,1). Hence, region $R^{(0)}$ is identified by $-\infty \leq v_1 \leq 0$ and $-\infty \leq i_2 \leq 1$. Substituting the parameters in this region into (3.29) and (3.30), we obtain:

$$\underline{B}^{(0)} = \begin{bmatrix} -1 & -1/2 & 0 \\ 5/4 & -1 & 0 \\ 0 & 1 & -1 \end{bmatrix}, \quad \text{and} \quad \underline{d}^{(0)} \triangleq [\underline{B}^{(0)}]^{-1} \underline{r} = \begin{bmatrix} 8/13 \\ 10/13 \\ 10/13 \end{bmatrix} \quad (3.47)$$

Since we are only interested in the range $(-7,7)$, $\omega = 1$ is used throughout the B-H algorithm in Section 3D. It follows from (3.31b) that

$$\Delta\rho_1^{(0)} = \frac{0 - (-4)}{8/13} = 13/2 \quad \text{and} \quad \Delta\rho_2^{(0)} = \frac{1 - (-5)}{10/13} = 39/5 \quad (3.48)$$

Since $\Delta\rho_1^{(0)} < \Delta\rho_2^{(0)}$, we identify $j_0 = 1$ and hence $\Delta\rho^{(0)} = \Delta\rho_1^{(0)} = 13/2$. Using (3.32) and (3.33), we calculate the next breakpoint:

$$\rho^{(1)} = -7 + 13/2 = -1/2, \quad \text{and} \quad \underline{x}^{(1)} = \begin{bmatrix} -4 \\ -5 \\ -5 \end{bmatrix} + 13/2 \begin{bmatrix} 8/13 \\ 10/13 \\ 10/13 \end{bmatrix} = \begin{bmatrix} 0 \\ 0 \\ 0 \end{bmatrix} \quad (3.49)$$

It follows from (3.48) that R_1 first arrives at its breakpoint $(0,0)$ when v_{in} increases from $\rho^{(0)} = -7$ to $\rho^{(1)} = -1/2$.

Step 2. The next region $R^{(1)}$ clearly corresponds to segment (2,1) and is characterized by $0 \leq v_1 \leq \infty$ and $-\infty \leq i_2 \leq 1$.

Steps 3,4,5. Using (3.35), (3.36), and (3.39), we obtain

$$\underline{d}^{(1)} = [2/5 \quad 6/5 \quad 6/5]^T \quad (3.50)$$

Steps 6,7. Since $d_1^{(1)} \cdot d_1^{(0)} \cdot \Delta\rho^{(0)} = 2/5 \cdot 8/13 \cdot 13/2 > 0$, the direction vector $\underline{d}^{(1)}$ points in the correct direction and it follows from (3.41b) that

$$\Delta\rho_1^{(1)} = \frac{\infty - 0}{2/5} = \infty, \quad \text{and} \quad \frac{1 - 0}{6/5} = 5/6 \quad (3.51)$$

Steps 8,9. Since $\Delta\rho_2^{(1)} < \Delta\rho_1^{(1)}$, we identify $j_1 = 2$ and hence $\Delta\rho^{(1)} = 5/6$.

Step 10. Using (3.44) and (3.45), we calculate the next breakpoint:

$$\rho^{(2)} = -1/2 + 5/6 = 1/3, \text{ and } \tilde{x}^{(2)} = \begin{bmatrix} 0 \\ 0 \\ 0 \end{bmatrix} + 5/6 \begin{bmatrix} 2/5 \\ 6/5 \\ 6/5 \end{bmatrix} = \begin{bmatrix} 1/3 \\ 1 \\ 1 \end{bmatrix} \quad (3.52)$$

It follows from (3.51) and (3.52) that R_2 first arrives at the next breakpoint $\tilde{x}^{(2)}$ when v_{in} increases from $\rho = -1/2$ to $\rho = 1/3$. We then return to Step 2 to find the next breakpoint.

Step 2. The next region $R^{(2)}$ clearly corresponds to segment (2,2) and is characterized by $0 \leq v_1 \leq \infty$ and $1 \leq i_2 \leq \infty$.

Steps 3,4,5. Using (3.35), (3.36), and (3.39) we obtain

$$\tilde{d}^{(2)} = [1/13 \quad 3/13 \quad 3/13]^T \quad (3.53)$$

Steps 6,7. Since $d_2^{(2)} \cdot d_2^{(1)} \cdot \Delta\rho^{(1)} = 3/13 \cdot 6/5 \cdot 5/6 > 0$, the direction vector $\tilde{d}^{(2)}$ points in the correct direction and it follows from (3.41b) that

$$\Delta\rho_1^{(2)} = \frac{\infty - 1/3}{1/13} = \infty, \text{ and } \Delta\rho_2^{(2)} = \frac{\infty - 1}{3/13} = \infty \quad (3.54)$$

Steps 8,9. $\Delta\rho^{(2)} = \infty$. (3.55)

Step 10(c). Equation (3.55) implies that region $R^{(2)}$ is an "unbounded" region having no other breakpoints as v_{in} increases from $\rho = 1/3$ to ∞ . Hence we simply choose the specified upper limit $\rho_{\max} = 7$ in (3.43) to obtain the end point (not a breakpoint) with $\Delta\rho^{(2)} = 7 - 1/3 = 20/3$:

$$\tilde{x}^{(3)} = \begin{bmatrix} 1/3 \\ 1 \\ 1 \end{bmatrix} + 20/3 \begin{bmatrix} 1/13 \\ 3/13 \\ 3/13 \end{bmatrix} = \begin{bmatrix} 11/13 \\ 33/13 \\ 33/13 \end{bmatrix} \quad (3.56)$$

To obtain the driving-point characteristic, we note from Fig. 18(a) that

$$y_0 = i_{in} = i_2 \quad (3.57)$$

Hence the breakpoints in the $i_{in} - v_{in}$ plane corresponding to $\tilde{x}^{(1)}$, $\tilde{x}^{(2)}$, and $\tilde{x}^{(3)}$ are trivially obtained from the third row of (3.49), (3.52), and (3.56), namely, $(-1/2, 0)$, $(1/3, 1)$, and $(7, 33/13)$. The initial point is of course just $(-7, -5)$. Connecting these points

by straight-line segments starting from (-7,-5) in the order indicated, we obtain the same driving-point characteristic in Fig. 18(d), as it should.

Example 3.2 (Fig. 19)

Consider next the circuit shown in Fig. 19(a), where the nonlinear resistor R_1 is described by the piecewise-linear characteristic shown in Fig. 19(b). Using the graphical method in [15], the driving-point characteristic for this circuit is easily obtained as shown in Fig. 19(c). Note that it is a multi-valued function of v_{in} .

To derive this driving-point characteristic using the breakpoint-hopping algorithm, we choose $\underline{x} = [v_1, i_{in}]^T$ and $\underline{y} = [i_1, v_{in}]^T$ and write the following associated canonical piecewise-linear equation (detailed calculation is given in Appendix D-2):

$$\begin{bmatrix} -1 & -2 \\ 1 & -1 \end{bmatrix} \begin{bmatrix} x_1 \\ x_2 \end{bmatrix} + \begin{bmatrix} 0 \\ -5/4 \end{bmatrix} |x_1 - 2| + \begin{bmatrix} 0 \\ 3/4 \end{bmatrix} |x_1 - 4| = \begin{bmatrix} 0 \\ -1/2 \end{bmatrix} + \rho \begin{bmatrix} -1 \\ 0 \end{bmatrix} \quad (3.58)$$

Suppose it is desired to trace the complete driving-point characteristic over the whole dynamic range $-\infty \leq v_{in} \leq \infty$. We start from $v_{in} = 9 \triangleq \rho^{(0)}$ where, by inspection of Fig. 19(c), there are three distinct solutions $\underline{x}_a = [3 \ 3]^T$, $\underline{x}_b = [7/4 \ 29/8]^T$, and $\underline{x}_c = [9/2 \ 9/4]^T$. Hence,

$$X = \{[3 \ 3]^T, [7/4 \ 29/8]^T, [9/2 \ 9/4]^T\} \quad (3.59)$$

Step 1. (b) We pick \underline{x}_a from X and denote it as $\underline{x}^{(0)}$, i.e., $\underline{x}^{(0)} \triangleq [3 \ 3]^T$.

We then delete it from X and

$$X = \{[7/4 \ 29/8]^T, [9/2 \ 9/4]^T\}. \text{ Choose } \omega = 1.$$

(c) $\underline{x}^{(0)}$ is located in segment 2 of the nonlinear resistor R_1 which is characterized by $\beta_1(i_1 - 1) = 2 < v_1 < 4 = \beta_1 i_1$. Hence, $i_1 = 2$.

(d) By (3.29)

$$\underline{B}^{(0)} = \begin{bmatrix} -1 & -2 \\ -1 & -1 \end{bmatrix} \quad (3.60)$$

(e) By (3.30)

$$\underline{d}^{(0)} = [\underline{B}^{(0)}]^{-1} \underline{r} = [-1 \ 1]^T \quad (3.61)$$

(f) $S^{(0)} = \{1\}$. Since $d_1^{(0)} \cdot \omega = -1 \cdot 1 = -1 < 0$, by (3.31a)

$$\Delta \rho_1^{(0)} = (3-2)/|-1| = 1. \quad (3.62)$$

(g) $\Delta \rho^{(0)} = \omega \cdot \Delta \rho_1^{(0)} = 1$, and $j_0 = 1$. (3.63)

(i) By (3.32) and (3.33),

$$\rho^{(1)} = 9 + 1 = 10, \text{ and } \tilde{x}^{(1)} = \begin{bmatrix} 3 \\ 3 \end{bmatrix} + 1 \cdot 1 \cdot \begin{bmatrix} -1 \\ 1 \end{bmatrix} = \begin{bmatrix} 2 \\ 4 \end{bmatrix} \quad (3.64)$$

Step 2. Since $d_1^{(0)} \cdot \Delta \rho^{(0)} = -1 \cdot 1 = -1 < 0$, by (3.34b) $i_1 = 2 - 1 = 1$ and the next region $R^{(1)}$ is located in segment 1 of R_1 which is characterized by $-\infty \leq v_1 \leq 2$.

Steps 3,4,5. Using (3.35), (3.36), and (3.39), we obtain

$$\tilde{d}^{(1)} = [1/4 \quad 3/8]^T \quad (3.65)$$

Step 6. $S^{(1)} = \{1\}$ and by (3.40)

$$g_1 = \text{sgn}\{1/4 \cdot 1/4 \cdot -1 \cdot 1\} = -1 \quad (3.66)$$

Step 7. By (3.41a) and (3.64)

$$\Delta \rho_1^{(1)} = [2 - (-\infty)]/|-1| = \infty \quad (3.67)$$

Steps 8,9. Since $d_1^{(1)} \cdot d_1^{(0)} \cdot \Delta \rho^{(0)} = 1/4 \cdot -1 \cdot 1 = -1/4 < 0$, by (3.42b) $\Delta \rho^{(1)} = -\infty$.

Step 10(b). Since $\Delta \rho^{(1)} = -\infty$ and $\rho^{(1)} = 10 > 9 = \rho^{(0)}$

$$(i) \rho^{(2)} = \rho^{(0)} = 9, \text{ and } \tilde{x}^{(2)} = \begin{bmatrix} 2 \\ 4 \end{bmatrix} + (9-10) \begin{bmatrix} 1/4 \\ 3/8 \end{bmatrix} = \begin{bmatrix} 7/4 \\ 29/8 \end{bmatrix}; \quad (3.68)$$

(ii) Since $\tilde{x}^{(2)} \in X$, we delete it from X and $X = \left\{ \begin{bmatrix} 9/2 \\ 9/4 \end{bmatrix} \right\}$.

Step 11. Set $\omega = -1$ and go to Step 1(f).

Step 1. (f) Since $d_1^{(0)} \cdot \omega = -1 \cdot -1 = 1 > 0$, by (3.31b)

$$\Delta \rho_1^{(0)} = (4-3)/|-1| = 1 \quad (3.69)$$

(g) $\Delta \rho^{(0)} = \omega \cdot \Delta \rho_1^{(0)} = -1 \cdot 1 = -1$, and $j_0 = 1$ (3.70)

(i) By (3.32) and (3.33),

$$\rho^{(1)} = 9 - 1 = 8, \text{ and } \tilde{x}^{(1)} = \begin{bmatrix} 3 \\ 3 \end{bmatrix} + (-1) \cdot 1 \cdot \begin{bmatrix} -1 \\ 1 \end{bmatrix} = \begin{bmatrix} 4 \\ 2 \end{bmatrix} \quad (3.71)$$

Step 2. Since $d_1^{(0)} \cdot \Delta\rho^{(0)} = -1 \cdot -1 = 1 > 0$, by (3.34a) $i_1 = 2 + 1 = 3$, and the next region $R^{(1)}$ is located in segment 3 of R_1 which is characterized by $4 \leq v_1 \leq \infty$.

Steps 3,4,5. Using (3.35), (3.36), and (3.39), we obtain

$$\tilde{d}^{(1)} = [1/2 \quad 1/4]^T \quad (3.72)$$

Step 6. $S^{(1)} = \{1\}$ and by (3.40)

$$g_1 = \text{sgn}\{1/2 \cdot 1/2 \cdot -1 \cdot -1\} = 1 > 0 \quad (3.73)$$

Step 7. By (3.41b) and (3.71)

$$\Delta\rho_1^{(1)} = (\infty - 4) / |1/2| = \infty \quad (3.74)$$

Steps 8,9. Since $d_1^{(1)} \cdot d_1^{(0)} \cdot \Delta\rho^{(0)} = 1/2 \cdot -1 \cdot -1 = 1 > 0$, by (3.42a) $\Delta\rho^{(1)} = \infty$.

Step 10(b). Since $\Delta\rho^{(1)} = \infty$ and $\rho^{(1)} = 8 < 9 = \rho^{(0)}$,

$$(i) \rho^{(2)} = \rho^{(0)} = 9, \text{ and } \tilde{x}^{(2)} = \begin{bmatrix} 4 \\ 2 \end{bmatrix} + (9-8) \begin{bmatrix} 1/2 \\ 1/4 \end{bmatrix} = \begin{bmatrix} 9/2 \\ 9/4 \end{bmatrix} \quad (3.75)$$

(ii) Since $\tilde{x}^{(2)} \in X$, we delete it from X and $X = \phi$.

Step 11. Since $\omega = -1$, go to Step 1(a).

Step 1(a). Since $X = \phi$, we stop the B-H algorithm.

To obtain the driving-point characteristic, we choose the breakpoints in (3.64), (3.68), (3.71), and (3.75), and start from the initial point $\tilde{x}^{(0)} = [3 \quad 3]^T$. Connecting these points by straight-line segments in the order indicated, we obtain the same driving-point characteristic in Fig. 19(c), as it should.

4. VALIDATING EXAMPLES

In this section we apply the B-H algorithm from Section 3D to derive the driving-point and/or transfer characteristic of the four piecewise-linear circuits studied earlier in Examples 2.1 (Fig. 5(a)), 2.2 (Fig. 6(a)), 2.3 (Fig. 7(a)), and 2.4 or 2.5 (Fig. 8(a)). Since these circuits are not of a series-parallel type, and some contain controlled sources, the graphical method in

[15] is no longer applicable. In spite of the simplicity of these circuits, their associated driving point and transfer characteristics are quite complicated. In particular, the characteristics of the circuits in Figs. 5(a), 6(a), 7(a), and 8(a) are multivalued function of v_{in} and can not be obtained by any existing computer simulation program (brute force approach), such as SPICE [17]. Consequently, these examples can be considered as "benchmark" circuits where future competing algorithms may be validated and their computational efficiency compared.

Since each circuit contains only two resistors, their solution curves Γ are piecewise-linear curves in the $x_1 - x_2$ plane and can be easily drawn. Consequently, in each of the following examples, we will sketch both the solution curve Γ and their associated driving-point and/or transfer characteristics in order to emphasize their relationships.

Example 4.1 (Fig. 5(a))

Let us derive the driving-point characteristic of the circuit in Fig. 5(a) whose canonical piecewise-linear equations have been derived in (2.17); namely,

$$\begin{bmatrix} -1 & -9/4 & 0 \\ 9/8 & 9/4 & -1 \\ 0 & -1 & 1 \end{bmatrix} \begin{bmatrix} x_1 \\ x_2 \\ x_3 \end{bmatrix} + \begin{bmatrix} 0 \\ 7/8 \\ 0 \end{bmatrix} |x_1 - 0| + \begin{bmatrix} -7/4 \\ 7/4 \\ 0 \end{bmatrix} |x_2 - 1| = \begin{bmatrix} -9/4 \\ 9/4 \\ 0 \end{bmatrix} + \rho \begin{bmatrix} -1 \\ 0 \\ 0 \end{bmatrix} \quad (4.1)$$

where $x_1 \triangleq v_1$, $x_2 \triangleq i_2$, and $x_3 \triangleq i_{in}$. Starting from the initial point $\tilde{x}^{(0)} = [-2 \ -2 \ -2]^T$ corresponding to $v_{in} = \rho^{(0)} = -7/2$, we apply the B-H algorithm to derive the solution curve Γ shown in Fig. 20(a). The detailed calculation is given in Appendix E-1. The three breakpoints of Γ are found to be located at:

$$\tilde{x}^{(1)} = [0 \ -1 \ -1]^T, \tilde{x}^{(2)} = [1/2 \ 1 \ 1]^T, \text{ and } \tilde{x}^{(3)} = [0 \ 4/3 \ 4/3]^T \quad (4.2a)$$

with

$$\rho^{(1)} = -1, \rho^{(2)} = 1/2, \text{ and } \rho^{(3)} = 4/3 \quad (4.2b)$$

The end segment of Γ is identified by a point $\tilde{x}^{(4)} = [-6 \ 11/6 \ 11/6]^T$ corresponding to $v_{in} = \rho^{(4)} = -8/3$.

To obtain the driving-point characteristic, we simply project the solution curve Γ along the $x_3 \triangleq i_{in}$ coordinate axis (parametrized by v_{in}). The result

is shown in Fig. 20(b). Observe that it is a multivalued function of v_{in} and is undefined for $v_{in} > 4/3$. It is also clear from Fig. 20(b) that whereas the direction vectors, $\underline{d}^{(0)}$, $\underline{d}^{(1)}$, and $\underline{d}^{(2)}$ are pointed in the correction direction, $\underline{d}^{(3)}$ is oppositely directed. \square

Example 4.2 (Fig. 6(a))

Consider the simple circuit shown in Fig. 6(a) whose canonical piecewise-linear equation has been derived earlier in (2.22); namely,

$$\begin{bmatrix} 7/4 & 0 & -1 \\ 0 & 4 & -1 \\ -1 & -1 & -3.2 \end{bmatrix} \begin{bmatrix} x_1 \\ x_2 \\ x_3 \end{bmatrix} + \begin{bmatrix} -25/18 \\ 0 \\ 0 \end{bmatrix} |x_1 - 1.2| + \begin{bmatrix} 41/36 \\ 0 \\ 0 \end{bmatrix} |x_1 - 3| + \begin{bmatrix} 0 \\ -7/2 \\ 0 \end{bmatrix} |x_2 - 0.8| \\ + \begin{bmatrix} 0 \\ 5/2 \\ 0 \end{bmatrix} |x_2 - 2| = \begin{bmatrix} 7/4 \\ 2.2 \\ 0 \end{bmatrix} + \rho \begin{bmatrix} 0 \\ 0 \\ -1 \end{bmatrix} \quad (4.3)$$

where $x_1 \triangleq v_1$, $x_2 \triangleq v_2$ and $x_3 \triangleq i_{in}$. Our objective here is to find the driving-point characteristic, as well as the two transfer characteristics $v_1 - v_s - v_{in}$ and $v_2 - v_s - v_{in}$.

As usual, the basic problem is to derive the solution curve Γ in the x_1 - x_2 plane via the B-H algorithm. Since the circuit in Fig. 6(a) is made of only passive resistors and contains no internal power supply, it is clear that the solution curve must pass through the origin $\underline{x}^{(0)} = \underline{0}$, as shown by Γ_1 in Fig. 21. It turns out that for this circuit a second solution curve through another initial point $\hat{\underline{x}}^{(0)} = [9/8 \ 67/40 \ 9/4]^T$ at $v_{in} = 10$ exists concurrently, as shown by Γ_2 in Fig. 21. The detailed calculation is given in Appendix E-2.

The breakpoints $\underline{x}^{(1)}$, $\underline{x}^{(2)}$, $\underline{x}^{(3)}$ and $\underline{x}^{(4)}$ plus one point in each end segment of Γ_1 are located as follow:

$$\underline{x}^{(0)} = \begin{bmatrix} 0 \\ 0 \\ 0 \end{bmatrix}, \underline{x}^{(1)} = \begin{bmatrix} 1.2 \\ 0.48 \\ 2.4 \end{bmatrix}, \underline{x}^{(2)} = \begin{bmatrix} 3 \\ 0.2 \\ 1 \end{bmatrix}, \underline{x}^{(3)} = \begin{bmatrix} 5 \\ 0.8 \\ 4 \end{bmatrix}, \\ \underline{x}^{(4)} = \begin{bmatrix} 3.4 \\ 2 \\ 1.6 \end{bmatrix}, \underline{x}^{(5)} = \begin{bmatrix} 4.9 \\ 2.75 \\ 3.86 \end{bmatrix} \quad (4.4a)$$

with

$$\rho^{(0)} = 0, \rho^{(1)} = 234/25, \rho^{(2)} = 6.4, \rho^{(3)} = 18.6, \rho^{(4)} = 10.52, \text{ and } \rho^{(5)} = 20 \quad (4.4b)$$

The second solution curve Γ_2 is cyclic with the following breakpoints:
(identified by a hat "^" to distinguish them from those of Γ_1)

$$\hat{x}^{(0)} = \begin{bmatrix} 9/8 \\ 67/40 \\ 9/4 \end{bmatrix}, \hat{x}^{(1)} = \begin{bmatrix} 1.2 \\ 1.6 \\ 2.4 \end{bmatrix}, \hat{x}^{(2)} = \begin{bmatrix} 78/35 \\ 2 \\ 1.6 \end{bmatrix}, \hat{x}^{(3)} = \begin{bmatrix} 1.2 \\ 34/15 \\ 2.4 \end{bmatrix}, \text{ and } \hat{x}^{(4)} = \begin{bmatrix} 0.8 \\ 2 \\ 1.6 \end{bmatrix} \quad (4.5a)$$

with

$$\hat{\rho}^{(0)} = 10, \hat{\rho}^{(1)} = 10.48, \hat{\rho}^{(2)} = 9.35, \hat{\rho}^{(3)} = 11.15, \text{ and } \hat{\rho}^{(4)} = 7.92 \quad (4.5b)$$

To derive the driving-point and transfer characteristics, we note from Fig. 6(a) that

$$i_{in} = x_3, v_1 = x_1, \text{ and } v_2 = x_2 \quad (4.6)$$

Consequently, these characteristics are trivially obtained from the respective components of \hat{x} at each breakpoint of Γ_1 and Γ_2 . The results are shown in Figs. 22(a), (b), and (c) respectively. Observe that the breakpoints of these three characteristics with the same $v_{in} = \rho^{(k)}$ corresponds to the breakpoint in the solution curve Γ_1 or Γ_2 with $\rho = \rho^{(k)}$. \square

Example 4.3 (Fig. 8(a))

For our final example, consider the one-transistor circuit in Fig. 8(a) whose canonical piecewise-linear equation has been derived earlier in (2.35); namely,

$$\begin{bmatrix} -5.59 & 74.8 & 0 \\ -42.7 & 1120 & 0 \\ 50.4 & -49.2 & -8000 \end{bmatrix} \begin{bmatrix} x_1 \\ x_2 \\ x_3 \end{bmatrix} + \begin{bmatrix} -0.25 \\ -2.68 \\ 2.11 \end{bmatrix} |x_1 - 0.4| + \begin{bmatrix} -5.59 \\ -60 \\ 47.3 \end{bmatrix} |x_1 - 0.6| \\ + \begin{bmatrix} 3.16 \\ 47.9 \\ -2.10 \end{bmatrix} |x_2 - 0.4| + \begin{bmatrix} 70.6 \\ 1071 \\ -47.1 \end{bmatrix} |x_2 - 0.6| = \begin{bmatrix} 40.2 \\ 625 \\ 0.146 \end{bmatrix} + \rho \begin{bmatrix} -1 \\ 0 \\ 0 \end{bmatrix} \quad (4.7)$$

where $x_1 \triangleq v_1$, $x_2 \triangleq v_2$, and $x_3 \triangleq i_{in}$. Our objective is to derive the driving-point characteristic.

Since this circuit is made of only passive elements and contains no internal power supply, $\underline{x} = \underline{0}$ is an operating point corresponding to $v_{in} = \rho = 0$. Applying the B-H algorithm with $\underline{x}^{(0)} = \underline{0}$ as the initial point, we obtain the solution curve Γ shown in Fig. 23(a). The detailed calculation is given in Appendix E-3. The breakpoints $\underline{x}^{(1)}$, $\underline{x}^{(2)}$, $\underline{x}^{(3)}$, and $\underline{x}^{(4)}$ and two points in each end segment of Γ are located as follows:

$$\underline{x}^{(0)} = \begin{bmatrix} 0 \\ 0 \\ 0 \end{bmatrix}, \quad \underline{x}^{(1)} = \begin{bmatrix} 0.4 \\ -8.03 \\ 5.02 \times 10^{-5} \end{bmatrix}, \quad \underline{x}^{(2)} = \begin{bmatrix} 0.6 \\ -10.9 \\ 1.81 \times 10^{-4} \end{bmatrix},$$

$$\underline{x}^{(3)} = \begin{bmatrix} 0.708 \\ 0.4 \\ 1.53 \times 10^{-3} \end{bmatrix}, \quad \underline{x}^{(4)} = \begin{bmatrix} 0.891 \\ 0.6 \\ 3.71 \times 10^{-3} \end{bmatrix}, \quad \underline{x}^{(5)} = \begin{bmatrix} 1.02 \\ 0.606 \\ 5.29 \times 10^{-3} \end{bmatrix} \quad (4.8a)$$

with

$$\rho^{(0)} = 0, \quad \rho^{(1)} = 7.93, \quad \rho^{(2)} = 10.9, \quad \rho^{(3)} = 0.78, \quad \rho^{(4)} = 1.41, \quad \text{and} \quad \rho^{(5)} = 2 \quad (4.8b)$$

The driving-point characteristic is obtained from the third coordinate, $x_3 = i_{in}$, of \underline{x} (parametrized by v_{in}) and is shown in Fig. 23(b). \square

5. ANALYSIS OF DEGENERATE CASES

A review of Section 3C would reveal that the breakpoint-hopping algorithm would get stuck under the following two degenerate situations:

1. The solution curve hits a corner point.
2. The Jacobian matrix $\underline{B}^{(k)}$ in region $R^{(k)}$ is singular for some region $R^{(k)}$ traversed by the solution curve Γ .

For canonical piecewise-linear equations with lattice structure, a corner is reached at $\rho = \rho^*$ where two or more nonlinear resistors arrive at their respective breakpoints simultaneously for the same input voltage $v_{in} = \rho^*$. The occurrence of a corner point in piecewise-linear analysis always costs more computational effort in tracing the solution curve since there is more than one possibility in determining the next region for the solution curve upon hitting a corner point. Moreover, the solution curve may split into several distinct branches as shown in the following example.

Example 5.1 (Fig. 24)

Consider the circuit shown in Fig. 24(a), where the nonlinear resistors

R_1 and R_2 are described by the piecewise-linear characteristics shown in Figs. 24(b) and (c) respectively. To trace the solution curve by using the B-H algorithm, we choose $\underline{x} = [v_1, v_2, i_{in}]^T$ and $\underline{y} = [i_1, i_2, v_{in}]^T$, and write the following associated canonical piecewise-linear equation (detailed calculation is given in Appendix D-3):

$$\begin{bmatrix} 0 & 0 & 0 \\ -1 & -1 & 0 \\ 0 & 0 & -1 \end{bmatrix} \begin{bmatrix} x_1 \\ x_2 \\ x_3 \end{bmatrix} + \begin{bmatrix} 1 \\ -1 \\ 0 \end{bmatrix} |x_1| + \begin{bmatrix} -1 \\ 0 \\ 0 \end{bmatrix} |x_2| = \begin{bmatrix} 0 \\ 2 \\ 0 \end{bmatrix} + \rho \begin{bmatrix} 0 \\ -1 \\ -1 \end{bmatrix} \quad (5.1)$$

We start from the initial point $\underline{x}^{(0)} = [-2 \ -2 \ 0]^T$ which corresponds to $\rho^{(0)} = 0$ and is located in segments (1,1) of the nonlinear resistors R_1 and R_2 . Hence, region $R^{(0)}$ is characterized by $-\infty \leq x_1 \leq 0$ and $-\infty \leq x_2 \leq 0$, and by (3.29) and (3.30),

$$\underline{B}^{(0)} = \begin{bmatrix} -1 & 1 & 0 \\ 0 & -1 & 0 \\ 0 & 0 & -1 \end{bmatrix}, \text{ and } \underline{d}^{(0)} = [\underline{B}^{(0)}]^{-1} \underline{r} = \begin{bmatrix} 1 \\ 1 \\ 1 \end{bmatrix} \quad (5.2)$$

It follows from (3.31b) that

$$\Delta\rho_1^{(0)} = (0 - (-2))/|1| = 2, \text{ and } \Delta\rho_2^{(0)} = (0 - (-2))/|1| = 2 \quad (5.3)$$

Hence, the solution curve Γ hits the boundary hyperplanes $x_1 = 0$ and $x_2 = 0$ simultaneously at the corner point

$$\underline{x}^{(1)} = [0 \ 0 \ 0]^T \quad \text{with} \quad \rho^{(0)} = 2 \quad (5.4)$$

It is shown in Fig. 24(e) that the corner point $\underline{x}^{(1)}$ belongs to regions $R^{(a)}$, $R^{(b)}$, and $R^{(c)}$ (corresponding to segments (1,2), (2,1) and (2,2) of the nonlinear resistors R_1 and R_2 respectively) in addition to region $R^{(0)}$ where the solution curve starts, and all these regions are possible candidates for the solution curve to enter. By (3.14a) and (3.15), the Jacobian matrix and the direction vector in each region can be found to be:

$$\underline{B}^{(a)} = \begin{bmatrix} -1 & -1 & 0 \\ 0 & -1 & 0 \\ 0 & 0 & -1 \end{bmatrix}, \underline{B}^{(b)} = \begin{bmatrix} 1 & 1 & 0 \\ -2 & -1 & 0 \\ 0 & 0 & -1 \end{bmatrix}, \text{ and } \underline{B}^{(c)} = \begin{bmatrix} 1 & -1 & 0 \\ -2 & -1 & 0 \\ 0 & 0 & -1 \end{bmatrix} \quad (5.5a)$$

$$\underline{d}^{(a)} = [-1 \ 1 \ 1]^T, \underline{d}^{(b)} = [1 \ -1 \ 1]^T, \text{ and } \underline{d}^{(c)} = [1/3 \ 1/3 \ 1]^T \quad (5.5b)$$

Since $\underline{d}^{(a)}$, $\underline{d}^{(b)}$, and $\underline{d}^{(c)}$ are in the direction of entering $R^{(a)}$, $R^{(b)}$, and $R^{(c)}$ respectively, each direction vector will define a trajectory for the solution curve and the solution curve starting from $\underline{x}^{(0)}$ will split into three different branches upon hitting the corner point $\underline{x}^{(1)} = [0 \ 0 \ 0]^T$ as shown in Fig. 24(e). \square

Since a corner can exist only for precise element parameter values, it is a pathological situation which occurs whenever $\Delta\rho_{j_1}^{(k)} = \Delta\rho_{j_2}^{(k)}$ for some $j_1 \neq j_2$. When this situation is detected, we simply remodel the circuit by perturbing one or more element parameters and repeat the analysis.

We next consider the second degenerate case when the solution curve traverses some region with a singular Jacobian matrix. In this case, the nullity of $\underline{B}^{(k)}$ is at least equal to one. We will focus our attention first in the case when the nullity is equal to one because in this case the solution in $R^{(k)}$ is a well-defined one-dimensional curve. When the nullity exceeds unity, we will see in Section 5B that the solution curve Γ in region $R^{(k)}$ is made up of points having nontrivial areas. When this happens, we must again remodel our circuit by perturbing some circuit elements until the nullity is at most equal to one.

A. One-Dimensional Degenerate Case: nullity of $\underline{B}^{(k)} = 1$

Suppose the solution curve Γ enters a region $R^{(k)}$ where the corresponding Jacobian matrix $\underline{B}^{(k)}$ has nullity equal to one. Let the circuit be characterized by the linear equation

$$\underline{B}^{(k)} \underline{x} = \underline{a}^{(k)} + \rho \cdot \underline{r} \quad (5.6)$$

within region $R^{(k)}$ where (5.6) is obtained by substituting all parameters in the canonical piecewise-linear equation of (2.12) corresponding to region $R^{(k)}$.

Since the breakpoint $\underline{x}^{(k)} \in R^{(k)}$ is a solution at $\rho = \rho^{(k)}$ where the solution curve Γ begins to enter region $R^{(k)}$. Hence,

$$\underline{B}^{(k)} \underline{x}^{(k)} = \underline{a}^{(k)} + \rho^{(k)} \cdot \underline{r} \quad (5.7)$$

Let $\underline{d}^{(k)}$ be a vector in the one-dimensional null space of $\underline{B}^{(k)}$ such that

$$\underline{B}^{(k)} \cdot \underline{d}^{(k)} = \underline{0} \quad (5.8)$$

By (5.7) and (5.8),

$$\underline{B}^{(k)}(\underline{x}^{(k)} + \lambda \underline{d}^{(k)}) = \underline{a}^{(k)} + \rho^{(k)} \underline{r} \quad (5.9)$$

Hence, $\underline{x}^{(k)} + \lambda \underline{d}^{(k)}$ is a solution of (2.12) at $\rho = \rho^{(k)}$ for any real value λ such that $\underline{x}^{(k)} + \lambda \underline{d}^{(k)} \in R^{(k)}$. Since $\underline{B}^{(k)}$ has nullity one, any vector satisfying (5.8) must be a multiple of $\underline{d}^{(k)}$. It follows that the solution curve of (2.12) within $R^{(k)}$ is a straight-line segment and the solution curve is still a one-dimensional curve in spite of the singularity of $\underline{B}^{(k)}$. However, the sweep voltage v_{in} is kept at a constant $v_{in} = \rho = \rho^{(k)}$ throughout region $R^{(k)}$.

It follows from (5.9) that the solution curve in $R^{(k)}$ follows the direction of $\underline{d}^{(k)}$ if $\underline{d}^{(k)}$ is chosen such that it points to the direction of entering $R^{(k)}$ instead of returning back to $R^{(k-1)}$. Hence, the direction vector $\underline{d}^{(k)}$ for the region $R^{(k)}$ with a singular Jacobian matrix can be determined as follows:

$$\underline{B}^{(k)} \cdot \underline{d}^{(k)} = 0 \quad (5.10a)$$

and

$$d_{j_{k-1}}^{(k)} \cdot d_{j_{k-1}}^{(k-1)} \cdot \Delta\rho^{(k-1)} > 0 \quad (5.10b)$$

Note that $\Delta\rho^{(k)} = 0$ since ρ is fixed at the constant $\rho = \rho^{(k)}$ for the solutions within $R^{(k)}$. Hence, the inequalities in (3.16), (3.17), (3.25), and (5.10) can no longer be applied if $\underline{B}^{(k-1)}$ is singular with $\Delta\rho^{(k-1)} = 0$. However, $\underline{d}^{(k-1)}$ will point to the correct direction if we follow the rule of (5.10) to choose $\underline{d}^{(k-1)}$ for $R^{(k-1)}$ with singular Jacobian matrix $\underline{B}^{(k-1)}$; namely,

$$\underline{B}^{(k-1)} \underline{d}^{(k-1)} = 0 \quad (5.11a)$$

$$d_{j_{k-2}}^{(k-1)} \cdot d_{j_{k-2}}^{(k-2)} \cdot \Delta\rho^{(k-2)} > 0 \quad (5.11b)$$

where we assume $\underline{B}^{(k-2)}$ is nonsingular and $\Delta\rho^{(k-2)} \neq 0$. In the case for $\Delta\rho^{(k-2)} = 0$, similar rule applies to the choice of $\underline{d}^{(k-2)}$.

It follows that if $\Delta\rho^{(k-1)} = 0$ then all the inequalities involving $\Delta\rho^{(k-1)}$ must be modified such that $\Delta\rho^{(k-1)}$ is aborted from these inequalities in determining the correct direction vector of the next region since $\underline{d}^{(k-1)}$ has been correctly chosen. For example, (5.10) should be modified as follows:

$$\tilde{B}^{(k)} \tilde{d}^{(k)} = \underline{0} \quad (5.12a)$$

$$d_{j_{k-1}}^{(k)} \cdot d_{j_{k-1}}^{(k-1)} \cdot \Delta\rho^{(k-1)} > 0 \quad \text{if } \Delta\rho^{(k-1)} \neq 0 \quad (5.12b)$$

$$d_{j_{k-1}}^{(k)} \cdot d_{j_{k-1}}^{(k-1)} > 0 \quad \text{if } \Delta\rho^{(k-1)} = 0 \quad (5.12c)$$

We now modify the B-H algorithm in Section 3D such that it is applicable for the more general case including the regions with singular Jacobian matrices of nullity equal to one. Only the steps needed to be modified are listed below, the other steps will remain unchanged and refer to Section 3D. The complete flowchart for this modified B-H algorithm is shown in Appendix C.

Modified Breakpoint-Hopping Algorithm:

Step 1. (e) If $\tilde{B}^{(0)}$ is nonsingular then same as Step 1(e) in Section 3D, else find the null space vector $\tilde{d}^{(0)}$ such that

$$\tilde{B}^{(0)} \tilde{d}^{(0)} = \underline{0} \quad (5.13)$$

(h) If $\tilde{B}^{(0)}$ is nonsingular then same as Step 1(h) in Section 3D, else if $\tilde{\Delta\rho}^{(0)}$ is finite then set $\Delta\rho^{(0)} = 0$, else go to Step 11.

Remark: If $\tilde{B}^{(0)}$ is singular and $\omega \cdot \Delta\rho_{j_0}^{(0)} = +\infty$ (resp.; $\omega \cdot \Delta\rho_{j_0}^{(0)} = -\infty$) then $\tilde{x}_0 = \tilde{x}^{(0)} + \lambda \tilde{d}^{(0)}$ is a solution at $\rho = \rho^{(0)}$ for all $\lambda \geq 0$ (resp.; $\lambda \leq 0$).

Step 2. If $\Delta\rho^{(k-1)} \neq 0$ then same as Step 2 in Section 3D, else if $k = 1$ then

$$i_j = \begin{cases} i_{j+1}, & \text{if } j = j_{k-1} \quad \text{and } \omega \cdot d_{j_{k-1}}^{(k-1)} > 0 \end{cases} \quad (5.14a)$$

$$i_j = \begin{cases} i_{j-1}, & \text{if } j = j_{k-1} \quad \text{and } \omega \cdot d_{j_{k-1}}^{(k-1)} < 0 \end{cases} \quad (5.14b)$$

$$i_j = \begin{cases} i_j, & \text{if } j \neq j_{k-1} \end{cases} \quad (5.14c)$$

else if $k > 1$ then

$$i_j = \begin{cases} i_{j+1}, & \text{if } j = j_{k-1} \quad \text{and } d_{j_{k-1}}^{(k-1)} > 0 \end{cases} \quad (5.15a)$$

$$i_j = \begin{cases} i_{j-1}, & \text{if } j = j_{k-1} \quad \text{and } d_{j_{k-1}}^{(k-1)} < 0 \end{cases} \quad (5.15b)$$

$$i_j = \begin{cases} i_j, & \text{if } j \neq j_{k-1} \end{cases}$$

Go to Step 3.

Step 3. If $\Delta\rho^{(k-1)} = 0$ then same as Step 3 in Section 3D, else go to Step 12.

Step 4. If $F \neq 0$ then same as Step 4 in Section 3D, else go to Step 13.

Step 6. If $\Delta\rho^{(k-1)} = 0$ then same as Step 6 in Section 3D, else let $S^{(k)} \triangleq \{j | d_j^{(k)} \neq 0, j = 1, 2, \dots, n\}$, and for $j \in S^{(k)}$ let

$$g_j = \text{sgn}\{d_j^{(k)} \cdot d_{j_{k-1}}^{(k)} \cdot d_{j_{k-1}}^{(k-1)}\} \quad (5.16)$$

Go to Step 7.

Step 9. If $\Delta\rho^{(k-1)} \neq 0$ then same as Step 9 in Section 3D,

$$\text{else if } k=1 \text{ then } \Delta\rho^{(k)} = \begin{cases} \Delta\rho^{(k)}, & \text{if } \omega \cdot d_{j_{k-1}}^{(k)} \cdot d_{j_{k-1}}^{(k-1)} > 0 \\ -\Delta\rho^{(k)}, & \text{if } \omega \cdot d_{j_{k-1}}^{(k)} \cdot d_{j_{k-1}}^{(k-1)} < 0 \end{cases} \quad (5.17a)$$

$$(5.17b)$$

$$\text{else } \Delta\rho^{(k)} = \begin{cases} \Delta\rho^{(k)}, & \text{if } d_{j_{k-1}}^{(k)} \cdot d_{j_{k-1}}^{(k-1)} > 0 \\ -\Delta\rho^{(k)}, & \text{if } d_{j_{k-1}}^{(k)} \cdot d_{j_{k-1}}^{(k-1)} < 0 \end{cases} \quad (5.17c)$$

$$(5.17d)$$

Go to Step 10.

Step 10. If $B^{(k)}$ is nonsingular then same as Step 10 in Section 3D, else

(a) if $\Delta\rho^{(k)}$ is infinite then choose

$$\rho^{(k+1)} = \rho^{(k)} \quad (5.18a)$$

$$\tilde{x}^{(k+1)} = \tilde{x}^{(k)} + \text{sgn}(\Delta\rho^{(k)}) \cdot \tilde{d}^{(k)} \quad (5.18b)$$

and go to Step 11;

(b) if $\Delta\rho^{(k)}$ is finite then compute

$$\tilde{x}^{(k+1)} = \tilde{x}^{(k)} + \Delta\rho^{(k)} \cdot \tilde{d}^{(k)} \quad (5.19a)$$

and choose

$$\Delta\rho^{(k)} = 0 \text{ and } \rho^{(k+1)} = \rho^{(k)} \quad (5.19b)$$

(c) set $k = k+1$;

(d) go to Step 2.

Step 12. Compute

$$\tilde{B}^{(k)} = \tilde{B} + \sum_{j=1}^n [(-\sum_{i=1}^{i_{j-1}} c_{ji} + \sum_{i=i_j}^{\sigma_j} c_{ji}) e_{j-1}^T] \quad (5.20)$$

If $\tilde{B}^{(k)}$ is nonsingular then compute $[\tilde{B}^{(k)}]^{-1}$ and go to Step 5, else find the null space vector $\tilde{d}^{(k)}$ such that

$$\tilde{B}^{(k)} \cdot \tilde{d}^{(k)} = 0 \quad (5.21a)$$

$$\omega \cdot d_{j_{k-1}}^{(k)} \cdot d_{j_{k-1}}^{(k-1)} > 0 \quad \text{if } k = 1 \quad (5.21b)$$

$$d_{j_{k-1}}^{(k)} \cdot d_{j_{k-1}}^{(k-1)} > 0 \quad \text{if } k > 1 \quad (5.21c)$$

Go to Step 6.

Step 13. Compute

$$\hat{d}^{(k)} = \begin{cases} -2[\tilde{B}^{(k-1)}]^{-1} c_{j_{k-1}} (i_{j_{k-1}} - 1), & \text{if } d_{j_{k-1}}^{(k-1)} \cdot \Delta \rho^{(k-1)} > 0 \\ -2[\tilde{B}^{(k-1)}]^{-1} c_{j_{k-1}} i_{j_{k-1}}, & \text{if } d_{j_{k-1}}^{(k-1)} \cdot \Delta \rho^{(k-1)} < 0 \end{cases} \quad (5.22a)$$

and choose $\tilde{d}^{(k)}$ the same as $\hat{d}^{(k)}$ except

$$d_{j_{k-1}}^{(k)} = \begin{cases} 1, & \text{if } d_{j_{k-1}}^{(k-1)} \cdot \Delta \rho^{(k-1)} > 0 \\ -1, & \text{if } d_{j_{k-1}}^{(k-1)} \cdot \Delta \rho^{(k-1)} < 0 \end{cases} \quad (5.23a)$$

$$d_{j_{k-1}}^{(k)} = \begin{cases} 1, & \text{if } d_{j_{k-1}}^{(k-1)} \cdot \Delta \rho^{(k-1)} > 0 \\ -1, & \text{if } d_{j_{k-1}}^{(k-1)} \cdot \Delta \rho^{(k-1)} < 0 \end{cases} \quad (5.23b)$$

Go to Step 6.

Remark: In the case of Step 13, $[\tilde{B}^{(k-1)}]^{-1}$ exists but $[\tilde{B}^{(k)}]^{-1}$ does not, we utilize $[\tilde{B}^{(k-1)}]^{-1}$ to compute the direction vector $\tilde{d}^{(k)}$ which satisfies (5.10). Since $\tilde{B}^{(k)} = \tilde{B}^{(k-1)} + 2c_{j_{k-1}}^T$ where $c = c_{j_{k-1}} (i_{j_{k-1}} - 1)$ (resp.;

$c = -c_{j_{k-1}} i_{j_{k-1}}$) if the solution curve is increasing (resp.; decreasing) in

the j_{k-1} -th coordinate axis in region $R^{(k-1)}$, i.e., if $d_{j_{k-1}}^{(k-1)} \cdot \Delta \rho^{(k-1)} > 0$

(resp.; $d_{j_{k-1}}^{(k-1)} \cdot \Delta\rho^{(k-1)} < 0$). By (5.10a),

$$\tilde{B}^{(k)} \tilde{d}^{(k)} = (\tilde{B}^{(k-1)} + 2c e_{j_{k-1}}^T) \tilde{d}^{(k)} = 0 \quad (5.24)$$

Multiplying (5.24) by $[\tilde{B}^{(k-1)}]^{-1}$, we obtain

$$\tilde{A} \tilde{d}^{(k)} = 0 \quad (5.25a)$$

where

$$\tilde{A} \triangleq I + 2[\tilde{B}^{(k-1)}]^{-1} c e_{j_{k-1}}^T \quad (5.25b)$$

Equation (5.25b) indicates that \tilde{A} differs from I only in the j_{k-1} -th column which is equal to $e_{j_{k-1}} + 2[\tilde{B}^{(k-1)}]^{-1} c$. Since \tilde{A} is singular, the j_{k-1} -th diagonal element must be zero and (5.25a) can be easily solved such that

$$\tilde{d}^{(k)} \triangleq -2[\tilde{B}^{(k-1)}]^{-1} c = -2[\tilde{B}^{(k-1)}]^{-1} c_{j_{k-1}} (i_{j_{k-1}} - 1) \quad (5.26a)$$

$$\text{(resp.; } \tilde{d}^{(k)} = 2[\tilde{B}^{(k-1)}]^{-1} c = -2[\tilde{B}^{(k-1)}]^{-1} c_{j_{k-1}} i_{j_{k-1}} \text{)} \quad (5.26b)$$

except the j_{k-1} -th component of $\tilde{d}^{(k)}$, $d_{j_{k-1}}^{(k)}$, is equal to 1 (resp; -1) if the solution curve is increasing (resp.; decreasing) in the j_{k-1} -th coordinate axis in region $R^{(k-1)}$, or more specifically, if $d_{j_{k-1}}^{(k-1)} \cdot \Delta\rho^{(k-1)} > 0$ (resp.; $d_{j_{k-1}}^{(k-1)} \cdot \Delta\rho^{(k-1)} < 0$).

Example 5.2 (Fig. 7(a))

Consider the simple circuit shown in Fig. 7(a) whose canonical piecewise-linear equation has been derived earlier in (2.27); namely,

$$\begin{aligned} & \begin{bmatrix} 1 & 1 & 0 \\ -1 & 1 & 0 \\ -1 & 0 & 1 \end{bmatrix} \begin{bmatrix} x_1 \\ x_2 \\ x_3 \end{bmatrix} + \begin{bmatrix} -1 \\ 0 \\ 0 \end{bmatrix} |x_1 - 2| + \begin{bmatrix} 1 \\ 0 \\ 0 \end{bmatrix} |x_1 - 3| + \begin{bmatrix} -2 \\ 0 \\ 0 \end{bmatrix} |x_2 - 4| \\ & + \begin{bmatrix} 2 \\ 0 \\ 0 \end{bmatrix} |x_2 - 5| = \begin{bmatrix} 3 \\ 0 \\ 0 \end{bmatrix} + \rho \begin{bmatrix} 1 \\ 0 \\ 0 \end{bmatrix} \end{aligned} \quad (5.27)$$

where $x_1 \triangleq i_1$, $x_2 \triangleq i_2$, and $x_3 \triangleq i_{in}$. Our goal is to find the driving-point

characteristic. Clearly, $\underline{x}^{(0)} = \underline{0}$ is an operating point corresponding to $\rho^{(0)} = 0$ since both R_1 and R_2 are passive and there exists no internal power supply. Note that $\omega = 1$ is used throughout the modified B-H algorithm because we are only interested in the range for $\rho \geq \rho^{(0)} = 0$.

Step 1. $\underline{x}^{(0)}$ is located in segment (1,1) of the nonlinear resistors R_1 and R_2 and region $R^{(0)}$ is characterized by

$$-\infty \leq x_1 \leq 2, \quad \text{and} \quad -\infty \leq x_2 \leq 4 \quad (5.28)$$

By (3.29) and (3.30),

$$\underline{B}^{(0)} = \begin{bmatrix} 1 & 1 & 0 \\ -1 & 1 & 0 \\ -1 & 0 & 1 \end{bmatrix}, \quad \text{and} \quad \underline{d}^{(0)} = [\underline{B}^{(0)}]^{-1} \underline{r} = \begin{bmatrix} 1/2 \\ 1/2 \\ 1/2 \end{bmatrix} \quad (5.29)$$

By (3.31b),

$$\Delta\rho_1^{(0)} = \frac{2-0}{1/2} = 4, \quad \text{and} \quad \Delta\rho_2^{(0)} = \frac{4-0}{1/2} = 8 \quad (5.30)$$

Since $\Delta\rho_1^{(0)} < \Delta\rho_2^{(0)}$, we identify $j_0 = 1$ and hence $\Delta\rho^{(0)} = \Delta\rho_1^{(0)} = 4$. Using (3.32) and (3.33), we calculate the next breakpoint:

$$\rho^{(1)} = 0 + 4 = 4, \quad \text{and} \quad \underline{x}^{(1)} = [0 \ 0 \ 0]^T + 4[1/2 \ 1/2 \ 1/2]^T = [2 \ 2 \ 2]^T \quad (5.31)$$

It follows from (5.30) that R_1 first arrives at its breakpoint when v_{in} increases from $\rho^{(0)} = 0$ to $\rho^{(1)} = 4$.

Step 2. The next region $R^{(1)}$ clearly corresponds to segment (2,1) and is characterized by $2 \leq x_1 \leq 3$ and $-\infty \leq x_2 \leq 4$.

Steps 3,4. Since

$$F = 1 + 2 \cdot [1 \ 0 \ 0] \begin{bmatrix} 1 & 1 & 0 \\ -1 & 1 & 0 \\ -1 & 0 & 1 \end{bmatrix}^{-1} \begin{bmatrix} -1 \\ 0 \\ 0 \end{bmatrix} = 0 \quad (5.32)$$

we are facing a degenerate case and should go to Step 13 of the modified B-H algorithm.

Step 13. By (5.22a) and (5.23a),

$$\hat{\underline{d}}^{(1)} = [1 \ 1 \ 1]^T \text{ and } \underline{d}^{(1)} = [1 \ 1 \ 1]^T \quad (5.33)$$

Step 6. $g_1 = \text{sgn}\{1 \cdot 1 \cdot 1/2 \cdot 4\} = 1$, $g_2 = \text{sgn}\{1 \cdot 1 \cdot 1/2 \cdot 4\} = 1$ (5.34)

Step 7. By (3.41b),

$$\Delta\rho_1^{(1)} = \frac{3-2}{1} = 1, \quad \Delta\rho_2^{(1)} = \frac{4-2}{1} = 2 \quad (5.35)$$

Step 8. $\Delta\rho^{(1)} = \Delta\rho_1^{(1)} = 1$ and $j_1 = 1$ (5.36)

Step 9. By (3.42a), $\Delta\rho^{(1)} = 1$.

Step 10. Since $\underline{B}^{(1)}$ is singular, we should follow Step 10 in the modified B-H algorithm. By (5.19),

$$\underline{x}^{(2)} = [2 \ 2 \ 2]^T + 1 \cdot [1 \ 1 \ 1]^T = [3 \ 3 \ 3]^T \quad (5.37a)$$

$$\rho^{(2)} = \rho^{(1)} = 4 \text{ and } \Delta\rho^{(1)} = 0 \quad (5.37b)$$

Step 2. Since $\Delta\rho^{(1)} = 0$, we should follow Step 2 in the modified B-H algorithm. The next region $R^{(2)}$ corresponds to segment (3,1) and is characterized by $3 \leq x_1 \leq \infty$ and $-\infty \leq x_2 \leq 4$.

Step 3. Since $\Delta\rho^{(1)} = 0$, we follow Step 3 in the modified B-H algorithm and go to Step 12.

Step 12. By (5.20),

$$\underline{B}^{(2)} = \begin{bmatrix} 1 & 1 & 0 \\ -1 & 1 & 0 \\ -1 & 0 & 1 \end{bmatrix} \quad (5.38)$$

Since $\underline{B}^{(2)}$ is nonsingular we can compute

$$[\underline{B}^{(2)}]^{-1} = \begin{bmatrix} 1/2 & -1/2 & 0 \\ 1/2 & 1/2 & 0 \\ 1/2 & -1/2 & 1 \end{bmatrix} \quad (5.39)$$

and go to Step 5.

Step 5. By (3.39),

$$\underline{d}^{(2)} = [1/2 \ 1/2 \ 1/2]^T \quad (5.40)$$

Step 6. Since $\Delta\rho^{(1)} = 0$, we follow Step 6 in the modified B-H algorithm and by (5.16),

$$g_1 = \text{sgn}\{1/2 \cdot 1/2 \cdot 1\} = 1, \quad g_2 = \text{sgn}\{1/2 \cdot 1/2 \cdot 1\} = 1 \quad (5.41)$$

Step 7. By (3.41b),

$$\Delta\rho_1^{(2)} = \frac{\infty-3}{1/2} = \infty, \quad \Delta\rho_2^{(2)} = \frac{4-3}{1/2} = 2 \quad (5.42)$$

Step 8. $\Delta\rho^{(2)} = 2$ and $j_2 = 2$.

Step 9. By (5.17a), $\Delta\rho^{(2)} = 2$. (5.43)

Step 10. By (3.44) and (3.45)

$$\rho^{(3)} = 4 + 2 = 6, \quad \tilde{x}^{(3)} = [3 \ 3 \ 3]^T + 2[1/2 \ 1/2 \ 1/2]^T = [4 \ 4 \ 4]^T \quad (5.44)$$

The remaining breakpoint-hopping procedures continue similarly as the above steps and it can be shown that $\tilde{x}^{(4)} = [5 \ 5 \ 5]^T$ with $\rho^{(4)} = 4$ is a breakpoint and $\tilde{x}^{(5)} = [7 \ 7 \ 7]^T$ with $\rho^{(5)} = 8$ is a point in the end segment of the solution curve shown in Fig. 25(a).

The driving-point characteristic is obtained from the third coordinate of \tilde{x} and is shown in Fig. 25(b). Note that all points on the vertical segment project into a single point $v_{in} = 4$. This corresponds to the region $R^{(1)}$ where $B^{(1)}$ has nullity equal to one. □

B. High-Dimensional Degenerate Case: nullity of $B^{(k)} = m > 1$

Suppose the solution curve Γ enters a region $R^{(k)}$ whose Jacobian matrix has nullity m with $m > 1$. Let the circuit be characterized by (5.6) within region $R^{(k)}$. Since the null space of $B^{(k)}$ has dimension $m > 1$, there are m independent vectors satisfying (5.8); namely,

$$\tilde{B}^{(k)} \tilde{d}^{(k)i} = 0 \quad i = 1, 2, \dots, m \quad (5.45)$$

By (5.7) and (5.45),

$$\tilde{B}^{(k)} \left(\tilde{x}^{(k)} + \sum_{i=1}^m \lambda_i \tilde{d}^{(k)i} \right) = \tilde{a}^{(k)} + \rho^{(k)} \cdot \tilde{r} \quad (5.46)$$

Hence, $\tilde{x}^{(k)} + \sum_{i=1}^m \lambda_i \tilde{d}^{(k)i}$ is a solution of (2.12) at $\rho = \rho^{(k)}$ for all real values $\lambda_1, \lambda_2, \dots, \lambda_m$ such that $\tilde{x}^{(k)} + \sum_{i=1}^m \lambda_i \tilde{d}^{(k)i} \in R^{(k)}$. It follows that the solutions of (2.12) within $R^{(k)}$ corresponding to $\rho = \rho^{(k)}$ are made up of points in a subset of m -dimensional hyperplane and can not be covered by any \hat{m} -dimensional hyperplane with $\hat{m} < m$. In this case, the solution curve Γ is

no longer a well-defined one-dimensional curve; it, however, will split into an m-dimensional hyperplane within $R^{(k)}$ upon hitting the breakpoint $\underline{x}^{(k)}$ (which is also a corner point) as shown in the following example:

Example 5.3 (Fig. 26(a))

Consider the circuit shown in Fig. 26(a), where the nonlinear resistors R_1 and R_2 are described by the piecewise-linear characteristics shown in Figs. 26(b) and (c) respectively. To trace the solution curve by using the modified B-H algorithm, we choose $\underline{x} = [v_1, v_2, i_{in}]^T$ and $\underline{y} = [i_1, i_2, v_{in}]^T$, and write the following associated canonical piecewise-linear equation (detailed calculation is given in Appendix D-4):

$$\begin{bmatrix} 1 & 0 & 0 \\ 0 & 3/2 & 0 \\ 0 & 0 & 1 \end{bmatrix} \begin{bmatrix} x_1 \\ x_2 \\ x_3 \end{bmatrix} + \begin{bmatrix} -1/2 \\ 0 \\ 0 \end{bmatrix} |x_1| + \begin{bmatrix} 1/2 \\ 0 \\ 0 \end{bmatrix} |x_1-2| + \begin{bmatrix} 0 \\ -1/2 \\ 0 \end{bmatrix} |x_2+1| + \begin{bmatrix} 0 \\ 1 \\ 0 \end{bmatrix} |x_2-1| = \begin{bmatrix} 0 \\ -1/2 \\ 0 \end{bmatrix} + \rho \begin{bmatrix} 1 \\ 1 \\ 1 \end{bmatrix} \quad (5.47)$$

We start from the initial point $\underline{x}^{(0)} = [-1 \ -2 \ 0]^T$ which corresponds to $\rho^{(0)} = 0$ and is located in segment (1,1) of the nonlinear resistors R_1 and R_2 . Hence, region $R^{(0)}$ is characterized by $-\infty \leq x_1 \leq 0$ and $-\infty \leq x_2 \leq -1$, and by (3.29) and (3.30),

$$\underline{B}^{(0)} = \begin{bmatrix} 1 & 0 & 0 \\ 0 & 1 & 0 \\ 0 & 0 & 1 \end{bmatrix}, \text{ and } \underline{d}^{(0)} = [\underline{B}^{(0)}]^{-1} \underline{r} = \begin{bmatrix} 1 \\ 1 \\ 1 \end{bmatrix} \quad (5.48)$$

It follows from (3.31b) that

$$\Delta\rho_1^{(0)} = \frac{0-(-1)}{1} = 1, \text{ and } \Delta\rho_2^{(0)} = \frac{-1-(-2)}{1} = 1 \quad (5.49)$$

Hence, the solution curve Γ hits the boundary hyperplanes $x_1 = 0$ and $x_2 = -1$ simultaneously at the corner point

$$\underline{x}^{(1)} = [0 \ -1 \ 1]^T \text{ with } \rho^{(1)} = 1 \quad (5.50)$$

which is identified as point A in Fig. 26(e). It is shown in Fig. 26(e) that

the corner point A belongs to regions $R^{(a)}$, $R^{(b)}$, and $R^{(c)}$ (corresponding to segments (1,2), (2,1), and (2,2) of the nonlinear resistors R_1 and R_2 respectively) in addition to region $R^{(0)}$, and all these regions are possible candidates for the solution curve to enter. By (3.15), the Jacobian matrices in these regions can be found to be

$$\underline{B}^{(a)} = \begin{bmatrix} 1 & 0 & 0 \\ 0 & 0 & 0 \\ 0 & 0 & 1 \end{bmatrix}, \quad \underline{B}^{(b)} = \begin{bmatrix} 0 & 0 & 0 \\ 0 & 1 & 0 \\ 0 & 0 & 1 \end{bmatrix}, \quad \text{and} \quad \underline{B}^{(c)} = \begin{bmatrix} 0 & 0 & 0 \\ 0 & 0 & 0 \\ 0 & 0 & 1 \end{bmatrix} \quad (5.51)$$

Note that $\underline{B}^{(a)}$ and $\underline{B}^{(b)}$ are singular with nullity equal to one. By (5.10), the direction vectors in these two regions can be found to be

$$\underline{d}^{(a)} = [0 \ 1 \ 0]^T \quad \text{and} \quad \underline{d}^{(b)} = [1 \ 0 \ 0]^T \quad (5.52)$$

The Jacobian matrix $\underline{B}^{(c)}$, however, has nullity equal to two and the direction vector in $R^{(c)}$ is not unique. Let

$$\underline{d}^{(c)1} = [1 \ 0 \ 0]^T \quad \text{and} \quad \underline{d}^{(c)2} = [0 \ 1 \ 0]^T \quad (5.53)$$

be two linearly independent vectors which satisfy (5.10). By (5.46), $\underline{x}^{(1)} + \lambda_1 \underline{d}^{(c)1} + \lambda_2 \underline{d}^{(c)2}$ is a solution of (5.47) at $\rho = \rho^{(1)} = 1$ for all real values λ_1 and λ_2 such that $\underline{x}^{(1)} + \lambda_1 \underline{d}^{(c)1} + \lambda_2 \underline{d}^{(c)2} \in R^{(c)}$. It follows that any point in $R^{(c)}$ is a solution of (5.47) at $\rho = \rho^{(1)} = 1$ and the solution curve Γ will split over the whole region of $R^{(c)}$ as shown in Fig. 26(e). Note that the direction vector $\underline{d}^{(a)}$ (resp.; $\underline{d}^{(b)}$) in (5.52) is in the direction of entering $R^{(a)}$ (resp.; $R^{(b)}$) and will define a trajectory for the solution curve in $R^{(a)}$ (resp.; $R^{(b)}$). But since $\underline{x}^{(1)}$ is a corner point, the solution curve in $R^{(a)}$ (resp.; $R^{(b)}$) follows the boundary line AD (resp.; AB) between regions $R^{(c)}$ and $R^{(a)}$ (resp.; $R^{(c)}$ and $R^{(b)}$) which is a boundary for region $R^{(c)}$ as shown in Fig. 26(e). There are three other corner points B, C, and D in $R^{(c)}$, it can be shown (by finding the direction vector in each neighboring region and checking whether it points to the correct direction) that point C is the next breakpoint and region $R^{(f)}$ is the next region for the solution curve with Jacobian matrix and direction vector

$$\underline{B}^{(f)} = \begin{bmatrix} 1 & 0 & 0 \\ 0 & 2 & 0 \\ 0 & 0 & 1 \end{bmatrix}, \quad \underline{d}^{(f)} = \begin{bmatrix} 1 \\ 1/2 \\ 0 \end{bmatrix} \quad (5.54)$$

The trajectory for the solution curve is shown in Fig. 26(e) where it splits into an area on a two-dimensional plane. The corresponding driving-point characteristic and $v_1 - v_s - v_{in}$, and $v_2 - v_s - v_{in}$ transfer characteristics are shown in Figs. 27(a), (b), and (c) respectively. \square

The high-dimensional degenerate case can be avoided by making a minor assumption as mentioned in Assumption A.1 in Section 3A; namely,

(i) the starting point lies in a region with a nonsingular Jacobian matrix; (5.55a)

(ii) the solution curve never hits a corner point. (5.55b)

Assumptions (5.55a) and (5.55b) can be easily satisfied by perturbing the element parameter values whenever the degenerate condition is detected. They guarantee the algorithm is free from the following two degeneracies: 1) hitting a corner point and 2) entering a region with the nullity of the Jacobian matrix greater than one.

C. Generic Properties of Solution Curves

We end this paper with a careful analysis of the generic properties of the solution curves. Such properties are best derived by answering the following questions:

1. Does the solution curve always follow a unique path in each region $R^{(k)}$ traversed by Γ ?
2. Can a solution curve Γ re-enter a region which it has previously traversed?
3. Can a solution curve Γ remain in a boundary hyperplane instead of penetrating it?

The above questions are general problems in piecewise-linear analysis and have been fully discussed in [16,18]. In the following, we describe the solutions to the above problems in the form of observations and use them to show that our breakpoint-hopping algorithm would not suffer the above problems under Assumption (5.55).

Observation 1. [16] If two regions $R^{(j)}$ and $R^{(k)}$, with Jacobian matrices $\underline{B}^{(j)}$ and $\underline{B}^{(k)}$ respectively, have a common $(n-1)$ -dimensional boundary hyperplane, then the ranks of $\underline{B}^{(j)}$ and $\underline{B}^{(k)}$ differ at most by one.

Observation 2. [16] If the solution curve Γ starts from an interior point of a region with a nonsingular Jacobian matrix, and assuming Γ never hits any corner point, then 1) Γ never enters a region with a Jacobian matrix of nullity two or more and 2) Γ intersects any boundary hyperplane at a single point.

Remark: The condition for nonsingular Jacobian matrix in the region where the starting point is located can be relaxed such that if the Jacobian matrix has nullity no greater than one and Γ never hits a corner point, then it also leads to the same result of 1) in Observation 2. This can be verified in Appendix A.

Observation 3. [18] If the nullity of the Jacobian matrix $B^{(k)}$ in region $R^{(k)}$ is not greater than one, and the solution curve Γ enters $R^{(k)}$ at $\tilde{x}^{(k)}$ and leaves $R^{(k)}$ at $\tilde{x}^{(k+1)}$, then Γ can not re-enter $R^{(k)}$ through a point other than $\tilde{x}^{(k)}$.

The answer to Question 1 in general is false as shown in Examples 5.1 and 5.3. It, however, is true under Assumption (5.55) as can be shown by Observation 2 and Appendix A: since the solution curve only traverses regions with the nullity of the corresponding Jacobian matrices no greater than one such that the direction vector in each region can be uniquely determined, and the solution curve will always follow a unique one-dimensional trajectory for each starting point.

The problem of Question 2 can be answered by Observation 3. Under Assumption (5.55), if the solution curve re-enters any previously traversed region, then this region must be $R^{(0)}$ where the starting point is located, and the solution curve becomes cyclic as shown in Fig. 28(a). The driving-point or transfer characteristic is periodic as shown in Fig. 28(b) if $\rho^{(m+2)} \neq \rho^{(1)}$ and is a closed cyclic curve as shown in Fig. 28(c) if $\rho^{(m+2)} = \rho^{(1)}$.

Under Assumption (5.55), the answer to Question 3 is negative in view of Observation 2 since the solution curve intersects any boundary hyperplane at a single point. It follows that both $d_{j_{k-1}}^{(k-1)}$ and $d_{j_{k-1}}^{(k)}$ are nonzero where $R^{(k-1)}$ and $R^{(k)}$ are separated by the boundary hyperplane $x_{j_{k-1}} = \text{constant}$. Hence, all the inequalities involving $d_{j_{k-1}}^{(k-1)}$ and $d_{j_{k-1}}^{(k)}$ which determine the correct direction vectors in the B-H algorithm would not suffer from the ill-conditioned case when $d_{j_{k-1}}^{(k-1)}$ or $d_{j_{k-1}}^{(k)}$ is zero, as long as Assumption (5.55) is satisfied.

As a final remark, if Assumption (5.55) is satisfied (which is true generically), then the breakpoint-hopping algorithm including the modifications

in Section 5A will trace every branch of the solution curves in the driving-point or transfer characteristics, provided one point in each branch is given.

APPENDIX

A. If the Jacobian matrix of the starting region has nullity no greater than one and Γ never hits a corner point, then it leads to the same result in 1) of Observation 2.

Proof: It is sufficient to show that if the nullity of $B^{(k-1)}$ is no greater than one and $\tilde{x}^{(k)}$ is not a corner point, then the nullity of $\tilde{B}^{(k)}$ is also no greater than one, where $B^{(k-1)}$ and $B^{(k)}$ are the Jacobian matrices in the regions $R^{(k-1)}$ and $R^{(k)}$ respectively, and the solution curve Γ enters $R^{(k)}$ from $R^{(k-1)}$ at $\tilde{x}^{(k)}$.

Since $\tilde{x}^{(k)}$ is not a corner point, $R^{(k)}$ and $R^{(k-1)}$ are separated by an $(n-1)$ -dimensional boundary hyperplane, $x_{j_{k-1}} = \text{constant}$. By (3.37), $\tilde{B}^{(k)}$ and $B^{(k-1)}$ are the same except the j_{k-1} -th column. Assume $B^{(k)}$ has nullity equal to two then $\tilde{B}^{(k-1)}$ has nullity equal to one since $B^{(k-1)}$ is assumed to have nullity no greater than one. Since $B^{(k)}$ has nullity equal to two, there exists $\tilde{z} \in \mathbb{R}^{n+1}$ such that $\tilde{B}^{(k)}\tilde{z} = \tilde{0}$ and $z_{j_{k-1}} = 0$. Hence, $\tilde{B}^{(k-1)}\tilde{z} = \tilde{0}$ because $\tilde{B}^{(k)}$ differs $B^{(k-1)}$ only in the j_{k-1} -th column. It follows from (5.10) that $\tilde{d}^{(k-1)}$ is parallel to \tilde{z} with $d_{j_{k-1}}^{(k-1)} = 0$ which implies that the solution curve within $R^{(k-1)}$ is parallel to the boundary hyperplane $x_{j_{k-1}} = \text{constant}$ and never enters $R^{(k)}$. Hence, $\tilde{B}^{(k)}$ can not have nullity equal to two and must have nullity no greater than one. \square

B. Correction to the ill-conditioned case in [2]

For ease of reference, we follow the same notations and list some equations of [2]. Assume circuit N in Sec. II of [2] can be characterized by the canonical piecewise-linear equation

$$\tilde{f}(\tilde{x}) = \tilde{a} + \tilde{B}\tilde{x} + \sum_{i=1}^p \tilde{c}_i |\langle \tilde{\alpha}_i, \tilde{x} \rangle - \beta_i| = 0 \quad (\text{B.1})$$

where $\tilde{B} \in \mathbb{R}^{n \times n}$, $\tilde{a}, \tilde{c}_i \in \mathbb{R}^n$, β_i is a scalar, and $\tilde{\alpha}_i$ is a unit vector along some coordinate axis for each $i = 1, 2, \dots, p$.

Consider an arbitrary k -th partition hyperplane H_k defined by

$$H_k : \langle \tilde{\alpha}_k, \tilde{x} \rangle - \beta_k = 0 \quad (\text{B.2})$$

In general, H_k will be further partitioned into several sections by other hyperplanes which intersect it. Let $\sigma_a \sigma_b$ be one arbitrary section on H_k such

that two regions R_a and R_b are separated by $\sigma_a\sigma_b$. For $\underline{x} \in \sigma_a\sigma_b$, we can expand the absolute-value term in (B.1) and obtain

$$\underline{f}(\underline{x}) = \underline{\bar{a}}_{k\sigma_a\sigma_b} + \underline{\bar{B}}_{k\sigma_a\sigma_b} \underline{x} \quad (B.3)$$

where

$$\underline{\bar{a}}_{k\sigma_a\sigma_b} = \underline{a} + \sum_{\substack{i=1 \\ i \neq k}}^p c_i (\mp \beta_i) \quad (B.4)$$

$$\underline{\bar{B}}_{k\sigma_a\sigma_b} = \underline{B} + \sum_{\substack{i=1 \\ i \neq k}}^p c_i (\pm \alpha_i^T) \quad (B.5)$$

and the choice of \pm sign in (B.4) and (B.5) depends on the sign of $\langle \alpha_i, \underline{x} \rangle - \beta_i$ for $i = 1, 2, \dots, p$ and $i \neq k$.

When $\underline{\bar{B}}_{k\sigma_a\sigma_b}$ is nonsingular, the image H'_k of H_k under the mapping $\underline{f}(\cdot)$ in (B.3) is an $(n-1)$ -dimensional hyperplane, we can follow Eqs. (20)-(23) in [2] to find H'_k and perform the sign test by Eq. (24).

We now discuss the ill-conditioned case that $\underline{\bar{B}}_{k\sigma_a\sigma_b}$ is singular or $\beta_k = 0$.

Degenerate Case I: $\underline{\bar{B}}_{k\sigma_a\sigma_b}$ is singular

In this case, the rank of $\underline{\bar{B}}_{k\sigma_a\sigma_b}$ is at most $n-1$ and the domain for the mapping $\underline{f}(\cdot)$ in (B.3) is the $(n-1)$ -dimensional hyperplane $H_k: \langle \alpha_k, \underline{x} \rangle - \beta_k = 0$ containing $\sigma_a\sigma_b$, hence the image $H'_k = \underline{f}(H_k)$ has at most a dimension equal to $n-1$ and it is still possible to perform the sign test when it is an $(n-1)$ -dimensional hyperplane.

The normal vector α_k for the hyperplane H_k is a unit vector along one of the coordinate axis. We assume $\alpha_k = e_j$ and H_k can be expressed as $x_j = \beta_k$. Let $\underline{\bar{b}}_j$ be the j -th column of $\underline{\bar{B}}_{k\sigma_a\sigma_b}$ and $\hat{\underline{B}}_{k\sigma_a\sigma_b}$ be the submatrix of $\underline{\bar{B}}_{k\sigma_a\sigma_b}$ obtained by deleting $\underline{\bar{b}}_j$ from $\underline{\bar{B}}_{k\sigma_a\sigma_b}$. For any $\underline{x} \in H_k$, we can decompose \underline{x} by $\underline{x} = \underline{\bar{x}} + x_j e_j = \underline{\bar{x}} + \beta_k e_j$, where $\underline{\bar{x}}$ is the same as \underline{x} except the j -th component of $\underline{\bar{x}}$ is zero.

Lemma B.1. If $\hat{\underline{B}}_{k\sigma_a\sigma_b}$ has rank $n-1$, then H'_k is an $(n-1)$ -dimensional hyperplane

and can be expressed as

$$H'_k : \langle \underline{\alpha}'_k, \underline{y} \rangle - \beta'_k = 0 \quad (\text{B.6})$$

where $\underline{\alpha}'_k$ is the basis of the null space of $\hat{B}_{\sim k \sigma_a \sigma_b}^T$, i.e.,

$$\hat{B}_{\sim k \sigma_a \sigma_b}^T \underline{\alpha}'_k = \underline{0} \quad (\text{B.7})$$

and

$$\beta'_k = (\underline{\alpha}'_k)^T [\bar{a}_{\sim k \sigma_a \sigma_b} + \beta_k \bar{b}_{\sim k-j}] \quad (\text{B.8})$$

Proof:

Let \underline{y} be any vector such that $\underline{y} \in H'_k$, then there exists an $\underline{x} \in H_k$ such that $\underline{y} = \hat{B}_{\sim k \sigma_a \sigma_b} \underline{x} + \bar{a}_{\sim k \sigma_a \sigma_b}$. Decomposing \underline{x} , we obtain $\underline{y} = \hat{B}_{\sim k \sigma_a \sigma_b} (\bar{x} + \beta_k \underline{e}_{\sim k-j}) + \bar{a}_{\sim k \sigma_a \sigma_b} = \hat{B}_{\sim k \sigma_a \sigma_b} \hat{\underline{x}} + (\beta_k \bar{b}_{\sim k-j} + \bar{a}_{\sim k \sigma_a \sigma_b})$, where $\hat{\underline{x}}$ is an $(n-1)$ -dimensional vector obtained by deleting the j -th component from \underline{x} . Since $\hat{B}_{\sim k \sigma_a \sigma_b}^T$ is an $(n-1) \times n$ matrix and has rank $n-1$, there exists a unique basis vector $\underline{\alpha}'_k$ (modulo scalar multiplication) in its null space. Hence each $\underline{y} \in H'_k$ must satisfy $\langle \underline{\alpha}'_k, \underline{y} \rangle = \underline{\alpha}'_k{}^T (\beta_k \bar{b}_{\sim k-j} + \bar{a}_{\sim k \sigma_a \sigma_b})$ and since $\underline{\alpha}'_k$ is unique, the span of \underline{y} in the range space has dimension $n-1$. Hence H'_k can be expressed as $\langle \underline{\alpha}'_k, \underline{y} \rangle = \beta'_k$ where $\beta'_k = \underline{\alpha}'_k{}^T (\beta_k \bar{b}_{\sim k-j} + \bar{a}_{\sim k \sigma_a \sigma_b})$. \square

Hence, if $\hat{B}_{\sim k \sigma_a \sigma_b}$ satisfies the condition of Lemma B.1, and $\beta'_k \neq 0$, we can still find the $(n-1)$ -dimensional hyperplane H'_k by (B.6)-(B.8) and perform the sign test.

If the condition of Lemma B.1 is not satisfied, then the rank of $\hat{B}_{\sim k \sigma_a \sigma_b}$ is at most $n-2$ and the image H'_k will shrink to a hyperplane with at most a dimension equal to $n-2$. Hence we can no longer perform the sign test. Due to a continuity, the image of R_a (or R_b) will be contained in a hyperplane with at most dimension $n-1$. Hence $J_{\sim a}$ (or $J_{\sim b}$), the Jacobian matrices in region R_a (or R_b), will be singular and we have two cases to discuss. For simplicity, we only present results concerning R_a , they can also be applied to R_b .

(a) If $J_{\sim a}$ has rank $n-1$, then the image R'_a of R_a is contained in an $(n-1)$ -dimensional hyperplane

$$H'_a : \langle \underline{\alpha}'_a, \underline{y} \rangle - \beta'_a = 0 \quad (\text{B.9})$$

where

$$J_{\tilde{a}\tilde{a}}^T \alpha'_a = 0 \quad (B.10)$$

$$\beta'_a = \alpha'_a{}^T \tilde{a}_a \quad (B.11)$$

and $f(\tilde{x}) = J_{\tilde{a}\tilde{a}} \tilde{x} + \tilde{a}_a$ for any $x \in R_a$. Equations (B.9)-(B.11) can be obtained similarly from the proof of Lemma B.1. If $\beta'_a \neq 0$ then there is no solution within R_a and there is no need to perform the sign test for R_a . However, we can utilize the hyperplane H'_a to perform the sign test on all the neighboring regions of R_a with nonsingular Jacobian matrices.

(b) If $J_{\tilde{a}\tilde{a}}$ has rank less than $n-1$ or has nullity m with $m \geq 2$, then the image R'_a of R_a is contained in an $(n-m)$ -dimensional hyperplane $H'_a = \bigcap_{i=1}^m H'_a(i)$ where

$$H'_a(i) : \langle \alpha'_a(i), \tilde{y} \rangle - \beta'_a(i) = 0 \quad (B.12)$$

$$J_{\tilde{a}\tilde{a}}^T \alpha'_a(i) = 0 \quad (B.13)$$

$$\beta'_a(i) = [\alpha'_a(i)]^T \tilde{a}_a \quad (B.14)$$

for $i = 1, 2, \dots, m$. If not all of $\beta'_a(i)$, $i = 1, 2, \dots, m$, are zero, then R_a contains no solution and there is no need to perform the sign test for R_a .

Degenerate Case II: $\beta' = 0$

(i) $\bar{B}_{\tilde{k}\sigma_a\sigma_b}$ is nonsingular and $\beta'_{\tilde{k}\sigma_a\sigma_b} = 0$.

In this case the origin of the range space is in the hyperplane H'_k defined in Eq. (21)-(23) of [2]. Hence $\bar{B}_{\tilde{k}\sigma_a\sigma_b} \tilde{x} + \bar{a}_{\tilde{k}\sigma_a\sigma_b} = 0$ has a solution $\tilde{x}^* = -\bar{B}_{\tilde{k}\sigma_a\sigma_b}^{-1} \bar{a}_{\tilde{k}\sigma_a\sigma_b}$, and if $\tilde{x}^* \in \sigma_a\sigma_b$, then \tilde{x}^* is a solution of (B.1).

If $J_{\tilde{a}\tilde{a}}$ (resp.; $J_{\tilde{b}\tilde{b}}$) is nonsingular, then there is no solution within the interior of R_a (resp.; R_b) since the image of the interior of R_a (resp.; R_b) is on one side of H'_k and does not contain the origin $\tilde{y} = 0$.

If $J_{\tilde{a}\tilde{a}}$ (resp.; $J_{\tilde{b}\tilde{b}}$) is singular then by continuity it must have rank $n-1$ and the image of R_a (resp.; R_b) must be contained in H'_k . Let $\eta_a \triangleq \{\tilde{x} | J_{\tilde{a}\tilde{a}} \tilde{x} + \tilde{a}_a = 0\}$ (resp.; $\eta_b \triangleq \{\tilde{x} | J_{\tilde{b}\tilde{b}} \tilde{x} + \tilde{a}_b = 0\}$), since H'_k is a boundary hyperplane for R_a (resp.; R_b), $\beta'_{\tilde{k}\sigma_a\sigma_b} = 0$ implies η_a (resp.; η_b) is nonempty. Hence $\tilde{x}^* \in \eta_a \cap R_a$ (resp.; $\tilde{x}^* \in \eta_b \cap R_b$) is a solution of (B.1) if the intersection is nonempty.

(ii) $\bar{B}_{k\sigma_a\sigma_b}$ is singular.

(a) $\hat{B}_{k\sigma_a\sigma_b}$ has rank $n-1$ and $\beta'_k = 0$ in (B.8). Let $\eta_{k\sigma_a\sigma_b} \triangleq \{x \mid \bar{B}_{k\sigma_a\sigma_b} x + \bar{a}_{k\sigma_a\sigma_b} = 0\}$, $\beta'_k = 0$ implies $\eta_{k\sigma_a\sigma_b} \neq \emptyset$, and $\tilde{x}^* \in \sigma_a\sigma_b \cap \eta_{k\sigma_a\sigma_b}$ is a solution of (B.1) if the intersection is nonempty.

If J_a (resp.; J_b) is nonsingular, then there is no solution within the interior of R_a (resp.; R_b).

If J_a (resp.; J_b) is singular, then $\beta'_k = 0$ implies η_a (resp.; η_b) is nonempty. Hence, $\tilde{x}^* \in \eta_a \cap R_a$ (resp.; $\tilde{x}^* \in \eta_b \cap R_b$) is a solution of (B.1) if the intersection is nonempty.

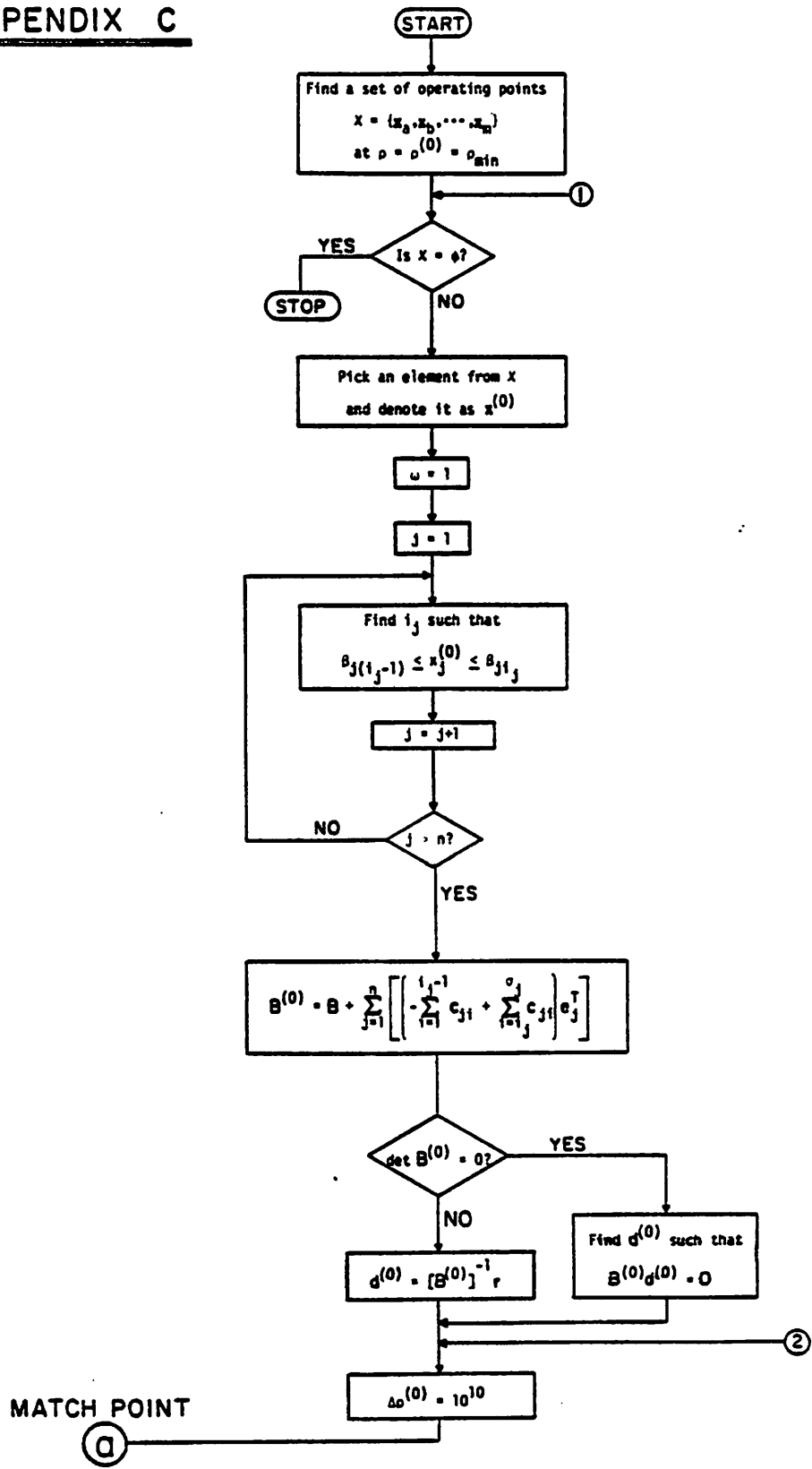
(b) $\hat{B}_{k\sigma_a\sigma_b}$ has rank less than $n-1$.

(1) J_a has rank $n-1$ and $\beta'_a = 0$ in (B.9). Since H_k is a boundary hyperplane for R_a , $\beta'_a = 0$ implies $\eta_a \neq \emptyset$, then $\tilde{x}^* \in \eta_a \cap R_a$ is a solution of (B.1) if the intersection is nonempty.

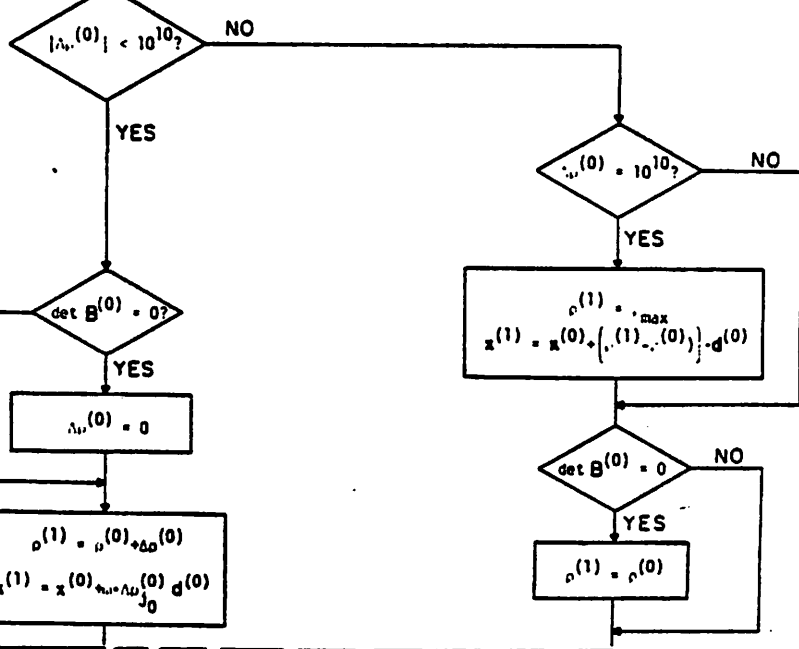
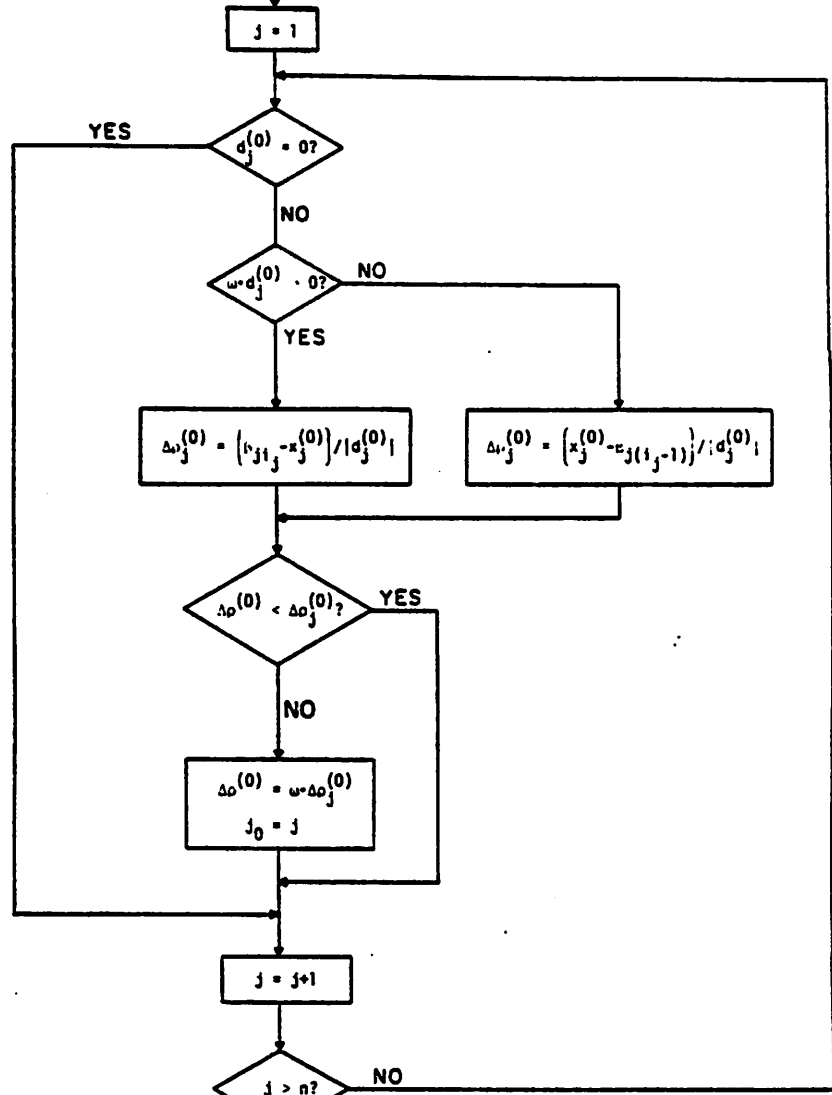
(2) J_a has rank less than $n-1$ or has nullity m with $m \geq 2$ and $\beta_a^{(i)} = 0$ for $i = 1, 2, \dots, m$ in (B.12).

$\beta_a^{(i)} = 0$ for $i = 1, 2, \dots, m$ implies $\eta_a \neq \emptyset$, then $\tilde{x}^* \in \eta_a \cap R_a$ is a solution of (B.1) if the intersection is nonempty. Cases (1) and (2) can also be applied to R_b .

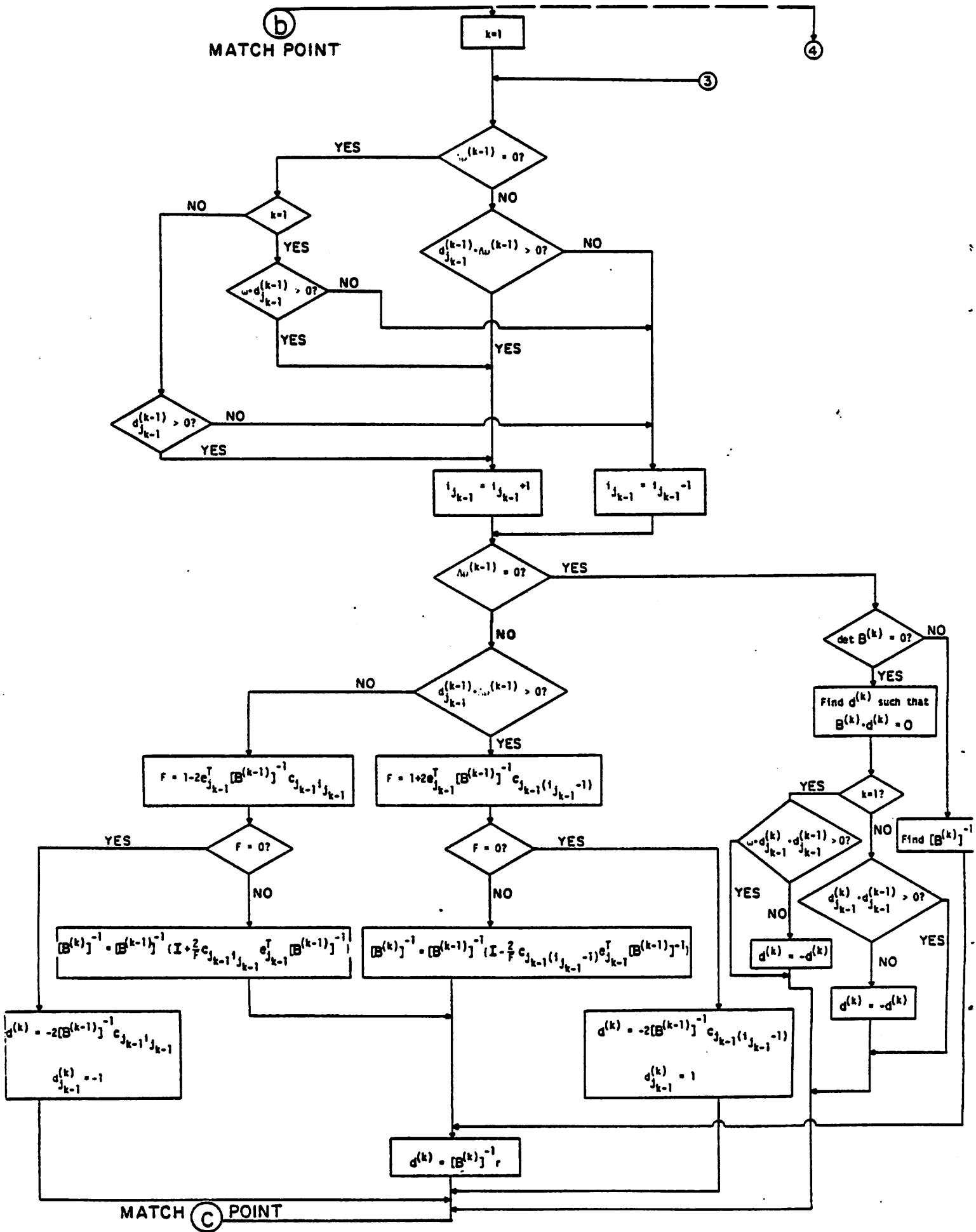
APPENDIX C



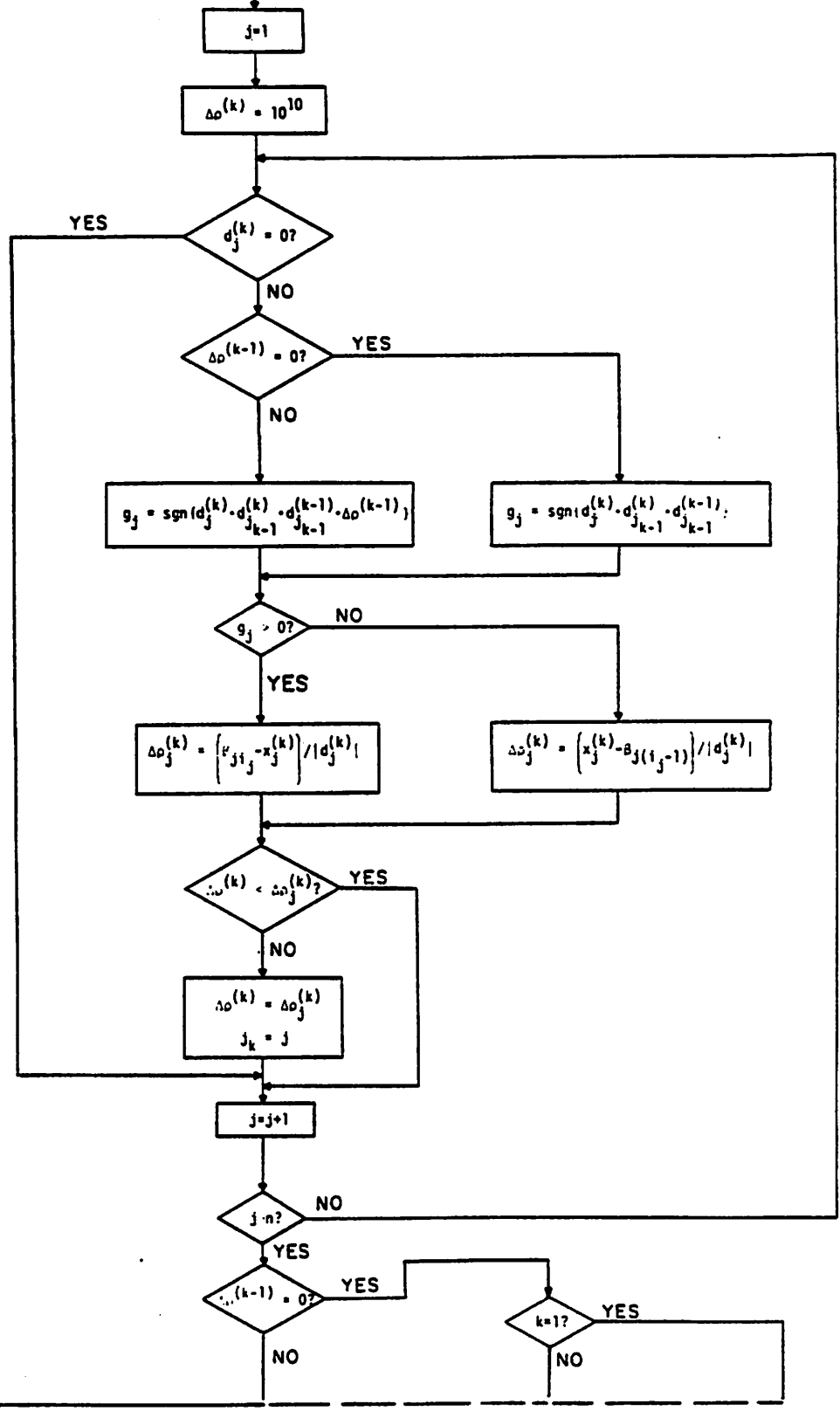
① MATCH POINT



MATCH POINT
②

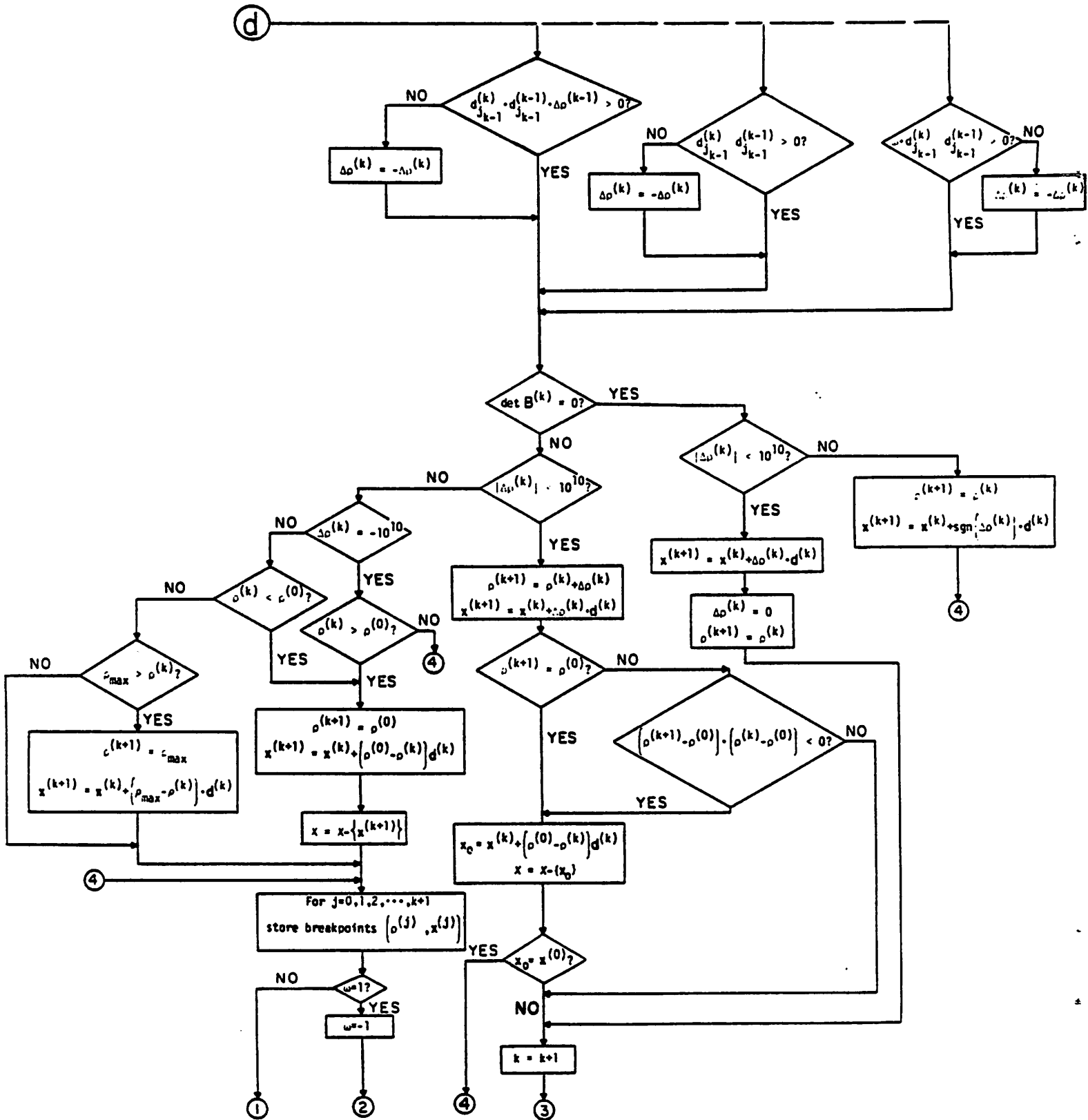


③
MATCH POINT



④
MATCH POINT

MATCH POINT



D. Formulation of the Canonical Piecewise-Linear Equations

1. Equation (3.46) in Example 3.1:

Using the explicit formulas in [1], we obtain the following canonical piecewise-linear equations for R_1 and R_2 :

$$R_1: i_1 = 9/8 v_1 + 7/8 |v_1| \quad (D.1a)$$

$$R_2: v_2 = 9/4 i_2 + 7/4 |i_2 - 1| - 9/4 \quad (D.1b)$$

Extracting the two nonlinear resistors, we obtain the linear 3-port \hat{N} shown in Fig. 18(e) which is described by the following generalized hybrid representation:

$$\underbrace{\begin{bmatrix} 1 & 0 & 0 \\ -1 & 1 & 0 \\ 0 & -1 & 1 \end{bmatrix}}_{\tilde{P}} \underbrace{\begin{bmatrix} v_1 \\ i_2 \\ i_{in} \end{bmatrix}}_{\tilde{x}} = \underbrace{\begin{bmatrix} 0 & -1 & 1 \\ 1 & 0 & 0 \\ 0 & 0 & 0 \end{bmatrix}}_{\tilde{Q}} \underbrace{\begin{bmatrix} i_1 \\ v_2 \\ v_{in} \end{bmatrix}}_{\tilde{y}} + \underbrace{\begin{bmatrix} 0 \\ 0 \\ 0 \end{bmatrix}}_{\tilde{s}} \quad (D.2)$$

Substituting (D.1) into (2.10) and (2.11), we obtain

$$\beta_{11} = 0, \beta_{21} = 1, \hat{\tilde{a}} = \begin{bmatrix} 0 \\ -9/4 \\ 0 \end{bmatrix}, \hat{\tilde{B}} = \begin{bmatrix} 9/8 & 0 & 0 \\ 0 & 9/4 & 0 \\ 0 & 0 & 0 \end{bmatrix}, \hat{\tilde{c}}_{11} = \begin{bmatrix} 7/8 \\ 0 \\ 0 \end{bmatrix}, \hat{\tilde{c}}_{21} = \begin{bmatrix} 0 \\ 7/4 \\ 0 \end{bmatrix} \quad (D.3)$$

Substituting (D.2) and (D.3) into (2.13), we obtain

$$\tilde{B} = \begin{bmatrix} -1 & -9/4 & 0 \\ 17/8 & -1 & 0 \\ 0 & 1 & -1 \end{bmatrix}, \tilde{a} = \begin{bmatrix} -9/4 \\ 0 \\ 0 \end{bmatrix}, \tilde{r} = \begin{bmatrix} -1 \\ 0 \\ 0 \end{bmatrix}, \tilde{c}_{11} = \begin{bmatrix} 0 \\ 7/8 \\ 0 \end{bmatrix}, \tilde{c}_{21} = \begin{bmatrix} -7/4 \\ 0 \\ 0 \end{bmatrix} \quad (D.4)$$

Substituting (D.4) into (2.12), we obtain the canonical piecewise-linear equation (3.46) for the circuit in Fig. 18(a).

2. Equation (3.58) in Example 3.2:

By Fig. 19(b), the canonical piecewise-linear equation of R_1 can be found to be

$$i_1 = -1/2 + v_1 - 5/4 |v_1 - 2| + 3/4 |v_1 - 4| \quad (D.5)$$

The generalized hybrid representation for the 2-port \hat{N} in Fig. 19(d) can be

found to be

$$\underbrace{\begin{bmatrix} 1 & 2 \\ 0 & 1 \end{bmatrix}}_{\tilde{P}} \underbrace{\begin{bmatrix} v_1 \\ i_{in} \end{bmatrix}}_{\tilde{x}} = \underbrace{\begin{bmatrix} 0 & 1 \\ 1 & 0 \end{bmatrix}}_{\tilde{Q}} \underbrace{\begin{bmatrix} i_1 \\ v_{in} \end{bmatrix}}_{\tilde{y}} + \underbrace{\begin{bmatrix} 0 \\ 1 \end{bmatrix}}_{\tilde{s}} \quad (D.6)$$

By (D.5), (2.10), and (2.11),

$$\beta_{11} = 2, \beta_{12} = 4, \hat{a} = \begin{bmatrix} -1/2 \\ 0 \end{bmatrix}, \hat{B} = \begin{bmatrix} 1 & 0 \\ 0 & 0 \end{bmatrix}, \hat{C}_{11} = \begin{bmatrix} -5/4 \\ 0 \end{bmatrix}, \hat{C}_{12} = \begin{bmatrix} 3/4 \\ 0 \end{bmatrix} \quad (D.7)$$

By (D.6), (D.7), and (2.13),

$$\tilde{B} = \begin{bmatrix} -1 & -2 \\ 1 & -1 \end{bmatrix}, \tilde{a} = \begin{bmatrix} 0 \\ -1/2 \end{bmatrix}, \tilde{r} = \begin{bmatrix} -1 \\ 0 \end{bmatrix}, \tilde{C}_{11} = \begin{bmatrix} 0 \\ -5/4 \end{bmatrix}, \tilde{C}_{12} = \begin{bmatrix} 0 \\ 3/4 \end{bmatrix} \quad (D.8)$$

Substituting (D.8) into (2.12), we obtain the canonical piecewise-linear equation (3.58) for the circuit in Fig. 19(a).

3. Equation (5.1) in Example 5.1:

By Figs. 24(b) and (c), the canonical piecewise-linear equations of R_1 and R_2 can be found to be

$$R_1: i_1 = 2 + v_1 + |v_1| \quad (D.8a)$$

$$R_2: i_2 = 2 + v_2 + |v_2| \quad (D.8b)$$

The generalized hybrid representation for the 3-port \hat{N} in Fig. 24(d) can be found to be

$$\underbrace{\begin{bmatrix} 1 & -1 & 0 \\ 0 & 1 & 0 \\ 0 & 0 & 1 \end{bmatrix}}_{\tilde{P}} \underbrace{\begin{bmatrix} v_1 \\ v_2 \\ i_{in} \end{bmatrix}}_{\tilde{x}} = \underbrace{\begin{bmatrix} 1 & -1 & 0 \\ -1 & 0 & 1 \\ 0 & 0 & 1 \end{bmatrix}}_{\tilde{Q}} \underbrace{\begin{bmatrix} i_1 \\ i_2 \\ v_{in} \end{bmatrix}}_{\tilde{y}} + \underbrace{\begin{bmatrix} 0 \\ 0 \\ 0 \end{bmatrix}}_{\tilde{s}} \quad (D.9)$$

By (D.8), (2.10), and (2.11),

$$\beta_{11} = 0, \beta_{21} = 0, \hat{\underline{a}} = \begin{bmatrix} 2 \\ 2 \\ 0 \end{bmatrix}, \hat{\underline{B}} = \begin{bmatrix} 1 & 0 & 0 \\ 0 & 1 & 0 \\ 0 & 0 & 0 \end{bmatrix}, \hat{\underline{c}}_{11} = \begin{bmatrix} 1 \\ 0 \\ 0 \end{bmatrix}, \hat{\underline{c}}_{21} = \begin{bmatrix} 0 \\ 1 \\ 0 \end{bmatrix} \quad (\text{D.10})$$

By (D.9), (D.10), and (2.13),

$$\underline{B} = \begin{bmatrix} 0 & 0 & 0 \\ -1 & -1 & 0 \\ 0 & 0 & -1 \end{bmatrix}, \underline{a} = \begin{bmatrix} 0 \\ 2 \\ 0 \end{bmatrix}, \underline{r} = \begin{bmatrix} 0 \\ -1 \\ -1 \end{bmatrix}, \underline{c}_{11} = \begin{bmatrix} 1 \\ -1 \\ 0 \end{bmatrix}, \underline{c}_{21} = \begin{bmatrix} -1 \\ 0 \\ 0 \end{bmatrix} \quad (\text{D.11})$$

Substituting (D.11) into (2.12), we obtain the canonical piecewise-linear equation (5.1) for the circuit in Fig. 24(a).

4. Equation (5.47) in Example 5.3:

By Figs. 26(b) and (c), the canonical piecewise-linear equations of R_1 and R_2 can be found to be

$$R_1: i_1 = v_1 - 1/2 |v_1| + 1/2 |v_1 - 2| \quad (\text{D.12a})$$

$$R_2: i_2 = 1/2 + 3/2 \cdot v_2 - 1/2 |v_2 + 1| + |v_2 - 1| \quad (\text{D.12b})$$

The generalized hybrid representation for the 3-port \hat{N} in Fig. 26(d) can be found to be

$$\underbrace{\begin{bmatrix} 0 & 0 & 0 \\ 0 & 0 & 0 \\ 0 & 0 & -1 \end{bmatrix}}_{\underline{P}} \underbrace{\begin{bmatrix} v_1 \\ v_2 \\ i_{in} \end{bmatrix}}_{\underline{x}} = \underbrace{\begin{bmatrix} 1 & 0 & -1 \\ 0 & 1 & -1 \\ 0 & 0 & -1 \end{bmatrix}}_{\underline{Q}} \underbrace{\begin{bmatrix} i_1 \\ i_2 \\ v_{in} \end{bmatrix}}_{\underline{y}} + \underbrace{\begin{bmatrix} 0 \\ 0 \\ 0 \end{bmatrix}}_{\underline{s}} \quad (\text{D.13})$$

By (D.12), (2.10), and (2.11),

$$\beta_{11} = 0, \beta_{12} = 2, \beta_{21} = -1, \beta_{22} = 1, \hat{\underline{a}} = \begin{bmatrix} 0 \\ 1/2 \\ 0 \end{bmatrix}, \hat{\underline{B}} = \begin{bmatrix} 1 & 0 & 0 \\ 0 & 3/2 & 0 \\ 0 & 0 & 0 \end{bmatrix},$$

$$\hat{\underline{c}}_{11} = \begin{bmatrix} -1/2 \\ 0 \\ 0 \end{bmatrix}, \hat{\underline{c}}_{12} = \begin{bmatrix} 1/2 \\ 0 \\ 0 \end{bmatrix}, \hat{\underline{c}}_{21} = \begin{bmatrix} 0 \\ -1/2 \\ 0 \end{bmatrix}, \hat{\underline{c}}_{22} = \begin{bmatrix} 0 \\ 1 \\ 0 \end{bmatrix} \quad (\text{D.14})$$

By (D.13), (D.14), and (2.13),

$$\begin{aligned} \tilde{B} &= \begin{bmatrix} 1 & 0 & 0 \\ 0 & 3/2 & 0 \\ 0 & 0 & 1 \end{bmatrix}, \quad \tilde{a} = \begin{bmatrix} 0 \\ -1/2 \\ 0 \end{bmatrix}, \quad \tilde{r} = \begin{bmatrix} 1 \\ 1 \\ 1 \end{bmatrix}, \quad \zeta_{11} = \begin{bmatrix} -1/2 \\ 0 \\ 0 \end{bmatrix}, \\ \zeta_{12} &= \begin{bmatrix} 1/2 \\ 0 \\ 0 \end{bmatrix}, \quad \zeta_{21} = \begin{bmatrix} 0 \\ -1/2 \\ 0 \end{bmatrix}, \quad \zeta_{22} = \begin{bmatrix} 0 \\ 1 \\ 0 \end{bmatrix} \end{aligned} \quad (D.15)$$

Substituting (D.15) into (2.12), we obtain the canonical piecewise-linear equation (5.47) for the circuit in Fig. 26(a).

E. Detailed Calculations in Examples 4.1, 4.2, and 4.3

1. Example 4.1:

Starting point $\tilde{x}^{(0)} = [-2 \ -2 \ -2]^T$ with $\rho = \rho^{(0)} = -7/2$ is located at $R^{(0)}: -\infty \leq x_1 \leq 0$ and $-\infty \leq x_2 \leq 1$. By (3.29) and (3.30),

$$\tilde{B}^{(0)} = \begin{bmatrix} -1 & -1/2 & 0 \\ 1/4 & 1/2 & -1 \\ 0 & -1 & 1 \end{bmatrix}, \quad \text{and} \quad \tilde{d}^{(0)} = \begin{bmatrix} 4/5 \\ 2/5 \\ 2/5 \end{bmatrix} \quad (E.1)$$

By (3.31b),

$$\Delta\rho_1^{(0)} = \frac{0 - (-2)}{4/5} = 5/2, \quad \Delta\rho_2^{(0)} = \frac{1 - (-2)}{2/5} = 15/2 \quad (E.2)$$

Since $\Delta\rho_1^{(0)} < \Delta\rho_2^{(0)}$, we identify $j_0 = 1$ and hence $\Delta\rho^{(0)} = \Delta\rho_1^{(0)} = 5/2$. Using (3.32) and (3.33), we calculate the next breakpoint:

$$\rho^{(1)} = -7/2 + 5/2 = -1, \quad \tilde{x}^{(1)} = \begin{bmatrix} -2 \\ -2 \\ -2 \end{bmatrix} + 5/2 \begin{bmatrix} 4/5 \\ 2/5 \\ 2/5 \end{bmatrix} = \begin{bmatrix} 0 \\ -1 \\ -1 \end{bmatrix} \quad (E.3)$$

The next region $R^{(1)}$ corresponds to segment (2,1) and is characterized by $0 \leq x_1 \leq \infty$ and $-\infty \leq x_2 \leq 1$. Using (3.35), (3.36), and (3.39), we obtain

$$\tilde{d}^{(1)} = [1/3 \ 4/3 \ 4/3]^T \quad (E.4)$$

Since $d_1^{(1)} \cdot d_1^{(0)} \cdot \Delta\rho^{(0)} = 1/3 \cdot 4/5 \cdot 5/2 > 0$, the direction vector $\tilde{d}^{(1)}$ points in

the correct direction and it follows from (3.41b) that

$$\Delta\rho_1^{(1)} = \frac{\infty-0}{1/3} = \infty, \quad \Delta\rho_2^{(1)} = \frac{1-(-1)}{4/3} = 3/2 \quad (\text{E.5})$$

Since $\Delta\rho_1^{(1)} > \Delta\rho_2^{(1)}$, we identify $j_1 = 2$ and hence $\Delta\rho^{(1)} = \Delta\rho_2^{(1)} = 3/2$. Using (3.44) and (3.45), we calculate the next breakpoint

$$\rho^{(2)} = -1 + 3/2 = 1/2 \text{ and } \underline{x}^{(2)} = \begin{bmatrix} 0 \\ -1 \\ -1 \end{bmatrix} + 3/2 \begin{bmatrix} 1/3 \\ 4/3 \\ 4/3 \end{bmatrix} = \begin{bmatrix} 1/2 \\ 1 \\ 1 \end{bmatrix} \quad (\text{E.6})$$

The next region $R^{(2)}$ corresponds to segment (2,2) and is characterized by $0 \leq x_1 \leq \infty$ and $1 \leq x_2 \leq \infty$. Using (3.35), (3.36), and (3.39), we obtain

$$\underline{d}^{(2)} = [-3/5 \quad 2/5 \quad 2/5]^T \quad (\text{E.7})$$

Since $d_2^{(2)} \cdot d_2^{(1)} \cdot \Delta\rho^{(1)} = 2/5 \cdot 4/3 \cdot 3/2 > 0$, $\underline{d}^{(2)}$ points to the correct direction and it follows from (3.41)

$$\Delta\rho_1^{(2)} = \frac{1/2-0}{|-3/5|} = 5/6, \quad \Delta\rho_2^{(2)} = \frac{\infty-1}{2/5} = \infty \quad (\text{E.8})$$

Since $\Delta\rho_1^{(2)} < \Delta\rho_2^{(2)}$, we identify $j_2 = 1$ and hence $\Delta\rho^{(2)} = \Delta\rho_1^{(2)} = 5/6$. Using (3.44) and (3.45), we calculate the next breakpoint

$$\rho^{(3)} = 1/2 + 5/6 = 4/3, \quad \underline{x}^{(3)} = \begin{bmatrix} 1/2 \\ 1 \\ 1 \end{bmatrix} + 5/6 \begin{bmatrix} -3/5 \\ 2/5 \\ 2/5 \end{bmatrix} = \begin{bmatrix} 0 \\ 4/3 \\ 4/3 \end{bmatrix} \quad (\text{E.9})$$

The next region $R^{(3)}$ corresponds to segment (1,2) and is characterized by $-\infty \leq x_1 \leq 0$ and $1 \leq x_2 \leq \infty$. Using (3.35), (3.36), and (3.39), we obtain

$$\underline{d}^{(3)} = [3/2 \quad -1/8 \quad -1/8]^T \quad (\text{E.10})$$

Since $d_1^{(3)} \cdot d_1^{(2)} \cdot \Delta\rho^{(2)} = 3/2 \cdot (-3/5) \cdot 5/6 < 0$, the solution curve in $R^{(3)}$ will follow the direction of $-\underline{d}^{(3)}$ and goes to infinity without hitting any boundary hyperplane of $R^{(3)}$. Hence, we choose

$$\Delta\rho^{(3)} = -4, \quad \rho^{(4)} = 4/3 - 4 = -8/3, \text{ and } \underline{x}^{(4)} = \begin{bmatrix} 0 \\ 4/3 \\ 4/3 \end{bmatrix} - 4 \begin{bmatrix} 3/2 \\ -1/8 \\ -1/8 \end{bmatrix} = \begin{bmatrix} -6 \\ 11/6 \\ 11/6 \end{bmatrix} \quad (\text{E.11})$$

as a point in the end segment of the solution curve. Equations (E.3), (E.6), (E.9) and (E.11) will give breakpoints $\underline{x}^{(1)}$, $\underline{x}^{(2)}$, $\underline{x}^{(3)}$ and a point $\underline{x}^{(4)}$ in the end segment.

2. Example 4.2:

(a) Γ_1 branch:

Starting point $\underline{x}^{(0)} = [0 \ 0 \ 0]^T$ with $\rho = \rho^{(0)} = 0$ is located at $R^{(0)} : -\infty \leq x_1 \leq 1.2$ and $-\infty \leq x_2 \leq 0.8$. By (3.29) and (3.30),

$$\underline{B}^{(0)} = \begin{bmatrix} 2 & 0 & -1 \\ 0 & 5 & -1 \\ -1 & -1 & -3.2 \end{bmatrix}, \quad \underline{d}^{(0)} = \begin{bmatrix} 5/39 \\ 2/39 \\ 10/39 \end{bmatrix} \quad (\text{E.12})$$

By (3.31b),

$$\Delta\rho_1^{(0)} = \frac{1.2-0}{5/39} = 234/25, \quad \Delta\rho_2^{(0)} = \frac{0.8-0}{2/39} = 78/5 \quad (\text{E.13})$$

Since $\Delta\rho_1^{(0)} < \Delta\rho_2^{(0)}$, we identify $j_0 = 1$ and hence $\Delta\rho^{(0)} = \Delta\rho_1^{(0)} = 234/25$. Using (3.32) and (3.33), we calculate the next breakpoint:

$$\rho^{(1)} = 0 + 234/25 = 234/25, \quad \underline{x}^{(1)} = \begin{bmatrix} 0 \\ 0 \\ 0 \end{bmatrix} + 234/25 \begin{bmatrix} 5/39 \\ 2/39 \\ 10/39 \end{bmatrix} = \begin{bmatrix} 1.2 \\ 0.48 \\ 2.4 \end{bmatrix} \quad (\text{E.14})$$

The next region $R^{(1)}$ corresponds to segment (2,1) and is characterized by $1.2 \leq x_1 \leq 3$ and $-\infty \leq x_2 \leq 0.8$. Using (3.35), (3.36), and (3.39), we obtain

$$\underline{d}^{(1)} = [-45/74 \ 7/74 \ 35/74]^T \quad (\text{E.15})$$

Since $d_1^{(1)} \cdot d_1^{(0)} \cdot \Delta\rho^{(0)} = -45/74 \cdot 5/39 \cdot 234/25 < 0$, $\underline{d}^{(1)}$ points in the opposite direction and it follows from (3.41) that

$$\Delta\rho_1^{(1)} = \frac{3-1.2}{|-45/74|} = 74/25, \quad \Delta\rho_2^{(1)} = \frac{0.48-(-\infty)}{7/74} = \infty \quad (\text{E.16})$$

Since $\Delta\rho_1^{(1)} < \Delta\rho_2^{(1)}$, we identify $j_1 = 1$ and hence $\Delta\rho^{(1)} = -\Delta\rho_1^{(1)} = -74/25$. Using (3.44) and (3.45), we calculate the next breakpoint

$$\rho^{(2)} = 234/25 - 74/25 = 6.4, \quad \tilde{x}^{(2)} = \begin{bmatrix} 1.2 \\ 0.48 \\ 2.4 \end{bmatrix} - 74/25 \begin{bmatrix} -45/74 \\ 7/74 \\ 35/74 \end{bmatrix} = \begin{bmatrix} 3 \\ 0.2 \\ 1 \end{bmatrix} \quad (\text{E.17})$$

The next region $R^{(2)}$ corresponds to segment (3,1) and is characterized by $3 \leq x_1 \leq \infty$ and $-\infty \leq x_2 \leq 0.8$. Using (3.35), (3.36), and (3.39), we obtain

$$\underline{d}^{(2)} = [10/61 \quad 3/61 \quad 15/61]^T \quad (\text{E.18})$$

Since $d_1^{(2)} \cdot d_1^{(1)} \cdot \Delta\rho^{(1)} = 10/61 \cdot (-45/74) \cdot (-74/25) > 0$, $\underline{d}^{(2)}$ points to the correct direction and it follows from (3.41),

$$\Delta\rho_1^{(2)} = \frac{\infty - 3}{10/61} = \infty, \quad \Delta\rho_2^{(2)} = \frac{0.8 - 0.2}{3/61} = 12.2 \quad (\text{E.19})$$

Since $\Delta\rho_2^{(2)} < \Delta\rho_1^{(2)}$, we identify $j_2 = 2$ and hence $\Delta\rho^{(2)} = \Delta\rho_2^{(2)} = 12.2$. Using (3.44) and (3.45), we calculate the next breakpoint

$$\rho^{(3)} = 6.4 + 12.2 = 18.6, \quad \tilde{x}^{(3)} = \begin{bmatrix} 3 \\ 0.2 \\ 1 \end{bmatrix} + 12.2 \cdot \begin{bmatrix} 10/61 \\ 3/61 \\ 15/61 \end{bmatrix} = \begin{bmatrix} 5 \\ 0.8 \\ 4 \end{bmatrix} \quad (\text{E.20})$$

The next region $R^{(3)}$ corresponds to segment (3,2) and is characterized by $3 \leq x_1 \leq \infty$ and $0.8 \leq x_2 \leq 2$. Using (3.35), (3.36), and (3.39), we obtain

$$\underline{d}^{(3)} = [20/101 \quad -15/101 \quad 30/101]^T \quad (\text{E.21})$$

Since $d_2^{(3)} \cdot d_2^{(2)} \cdot \Delta\rho^{(2)} = -15/101 \cdot 3/61 \cdot 12.2 < 0$, $\underline{d}^{(3)}$ points to the opposite direction and it follows from (3.41),

$$\Delta\rho_1^{(3)} = \frac{5 - 3}{20/101} = 10.1, \quad \Delta\rho_2^{(3)} = \frac{2 - 0.8}{|-15/101|} = 202/25 \quad (\text{E.22})$$

Since $\Delta\rho_2^{(3)} < \Delta\rho_1^{(3)}$, we identify $j_3 = 2$ and hence $\Delta\rho^{(3)} = -\Delta\rho_2^{(3)} = -202/25$. Using (3.44) and (3.45), we calculate the next breakpoint

$$\rho^{(4)} = 18.6 - 202/25 = 10.52, \quad \tilde{x}^{(4)} = \begin{bmatrix} 5 \\ 0.8 \\ 4 \end{bmatrix} - 202/25 \cdot \begin{bmatrix} 20/101 \\ -15/101 \\ 30/101 \end{bmatrix} = \begin{bmatrix} 3.4 \\ 2 \\ 1.6 \end{bmatrix} \quad (\text{E.23})$$

The next region $R^{(4)}$ corresponds to segment (3,3) and is characterized by

$3 \leq x_1 \leq \infty$ and $2 \leq x_2 \leq \infty$. Using (3.35), (3.36), and (3.39), we obtain

$$\underline{d}^{(4)} = [10/63 \quad 5/63 \quad 5/21]^T \quad (E.24)$$

Since $\underline{d}_2^{(4)} \cdot \underline{d}_2^{(3)} \cdot \Delta\rho^{(3)} = 5/63 \cdot (-15/101) \cdot (-202/25) > 0$, $\underline{d}^{(4)}$ points to the correct direction and it follows from (3.41) that

$$\Delta\rho_1^{(4)} = \frac{\infty - 3.4}{10/63} = \infty, \quad \Delta\rho_2^{(4)} = \frac{\infty - 2}{5/63} = \infty \quad (E.25)$$

Hence, the solution curve goes to infinity without hitting any boundary of $R^{(4)}$. Hence, we choose

$$\Delta\rho^{(4)} = 9.48, \quad \rho^{(5)} = 10.52 + 9.48 = 20, \quad \underline{x}^{(5)} = \begin{bmatrix} 3.4 \\ 2 \\ 1.6 \end{bmatrix} + 9.48 \cdot \begin{bmatrix} 10/63 \\ 5/63 \\ 5/21 \end{bmatrix} = \begin{bmatrix} 4.9 \\ 2.75 \\ 3.86 \end{bmatrix} \quad (E.26)$$

as a point in the end segment of the solution curve. Equations (E.14), (E.17), (E.20), (E.23), and (E.26) will give breakpoints $\underline{x}^{(1)}$, $\underline{x}^{(2)}$, $\underline{x}^{(3)}$, $\underline{x}^{(4)}$, and a point $\underline{x}^{(5)}$ in the end segment.

(b) Γ_2 branch:

Starting point $\hat{\underline{x}}^{(0)} = [9/8 \quad 67/40 \quad 9/4]^T$ with $\hat{\rho}^{(0)} = 10$ is located at $\hat{R}^{(0)} : -\infty \leq x_1 \leq 1.2$ and $0.8 \leq x_2 \leq 2$. By (3.29) and (3.30),

$$\hat{\underline{B}}^{(0)} = \begin{bmatrix} 2 & 0 & -1 \\ 0 & -2 & -1 \\ -1 & -1 & -3.2 \end{bmatrix}, \quad \hat{\underline{d}}^{(0)} = \begin{bmatrix} 5/32 \\ -5/32 \\ 5/16 \end{bmatrix} \quad (E.27)$$

By (3.31b),

$$\Delta\hat{\rho}_1^{(0)} = \frac{1.2 - 9/8}{5/32} = 12/25, \quad \Delta\hat{\rho}_2^{(0)} = \frac{67/40 - 0.8}{|-5/32|} = 28/5 \quad (E.28)$$

Since $\Delta\hat{\rho}_1^{(0)} < \Delta\hat{\rho}_2^{(0)}$, we identify $\hat{j}_0 = 1$ and hence $\Delta\hat{\rho}^{(0)} = \Delta\hat{\rho}_1^{(0)} = 12/25$. Using (3.32) and (3.33), we calculate the next breakpoint:

$$\hat{\rho}^{(1)} = 10 + 12/25 = 10.48, \quad \hat{\underline{x}}^{(1)} = \begin{bmatrix} 9/8 \\ 67/40 \\ 9/4 \end{bmatrix} + 12/25 \cdot \begin{bmatrix} 5/32 \\ -5/32 \\ 5/16 \end{bmatrix} = \begin{bmatrix} 1.2 \\ 1.6 \\ 2.4 \end{bmatrix} \quad (E.29)$$

The next region $\hat{R}^{(1)}$ corresponds to segment (2,2) and is characterized by $1.2 \leq x_1 \leq 3$ and $0.8 \leq x_2 \leq 2$. Using (3.35), (3.36), and (3.39), we obtain

$$\hat{d}^{(1)} = [-10/11 \quad -35/99 \quad 70/99]^T \quad (\text{E.30})$$

Since $\hat{d}_1^{(1)} \cdot \hat{d}_1^{(0)} \cdot \Delta \hat{\rho}^{(0)} = -10/11 \cdot 5/32 \cdot 12/25 < 0$, $\hat{d}^{(1)}$ points in the opposite direction and it follows from (3.41) that

$$\Delta \hat{\rho}_1^{(1)} = \frac{3-1.2}{|-10/11|} = 1.98, \quad \Delta \hat{\rho}^{(1)} = \frac{2-1.6}{|-35/99|} = 198/175 \quad (\text{E.31})$$

Since $\Delta \hat{\rho}_2^{(1)} < \Delta \hat{\rho}_1^{(1)}$, we identify $\hat{j}_1 = 2$ and hence $\Delta \hat{\rho}^{(1)} = -\Delta \hat{\rho}_2^{(1)} = -198/175$. Using (3.44) and (3.45), we calculate the next breakpoint:

$$\hat{\rho}^{(2)} = 10.48 - 198/175 = 9.35, \quad \hat{x}^{(2)} = \begin{bmatrix} 1.2 \\ 1.6 \\ 2.4 \end{bmatrix} - 198/175 \cdot \begin{bmatrix} -10/11 \\ -35/99 \\ 70/99 \end{bmatrix} = \begin{bmatrix} 78/35 \\ 2 \\ 1.6 \end{bmatrix} \quad (\text{E.32})$$

The next region $\hat{R}^{(2)}$ is characterized by $1.2 \leq x_1 \leq 3$ and $2 \leq x_2 \leq \infty$ and corresponds to segment (2,3). Using (3.35), (3.36), and (3.39), we obtain

$$\hat{d}^{(2)} = [-135/236 \quad 35/236 \quad 105/236]^T \quad (\text{E.33})$$

Since $\hat{d}_2^{(2)} \cdot \hat{d}_2^{(1)} \cdot \Delta \hat{\rho}^{(1)} = 35/236 \cdot (-35/99) \cdot (-198/175) > 0$, $\hat{d}^{(2)}$ points in the correct direction and it follows from (3.41) that

$$\Delta \hat{\rho}_1^{(2)} = \frac{78/35-1.2}{|-135/236|} = 1.8, \quad \Delta \hat{\rho}_2^{(2)} = \frac{\infty-2}{35/236} = \infty \quad (\text{E.34})$$

Since $\Delta \hat{\rho}_1^{(2)} < \Delta \hat{\rho}_2^{(2)}$, we identify $\hat{j}_2 = 1$ and $\Delta \hat{\rho}^{(2)} = \Delta \hat{\rho}_1^{(2)} = 1.8$. Using (3.44) and (3.45), we calculate the next breakpoint:

$$\hat{\rho}^{(3)} = 9.35 + 1.8 = 11.15, \quad \hat{x}^{(3)} = \begin{bmatrix} 78/35 \\ 2 \\ 1.6 \end{bmatrix} + 1.8 \cdot \begin{bmatrix} -135/236 \\ 35/236 \\ 105/236 \end{bmatrix} = \begin{bmatrix} 1.2 \\ 34/15 \\ 2.4 \end{bmatrix} \quad (\text{E.35})$$

The next region $\hat{R}^{(3)}$ is characterized by $-\infty \leq x_1 \leq 1.2$ and $2 \leq x_2 \leq \infty$ and corresponds to segment (1,3). Using (3.35), (3.36), and (3.39), we obtain

$$\hat{d}^{(3)} = [15/121 \quad 10/121 \quad 30/121]^T \quad (\text{E.36})$$

Since $\hat{d}_1^{(3)} \cdot \hat{d}_1^{(2)} \cdot \Delta\rho^{(2)} = 15/121 \cdot (-135/236) \cdot 1.8 < 0$, $\hat{d}^{(3)}$ points to the opposite direction and it follows from (3.41) that

$$\Delta\hat{\rho}_1^{(3)} = \frac{1.2 - (-\infty)}{15/121} = \infty, \quad \Delta\hat{\rho}_2^{(3)} = \frac{34/15 - 2}{10/121} = 242/75 \quad (\text{E.37})$$

Since $\Delta\hat{\rho}_2^{(3)} < \Delta\hat{\rho}_1^{(3)}$, we identify $\hat{j}_3 = 2$ and hence $\Delta\hat{\rho}^{(3)} = -\Delta\hat{\rho}_2^{(3)} = -242/75$. Using (3.44) and (3.45), we calculate the next breakpoint:

$$\hat{\rho}^{(4)} = 11.15 - 242/75 = 7.92, \quad \hat{x}^{(4)} = \begin{bmatrix} 1.2 \\ 34/15 \\ 2.4 \end{bmatrix} - 242/75 \begin{bmatrix} 15/121 \\ 10/121 \\ 30/121 \end{bmatrix} = \begin{bmatrix} 0.8 \\ 2 \\ 1.6 \end{bmatrix} \quad (\text{E.38})$$

The next region $R^{(4)}$ corresponds to segment (1,2) and is characterized by $-\infty \leq x_1 \leq 1.2$ and $0.8 \leq x_2 \leq 2$, which is exactly the same as region $R^{(0)}$. It follows that the solution curve re-enters region $R^{(0)}$ and by Observation 3 in Section 5C, it becomes cyclic as shown in Fig. 21. Equations (E.29), (E.32), (E.35), and (E.38) will give breakpoints $\hat{x}^{(1)}$, $\hat{x}^{(2)}$, $\hat{x}^{(3)}$, and $\hat{x}^{(4)}$.

3. Example 4.3

Starting point $\underline{x}^{(0)} = [0 \ 0 \ 0]^T$ with $\rho^{(0)} = 0$ is located at $R^{(0)} : -\infty \leq x_1 \leq 0.4$ and $-\infty \leq x_2 \leq 0.4$. By (3.29) and (3.30),

$$\underline{B}^{(0)} = \begin{bmatrix} 0.25 & 1 & 0 \\ 20 & 1 & 0 \\ 1 & 0 & -8000 \end{bmatrix}, \quad \underline{d}^{(0)} = \begin{bmatrix} 5.05 \times 10^{-2} \\ -1.01 \\ 6.33 \times 10^{-6} \end{bmatrix} \quad (\text{E.39})$$

By (3.31b),

$$\Delta\rho_1^{(0)} = \frac{0.4 - 0}{5.05 \times 10^{-2}} = 7.93, \quad \Delta\rho_2^{(0)} = \frac{0 - (-\infty)}{|-1.01|} = \infty \quad (\text{E.40})$$

Since $\Delta\rho_1^{(0)} < \Delta\rho_2^{(0)}$, we identify $j_0 = 1$ and hence $\Delta\rho^{(0)} = \Delta\rho_1^{(0)} = 7.93$. Using (3.32) and (3.33), we calculate the next breakpoint:

$$\rho^{(1)} = 0 + 7.93 = 7.93, \quad \underline{x}^{(1)} = \begin{bmatrix} 0 \\ 0 \\ 0 \end{bmatrix} + 7.93 \cdot \begin{bmatrix} 5.05 \times 10^{-2} \\ -1.01 \\ 6.33 \times 10^{-6} \end{bmatrix} = \begin{bmatrix} 0.4 \\ -8.03 \\ 5.02 \times 10^{-5} \end{bmatrix} \quad (\text{E.41})$$

The next region $R^{(1)}$ corresponds to segment (2,1) and is characterized by $0.4 \leq x_1 \leq 0.6$ and $-\infty \leq x_2 \leq 0.4$. Using (3.35), (3.36), and (3.39), we obtain

$$\underline{d}^{(1)} = [6.69 \times 10^{-2} \quad -9.84 \times 10^{-1} \quad 4.37 \times 10^{-5}]^T \quad (\text{E.42})$$

Since $\underline{d}_1^{(1)} \cdot \underline{d}_1^{(0)} \cdot \Delta\rho^{(0)} = 6.69 \times 10^{-2} \cdot 5.05 \times 10^{-2} \cdot 0.4 > 0$, $\underline{d}^{(1)}$ points to the correct direction and by (3.41),

$$\Delta\rho_1^{(1)} = \frac{0.6-0.4}{6.69 \times 10^{-2}} = 2.97, \quad \Delta\rho_2^{(1)} = \frac{-8.03-(-\infty)}{|-9.84 \times 10^{-1}|} = \infty \quad (\text{E.43})$$

Since $\Delta\rho_1^{(1)} < \Delta\rho_2^{(1)}$, we identify $j_1 = 1$ and hence $\Delta\rho^{(1)} = \Delta\rho_1^{(1)} = 2.97$. Using (3.44) and (3.45), we calculate the next breakpoint:

$$\rho^{(2)} = 7.93 + 2.97 = 10.9, \quad \underline{x}^{(2)} = \begin{bmatrix} 0.4 \\ -8.03 \\ 5.02 \times 10^{-5} \end{bmatrix} + 2.97 \begin{bmatrix} 6.69 \times 10^{-2} \\ -9.84 \times 10^{-1} \\ 4.37 \times 10^{-5} \end{bmatrix} = \begin{bmatrix} 0.6 \\ -10.9 \\ 1.81 \times 10^{-4} \end{bmatrix} \quad (\text{E.44})$$

The next region $R^{(2)}$ is characterized by $0.6 \leq x_1 \leq \infty$ and $-\infty \leq x_2 \leq 0.4$ and corresponds to segment (3,1). Using (3.35), (3.36), and (3.39), we obtain

$$\underline{d}^{(2)} = [-1.06 \times 10^{-2} \quad -1.12 \quad -1.33 \times 10^{-4}]^T \quad (\text{E.45})$$

Since $\underline{d}_1^{(2)} \cdot \underline{d}_1^{(1)} \cdot \Delta\rho^{(1)} = -1.06 \times 10^{-2} \cdot 6.69 \times 10^{-2} \cdot 2.97 < 0$, $\underline{d}^{(2)}$ points to the opposite direction and by (3.41),

$$\Delta\rho_1^{(2)} = \frac{\infty-0.6}{|-1.06 \times 10^{-2}|} = \infty, \quad \Delta\rho_2^{(2)} = \frac{0.4-(-10.9)}{|-1.12|} = 10.12 \quad (\text{E.46})$$

Since $\Delta\rho_2^{(2)} < \Delta\rho_1^{(2)}$, we identify $j_2 = 2$ and hence $\Delta\rho^{(2)} = -\Delta\rho_2^{(2)} = -10.12$. Using (3.44) and (3.45), we calculate the next breakpoint:

$$\rho^{(3)} = 10.9 - 10.12 = 0.78, \quad \underline{x}^{(3)} = \begin{bmatrix} 0.6 \\ -10.9 \\ 1.81 \times 10^{-4} \end{bmatrix} - 10.12 \begin{bmatrix} -1.06 \times 10^{-2} \\ -1.12 \\ -1.33 \times 10^{-4} \end{bmatrix} = \begin{bmatrix} 0.708 \\ 0.4 \\ 1.53 \times 10^{-3} \end{bmatrix} \quad (\text{E.47})$$

The next region $R^{(3)}$ corresponds to segment (3,2) and is characterized by

$0.6 \leq x_1 \leq \infty$ and $0.4 \leq x_2 \leq 0.6$. Using (3.35), (3.36), and (3.39), we obtain

$$\underline{d}^{(3)} = [0.289 \quad 0.315 \quad 3.44 \times 10^{-3}]^T \quad (\text{E.48})$$

Since $d_2^{(3)} \cdot d_2^{(2)} \cdot \Delta\rho^{(2)} = 0.315 \cdot (-1.12) \cdot (-10.12) > 0$, $\underline{d}^{(3)}$ points to the correct direction and by (3.41),

$$\Delta\rho_1^{(3)} = \frac{\infty - 0.708}{0.289} = \infty, \quad \Delta\rho_2^{(3)} = \frac{0.6 - 0.4}{0.315} = 0.63 \quad (\text{E.49})$$

Since $\Delta\rho_2^{(3)} < \Delta\rho_1^{(3)}$, we identify $j_3 = 2$ and hence $\Delta\rho^{(3)} = \Delta\rho_2^{(3)} = 0.63$. Using (3.44) and (3.45), we calculate the next breakpoint:

$$\rho^{(4)} = 0.78 + 0.63 = 1.41, \quad \underline{x}^{(4)} = \begin{bmatrix} 0.708 \\ 0.4 \\ 1.53 \times 10^{-3} \end{bmatrix} + 0.63 \cdot \begin{bmatrix} 0.289 \\ 0.315 \\ 3.44 \times 10^{-3} \end{bmatrix} = \begin{bmatrix} 0.891 \\ 0.6 \\ 3.71 \times 10^{-3} \end{bmatrix} \quad (\text{E.50})$$

The next region $R^{(4)}$ corresponds to segment (3,3) and is characterized by $0.6 \leq x_1 \leq \infty$ and $0.6 \leq x_2 \leq \infty$. Using (3.35), (3.36), and (3.39), we obtain

$$\underline{d}^{(4)} = [0.225 \quad 1.06 \times 10^{-2} \quad 2.68 \times 10^{-3}]^T \quad (\text{E.51})$$

Since $d_2^{(4)} \cdot d_2^{(3)} \cdot \Delta\rho^{(3)} = 1.06 \times 10^{-2} \cdot 0.315 \cdot 0.63 > 0$, the solution curve follows the direction of $\underline{d}^{(4)}$ and goes to infinity without hitting any boundary of $R^{(4)}$. Hence, we choose

$$\begin{aligned} \Delta\rho^{(4)} = 0.59, \quad \rho^{(5)} = 1.41 + 0.59 = 2.0, \quad \underline{x}^{(5)} &= \begin{bmatrix} 0.891 \\ 0.6 \\ 3.71 \times 10^{-3} \end{bmatrix} + 0.59 \begin{bmatrix} 0.225 \\ 1.06 \times 10^{-2} \\ 2.68 \times 10^{-3} \end{bmatrix} \\ &= \begin{bmatrix} 1.02 \\ 0.606 \\ 5.29 \times 10^{-3} \end{bmatrix} \end{aligned} \quad (\text{E.52})$$

as a point in the end segment of the solution curve. Equations (E.41), (E.44), (E.47), (E.50), and (E.52) will give breakpoints $\underline{x}^{(1)}$, $\underline{x}^{(2)}$, $\underline{x}^{(3)}$, $\underline{x}^{(4)}$ and $\underline{x}^{(5)}$ in the end segment of the solution curve.

REFERENCES

- [1] L. O. Chua and R. Ying, "Canonical piecewise-linear analysis," IEEE Trans. Circuits and Systems, Vol. CAS-30, pp. 125-140, Mar. 1983.
- [2] L. O. Chua and R. Ying, "Finding all solutions of piecewise-linear circuits," Int. J. Circuit Theory and Applications, Vol. 10, pp. 201-229, 1982.
- [3] L. O. Chua and S. M. Kang, "Section-wise piecewise-linear functions: canonical representation, properties, and applications," Proceedings of the IEEE, Vol. 65, pp. 915-929, June 1977.
- [4] L. O. Chua and P. M. Lin, Computer Aided Analysis of Electronic Circuits: Algorithms and Computational Techniques, Prentice-Hall, Englewood Cliffs, NJ, 1975.
- [5] L. O. Chua, J. Yu, and Y. Yu, "Negative resistance devices," Int. J. Circuit Theory and Applications, Vol. 11, pp. 161-186, April 1983.
- [6] L. O. Chua, J. Yu, and Y. Yu, "Bipolar-JFET-MOSFET negative resistance devices," University of California, Berkeley, Memorandum No. UCB/ERL M82/84, Nov. 15, 1982.
- [7] L. O. Chua and A. Ushida, "A switching-parameter algorithm for finding multiple solutions of nonlinear resistive circuits," Int. J. Circuit Theory and Applications, Vol. 4, pp. 215-239, 1976.
- [8] C. W. Yun and K. S. Chao, "Simple solution curves of nonlinear resistive networks," Int. J. Circuit Theory and Applications, Vol. 11, pp. 47-55, 1983.
- [9] F. H. Branin, "Widely convergent method for finding multiple solutions of simultaneous nonlinear equations," IBM J. Res. Develop., Vol. 16, pp. 504-522, 1972.
- [10] A. Ushida and L. O. Chua, "Tracing solution curves of nonlinear equation with sharp turning points," Int. J. Circuit Theory and Applications, to appear.
- [11] M. J. Chien, "Searching for multiple solutions of nonlinear systems," IEEE Trans. Circuits and Systems, Vol. CAS-26, pp. 817-827, Oct. 1979.
- [12] S. M. Lee and K. S. Chao, "Multiple solutions of piecewise-linear resistive networks," IEEE Trans. Circuits and Systems, Vol. CAS-30, pp. 84-88, Feb. 1983.
- [13] L. O. Chua and R. A. Rohrer, "On the dynamic equation of a class of nonlinear RLC networks," IEEE Trans. on Circuit Theory, Vol. 12, pp. 475-489, Dec. 1965.
- [14] L. O. Chua and N. N. Wang, "On the application of degree theory to the analysis of resistive nonlinear networks," Int. J. Circuit Theory and Applications, Vol. 5, pp. 35-68, 1977.
- [15] L. O. Chua, Introduction to Nonlinear Network Theory, McGraw-Hill, 1969.
- [16] T. Ohtsuki, T. Fujisawa, and S. Kumagai, "Existence theorems and a solution algorithm for piece-wise linear resistor networks," SIAM J. Math. Anal., Vol. 8, No. 1, pp. 69-99, Feb. 1977.
- [17] A. Vladimirescu, K. Zhang, A. R. Newton, D. O. Pederson, and A. Sangiovanni-Vincentelli, "SPICE Version 2G Users Guide," University of California, Berkeley, Aug. 10, 1981 (unpublished).
- [18] M. J. Chien and E. S. Kuh, "Solving piecewise-linear equation for resistive networks," Int. J. Circuit Theory and Applications, Vol. 4, pp. 3-24, 1976.

FIGURE CAPTIONS

- Fig. 1. (a) A piecewise-linear one-port N driven by y_{in} , which can be either a voltage source v_{in} , or a current source i_{in} . (b) Typical piecewise-linear driving-point characteristic plotted with $y_{in} = v_{in}$ as the independent variable. (c) Typical piecewise-linear driving-point characteristic plotted with $y_{in} = i_{in}$ as the independent variable.
- Fig. 2. (a) A piecewise-linear two-port N driven by y_{in} , which can be either a voltage source v_{in} , or a current source i_{in} , and the open-circuit voltage v_0 taken as the output variable. (b) Same as in (a) but with the short-circuit current i_0 taken as the output variable. (c) Typical piecewise-linear transfer characteristic.
- Fig. 3. (a) Resistor R_1 with two breakpoints $v_1 = -1$ and $v_1 = 2$. (b) Resistor R_2 with one breakpoint at $i_2 = 3$. (c) The two vertical lines (parallel to x_2) $x_1 = -1$ and $x_1 = 2$ and the horizontal line (parallel to x_1) $x_2 = 3$ partition the $x_1 - x_2$ plane into 6 distinct rectangular regions inside each of which the circuit is described by an affine function. Region (j,k) corresponds to the linear circuit where resistor R_1 is operating in segment j and resistor R_2 is operating in segment k .
- Fig. 4. (a) Linear $(n+1)$ -port \hat{N} terminated by voltage-controlled resistors R_1, R_2, \dots, R_ℓ on the left, current-controlled resistors $R_{\ell+1}, R_{\ell+2}, \dots, R_n$ on the right and the input voltage source v_{in} across the driving port $(n+1)$. (b) Linear $(n+1)$ -port \hat{N} from (a) terminated by voltage sources v_1, v_2, \dots, v_ℓ on the left, current sources $i_{\ell+1}, i_{\ell+2}, \dots, i_n$ on the right, and the input voltage source v_{in} across port $(n+1)$.
- Fig. 5. (a) Circuit for Example 2.1. (b) Linear 3-port \hat{N} terminated by nonlinear resistors R_1 and R_2 and voltage source v_{in} . (c) Voltage-controlled $v_1 - i_1$ curve for R_1 . (d) Current-controlled $i_2 - v_2$ curve for R_2 .
- Fig. 6. (a) Circuit for Example 2.2. (b) Linear 3-port \hat{N} terminated by voltage-controlled resistors R_1 and R_2 and voltage source v_{in} . (c) $v_1 - i_1$ curve for R_1 . (d) $v_2 - i_2$ curve for R_2 .
- Fig. 7. (a) Circuit for Example 2.3. (b) Linear 3-Port \hat{N} terminated by current-controlled resistors R_1 and R_2 and voltage source v_{in} . (c) $v_1 - i_1$ curve for R_1 . (d) $v_2 - i_2$ curve for R_2 .
- Fig. 8. (a) Circuit for Example 2.4. (b) Linear 3-port \hat{N} terminated by

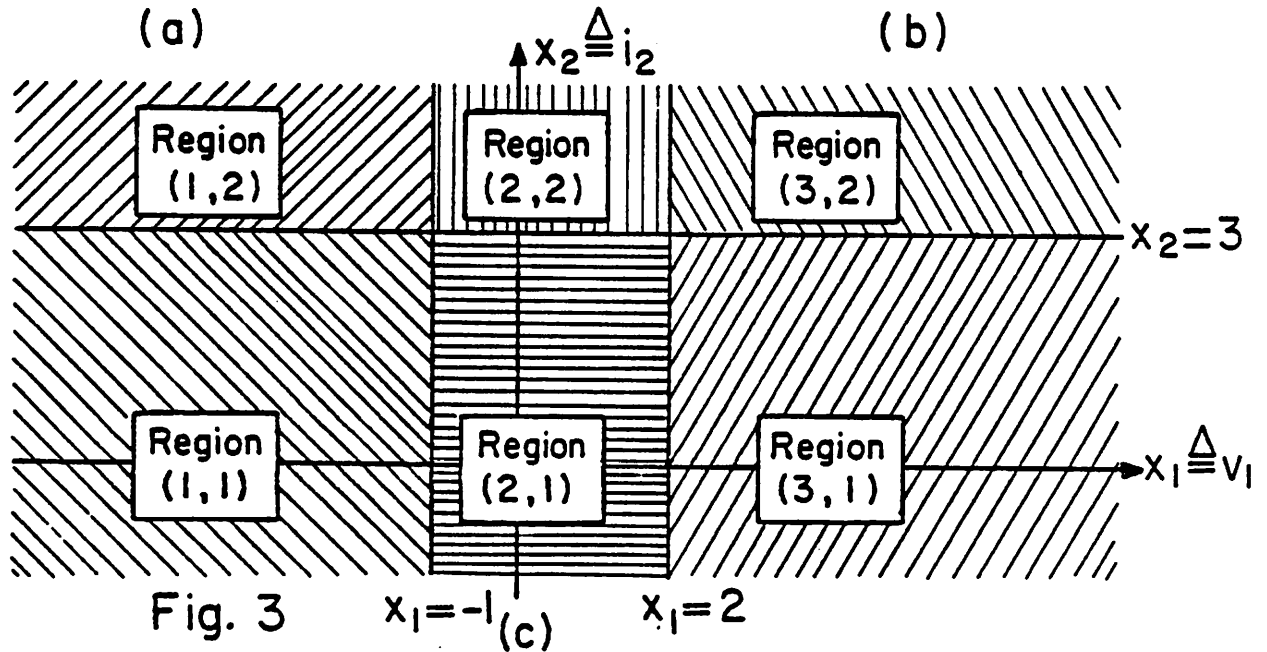
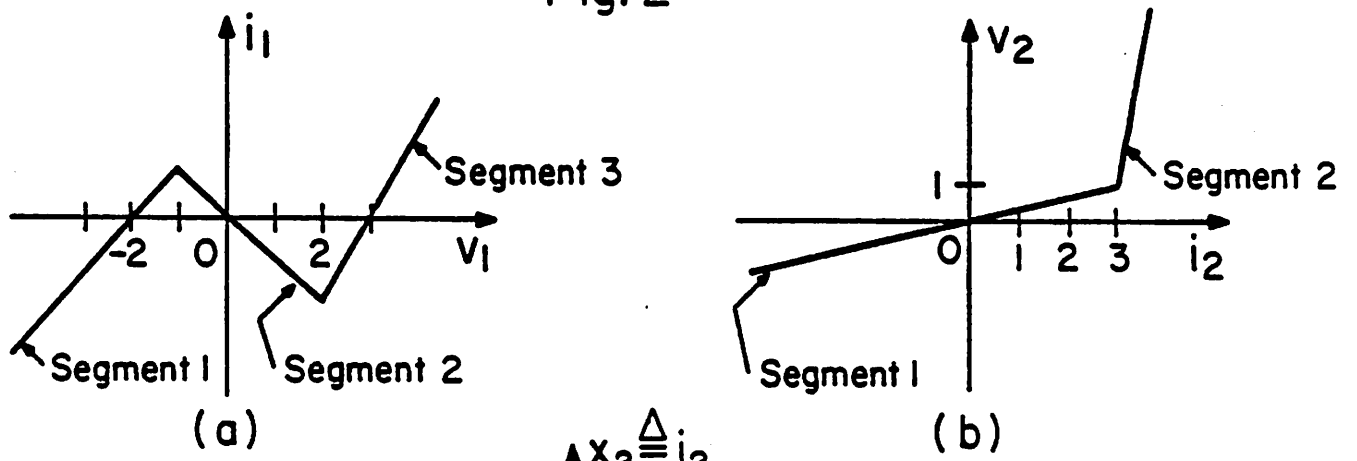
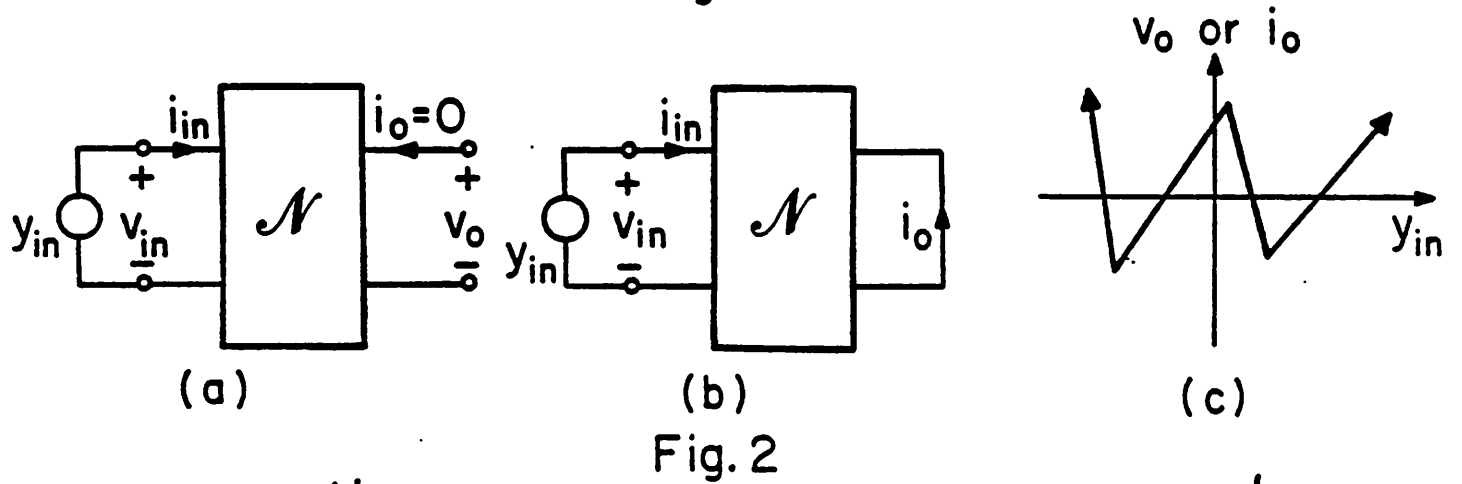
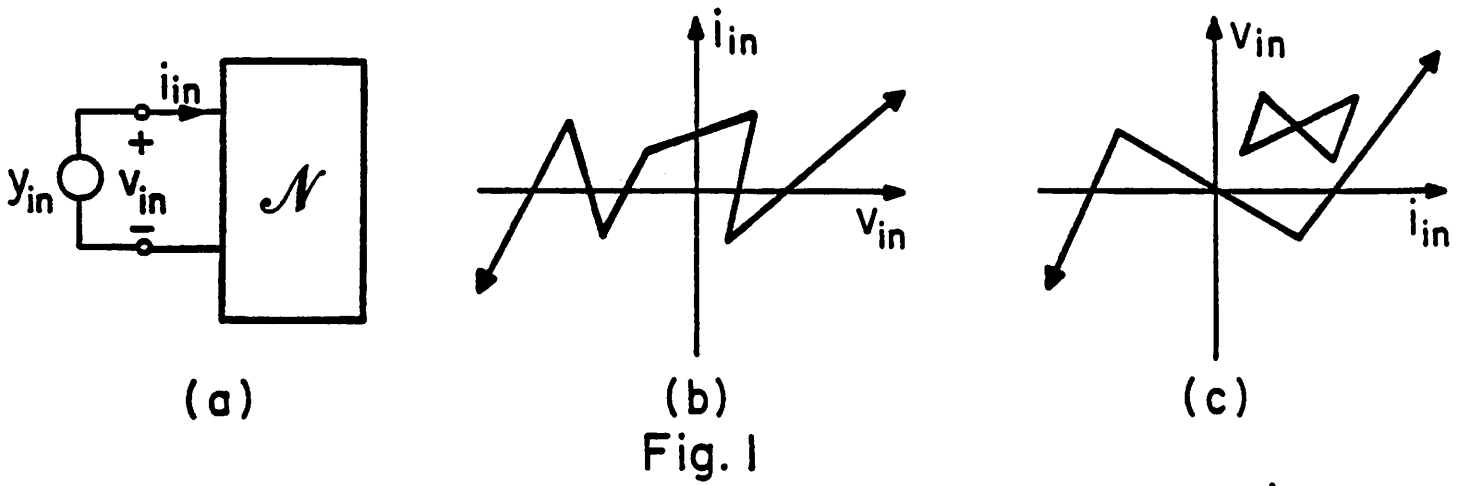
voltage-controlled resistors R_1 and R_2 and voltage source v_{in} .

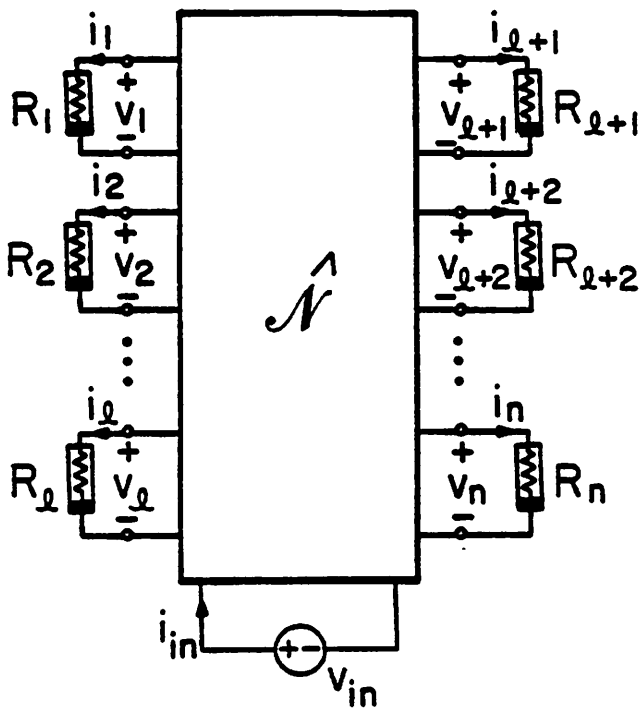
(c) Ebers-Moll circuit model of npn transistor. (d) The exponential law of the pn junction diode in Ebers-Moll circuit model in (c) is modeled by a 3-segment piecewise-linear function $\hat{f}(\cdot)$.

- Fig. 9. (a) The circuit in Fig. 8(a) redrawn with transistor and voltage source v_{in} extracted across the new (without controlled-sources) 3-port \hat{N} . (b) Representing the 3-terminal device in (a) by two coupled 2-terminal resistors R_1 and R_2 .
- Fig. 10. A hypothetical piecewise-linear solution curve Γ traced on the $x_1 - x_2$ plane in Fig. 3. Note that Γ does not pass through region (1,2). The notation $\tilde{x}^{(j)}(\rho^{(j)})$ means the location of $\tilde{x}^{(j)}$ corresponding to $\rho = \rho^{(j)}$.
- Fig. 11. (a) The direction vector $\tilde{d}^{(0)}$ originating from $\tilde{x}^{(0)}$ intersects the boundary line $x_1 = \beta_1 i_1$ at $\tilde{x}^{(1)}$ before its extension (shown dotted) intersects the second boundary line $x_2 = \beta_2 i_2$ at $\tilde{x}^{(1)'}$. (b) The direction vector $\tilde{d}^{(0)}$ from $\tilde{x}^{(0)}$ intersects the boundary plane $x_2 = \beta_2 i_2$ at $\tilde{x}^{(1)}$ before its extension (shown dotted) intersects the boundary plane $x_1 = \beta_1(i_1 - 1)$ (back side) at $\tilde{x}^{(1)'}$ and finally the boundary plane $x_3 = \beta_3 i_3$ (top) at $\tilde{x}^{(1)''}$.
- Fig. 12. (a) Solution curve in region $R^{(1)}$ connects two breakpoints $\tilde{x}^{(1)}$ and $\tilde{x}^{(2)}$. (b) Solution curve in region $R^{(1)}$ goes from $\tilde{x}^{(1)}$ to ∞ .
- Fig. 13. Typical example showing the direction vector $\tilde{d}^{(k)}$ lying along the solution curve Γ on $R^{(k)}$ but pointing outwards; i.e. back towards the region $R^{(k-1)}$ where we came from. The horizontal axis is labelled as $x_{j_{k-1}}$.
- Fig. 14. (a) A current-controlled driving-point characteristic which is not a single-valued function of $v_{in} = \rho$. (b) A multivalued driving-point characteristic which is not a single-valued function of $v_{in} = \rho$. (c) A driving-point characteristic which is a single-valued function of $v_{in} = \rho$ except at one point $v_{in} = \rho^*$ where the entire vertical line segment maps into one-point $v_{in} = \rho^*$.
- Fig. 15. (a) A bow-tie shape driving-point characteristic which does not intersect the load line $v_{in} = \rho_{min}$. (b) A driving-point characteristic which intersects the load line $v_{in} = \rho_{min}$ at three points.
- Fig. 16. (a) A driving-point characteristic having a vertical end segment located at $\rho^* < \rho_{max}$. (b) A driving-point characteristic which does not intersect the load line $v_{in} = \rho_{max}$.
- Fig. 17. The load line $v_{in} = \rho_{min}$ intersects one branch at 3 points but not

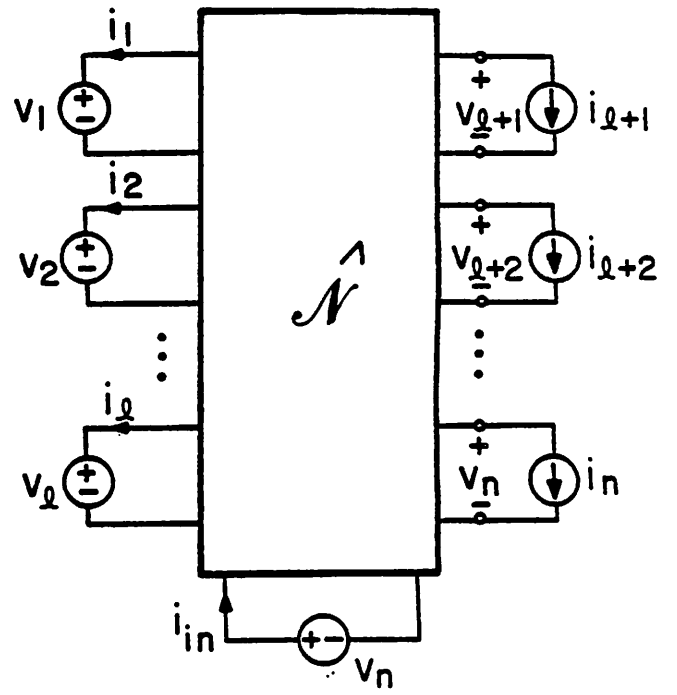
the second branch.

- Fig. 18. (a) Circuit for Example 3.1. (b) $v_1 - i_1$ characteristic for R_1 . (c) $i_2 - v_2$ characteristic for R_2 . (d) Driving-point characteristic derived by graphical method and by the breakpoint-hopping algorithm. (e) Linear 3-port \hat{N} terminated by voltage-controlled nonlinear resistor R_1 , current-controlled nonlinear resistor R_2 and voltage source v_{in} .
- Fig. 19. (a) Circuit for Example 3.2. (b) $v_1 - i_1$ characteristic for R_1 . (c) Driving-point characteristic derived by the breakpoint-hopping algorithm. (d) Linear 2-port \hat{N} terminated by voltage-controlled nonlinear resistor R_1 and voltage source v_{in} .
- Fig. 20. (a) Solution curve Γ of the circuit in Fig. 5(a). (b) Driving-point characteristic of the circuit in Fig. 5(a).
- Fig. 21. Two distinct solution curves Γ_1 and Γ_2 for the circuit in Fig. 6(a). Horizontal axis denotes $x_1 \triangleq v_1$ and vertical axis denotes $x_2 \triangleq v_2$.
- Fig. 22. (a) Two distinct branches of the driving-point characteristic of the circuit in Fig. 6(a). (b) $v_1 - v_s - v_{in}$ transfer characteristics. (c) $v_2 - v_s - v_{in}$ transfer characteristic.
- Fig. 23. (a) Solution curve Γ of the circuit in Fig. 8(a). (b) Driving-point characteristic of the circuit in Fig. 8(a).
- Fig. 24. (a) Circuit for Example 5.1. (b) $v_1 - i_1$ characteristic for R_1 . (c) $v_2 - i_2$ characteristic for R_2 . (d) Linear 3-port \hat{N} terminated by voltage-controlled nonlinear resistors R_1 and R_2 and voltage source v_{in} . (e) Solution curve of the circuit in (a). Note that it splits into 3 branches upon hitting the corner point $x^{(1)}$.
- Fig. 25. (a) Solution curve of the circuit in Fig. 7(a). (b) Driving-point characteristic of the circuit in Fig. 7(a).
- Fig. 26. (a) Circuit for Example 5.3. (b) $v_1 - i_1$ characteristic for R_1 . (c) $v_2 - i_2$ characteristic for R_2 . (d) Linear 3-port \hat{N} terminated by voltage-controlled nonlinear resistors R_1 and R_2 and voltage source v_{in} . (e) Solution "curve" for the circuit in (a).
- Fig. 27. (a) Driving-point characteristic for the circuit in Fig. 26(a). (b) $v_1 - v_s - v_{in}$ transfer characteristic. (c) $v_2 - v_s - v_{in}$ transfer characteristic. Note that the solution curve splits into the whole 2-dimensional area of region $R^{(c)}$.
- Fig. 28. (a) Solution curve re-entering a previously traversed region. (b) Driving-point or transfer characteristic for $\rho^{(m+2)} \neq \rho^{(1)}$. (c) Driving-point or transfer characteristic for $\rho^{(m+2)} = \rho^{(1)}$.



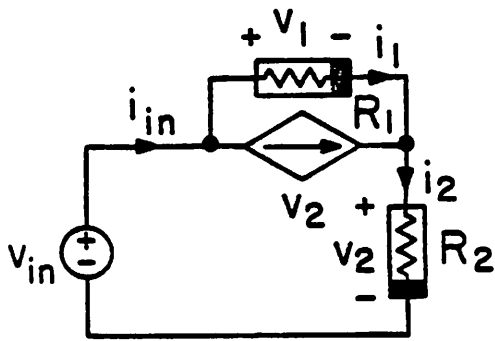


(a)

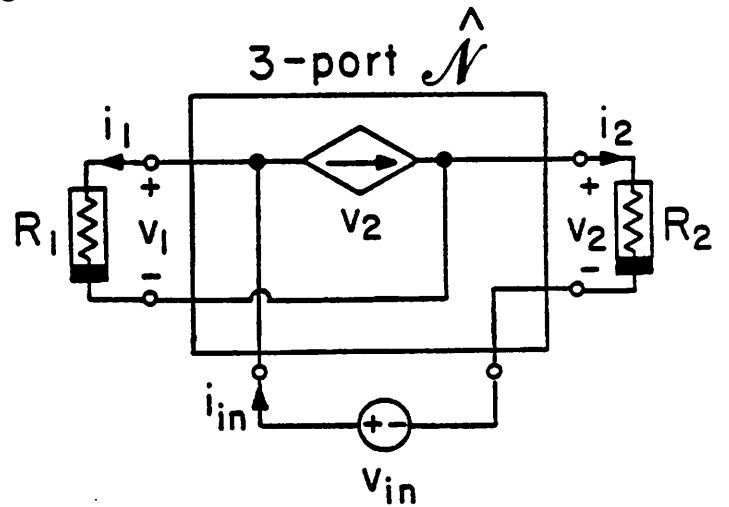


(b)

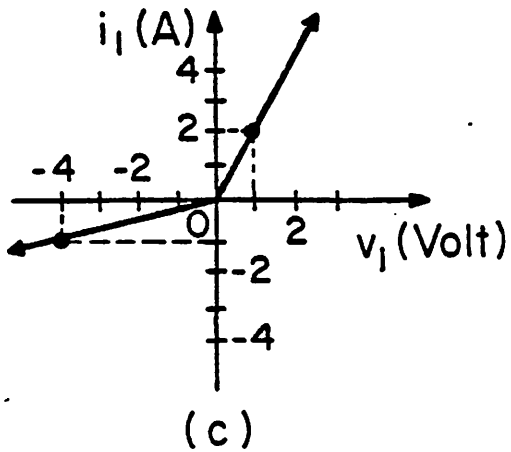
Fig. 4



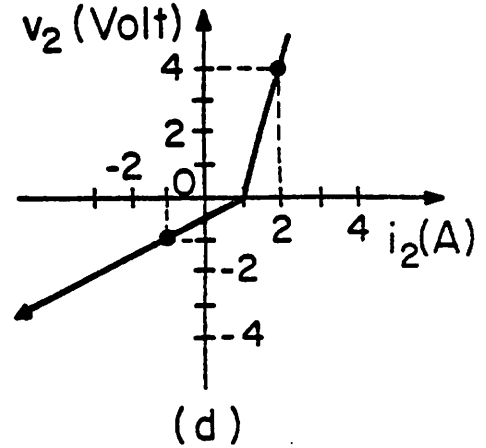
(a)



(b)



(c)



(d)

Fig. 5

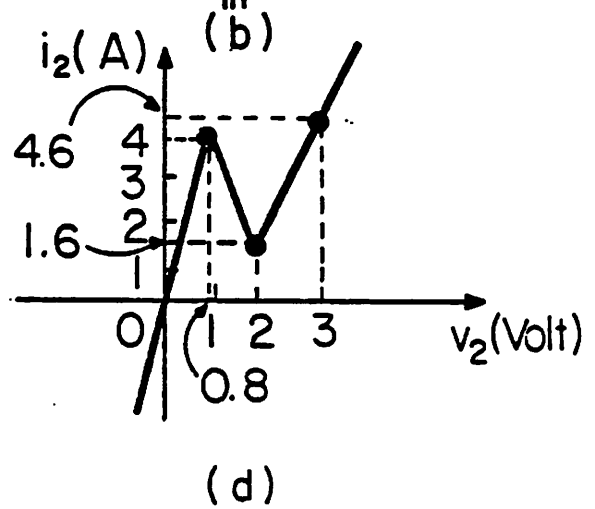
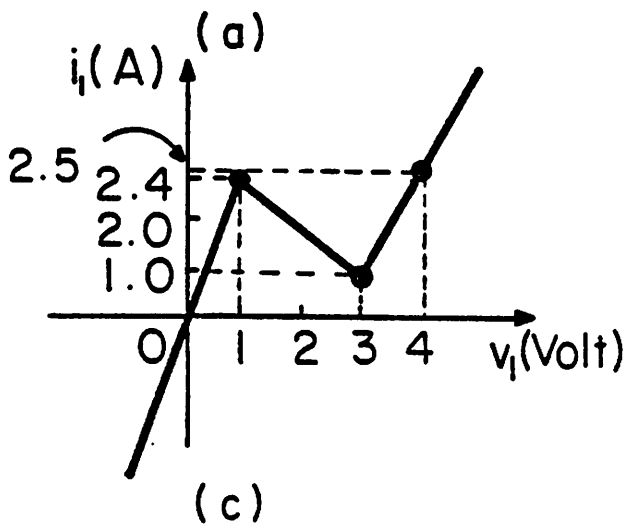
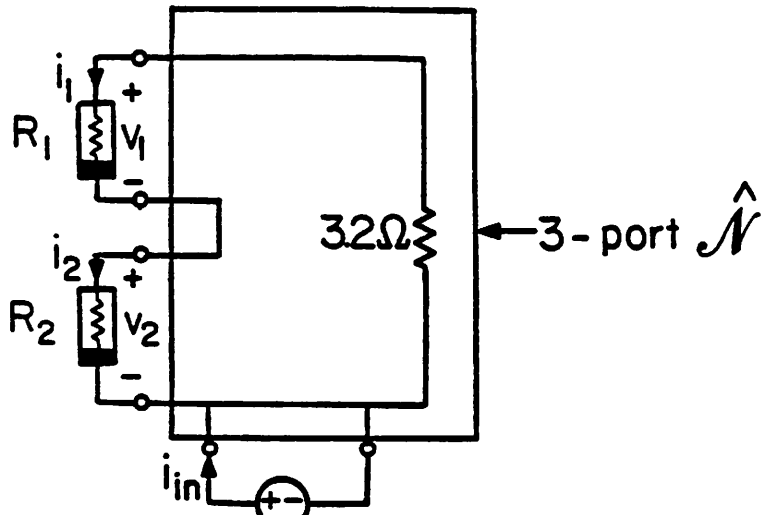
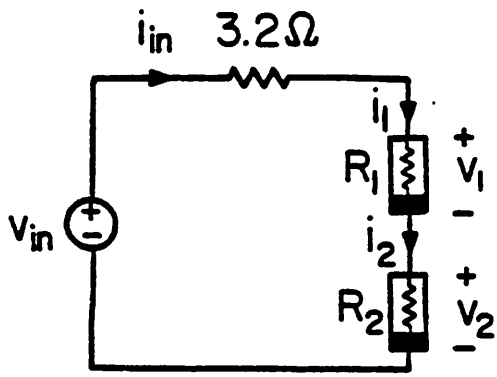


Fig.6

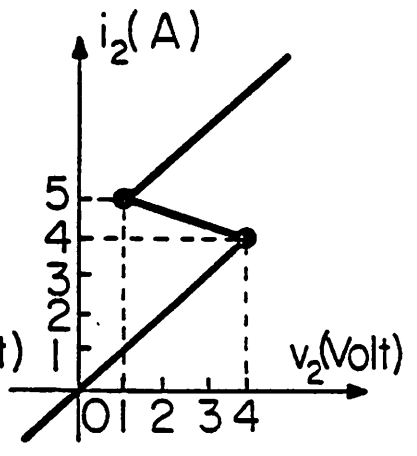
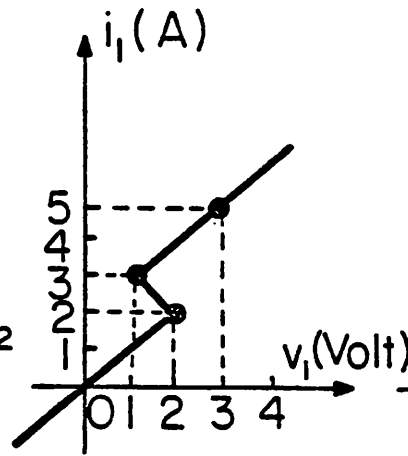
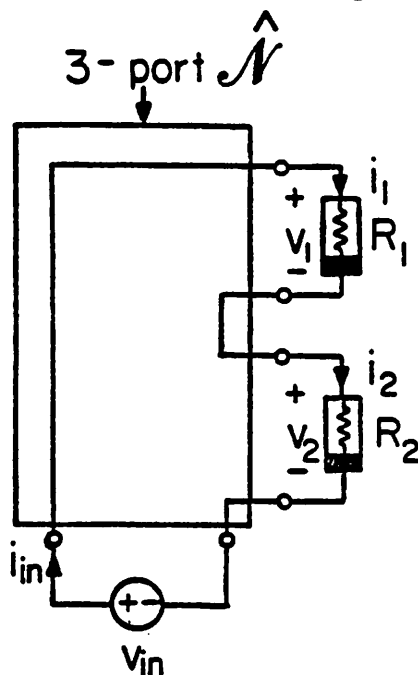
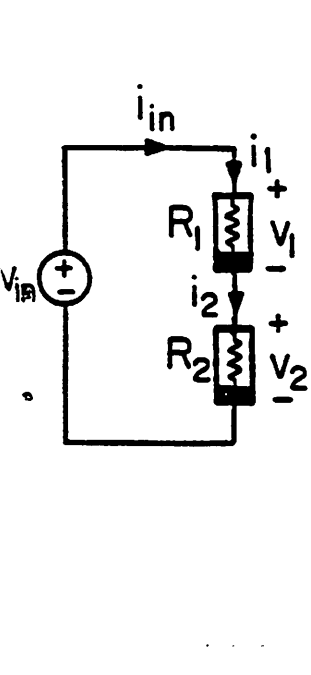


Fig.7

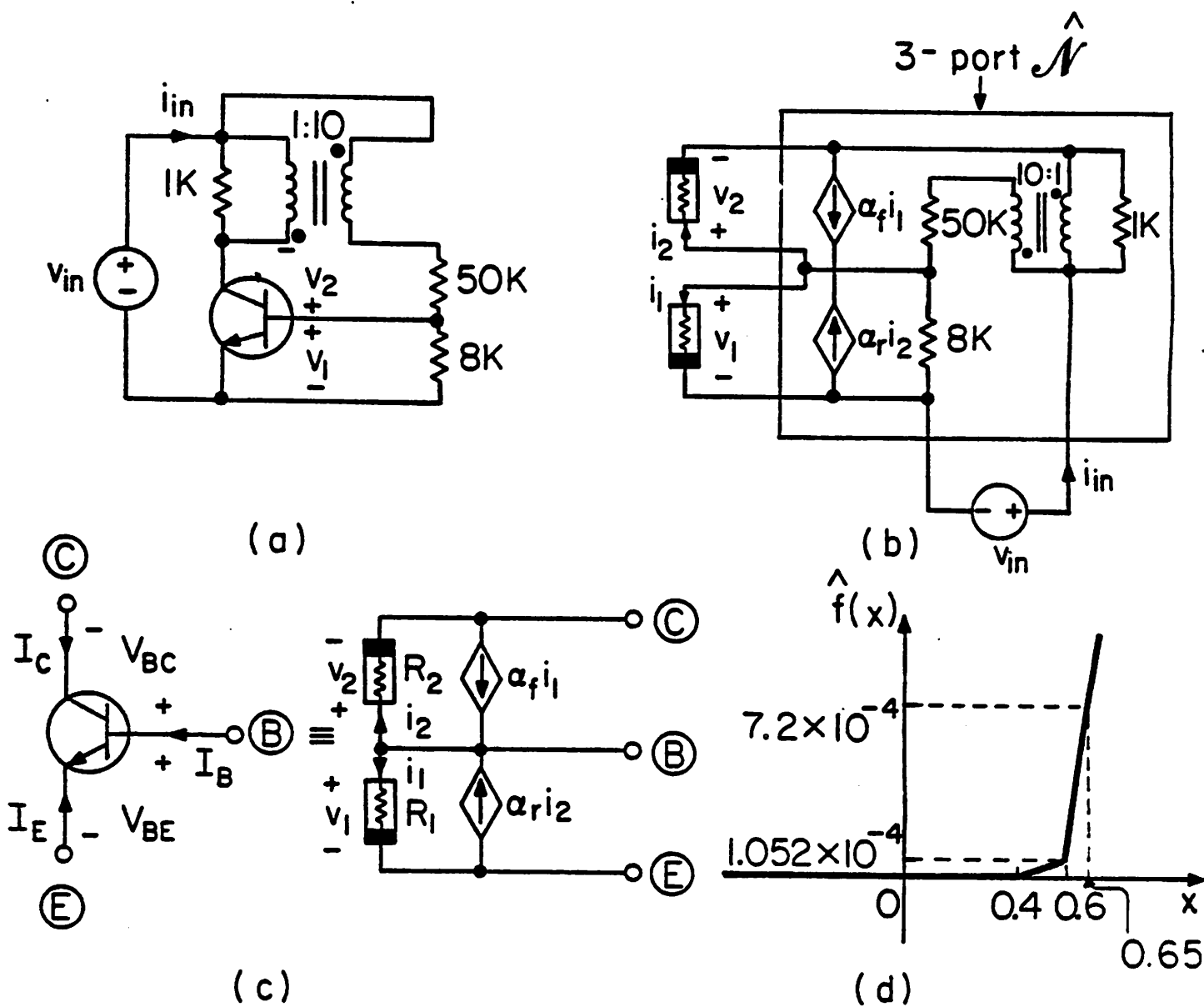


Fig.8

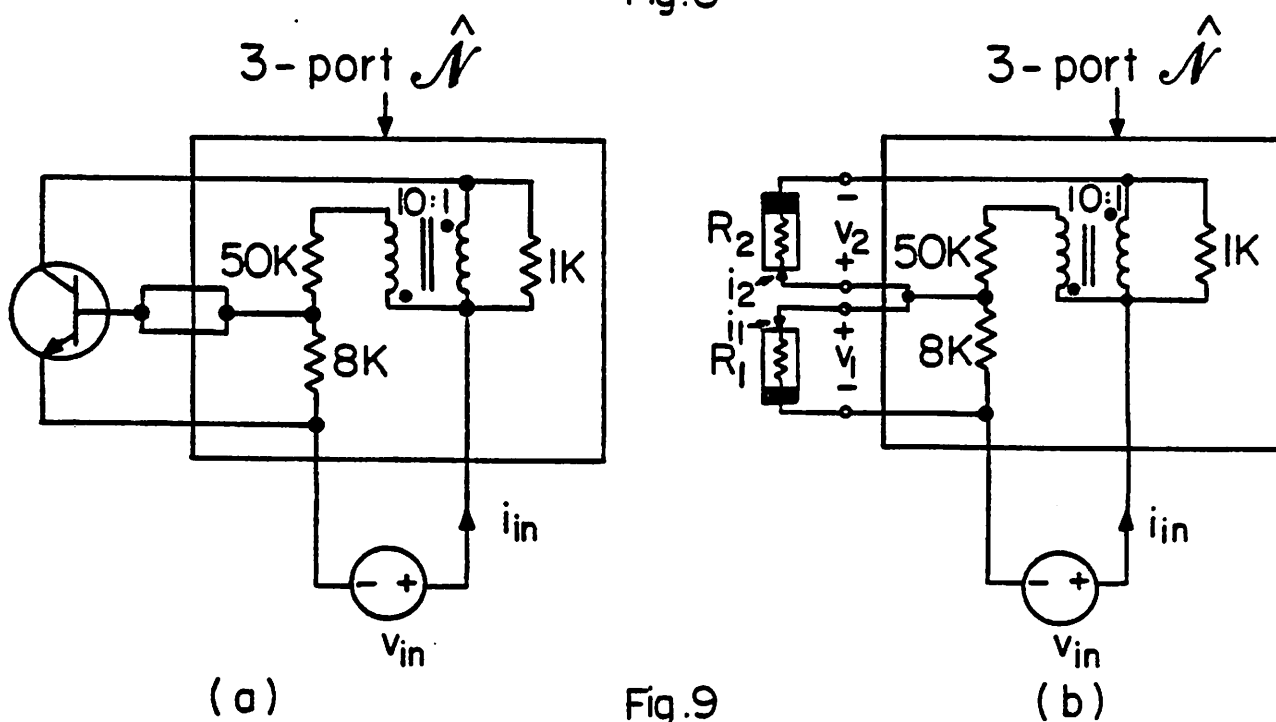


Fig.9

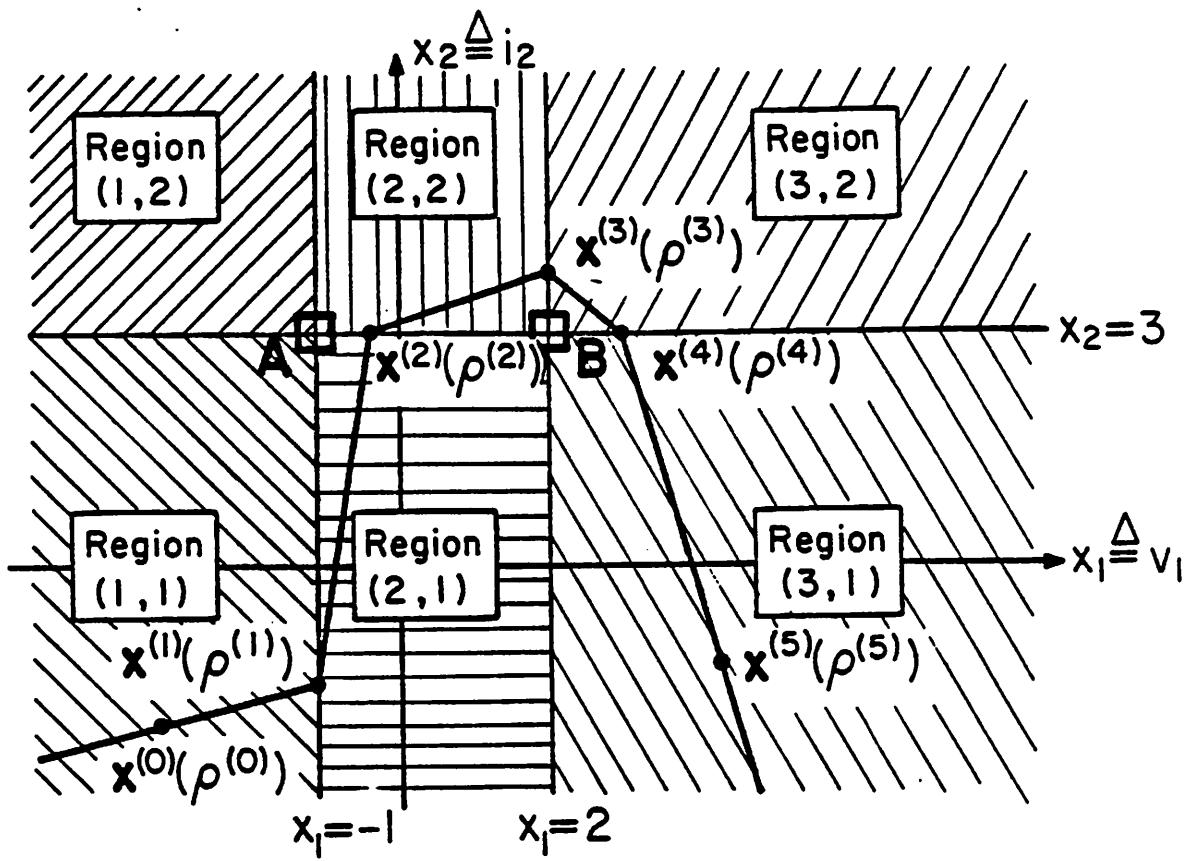


Fig. 10

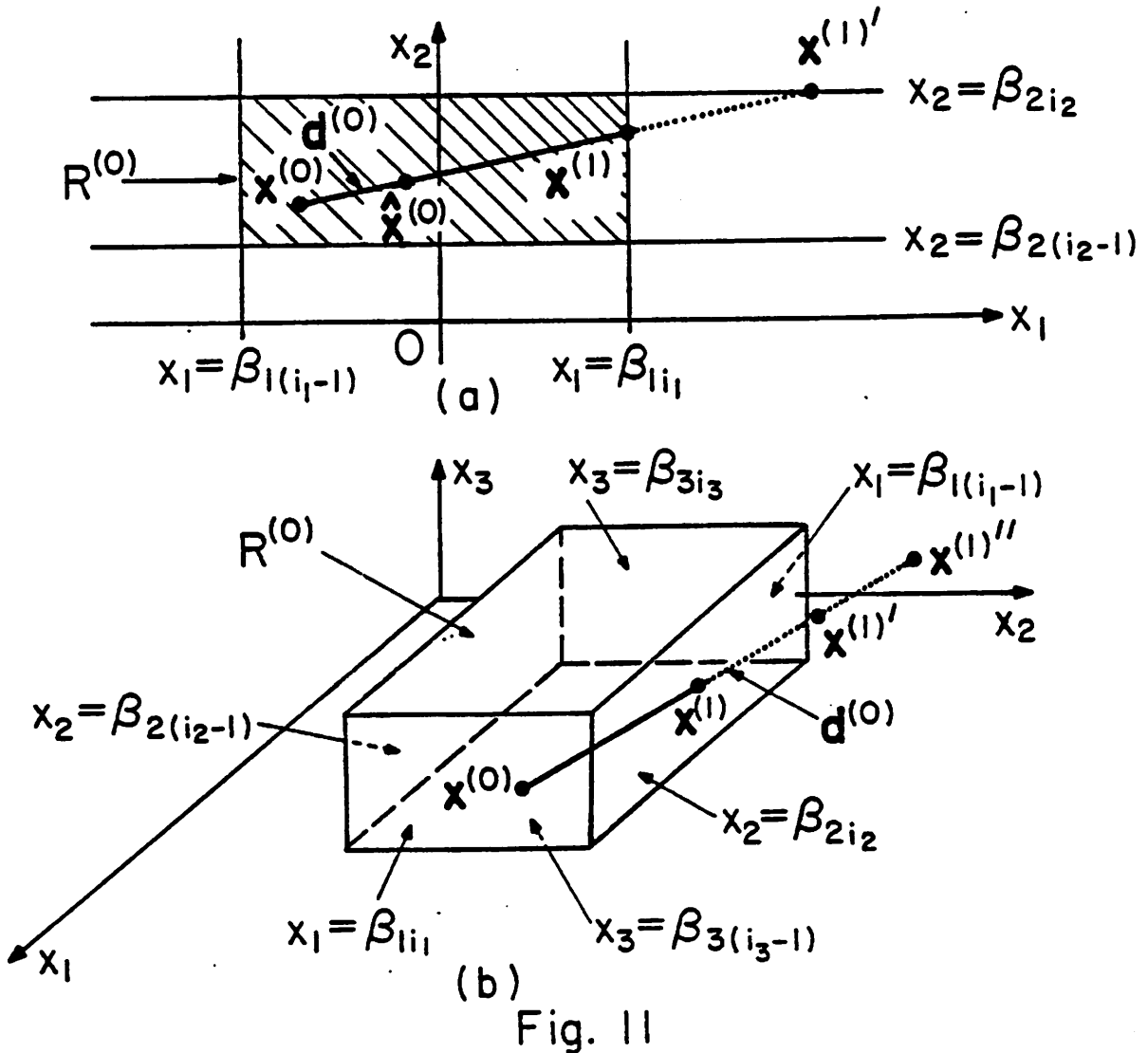


Fig. 11

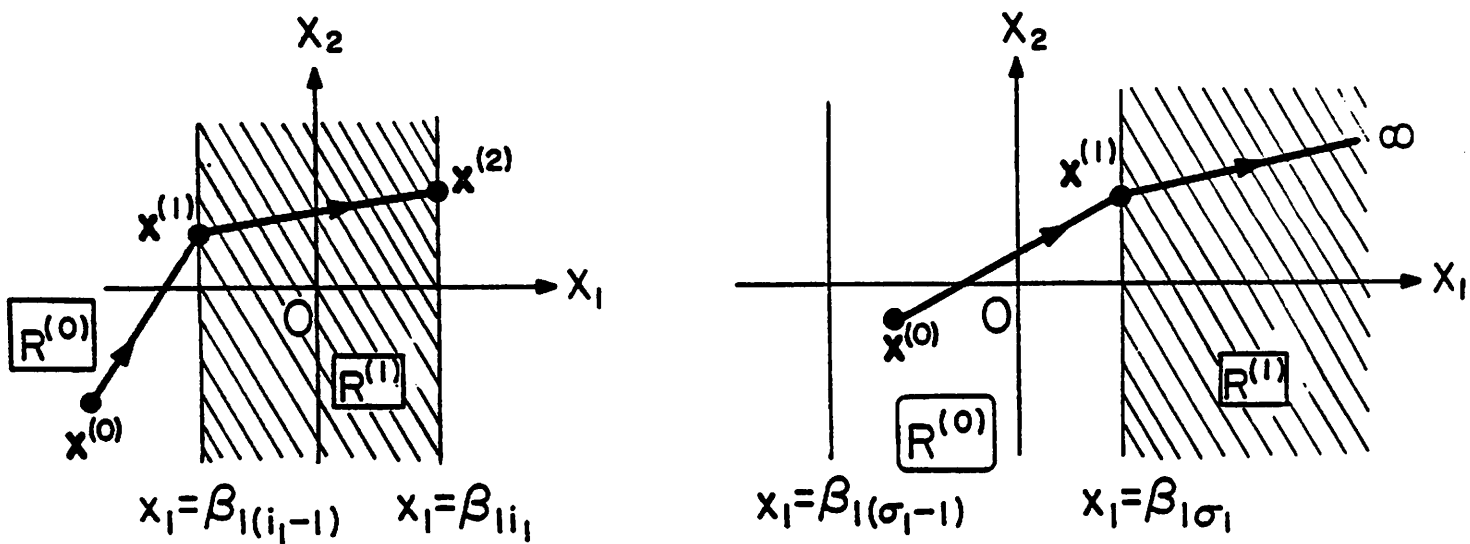


Fig.12

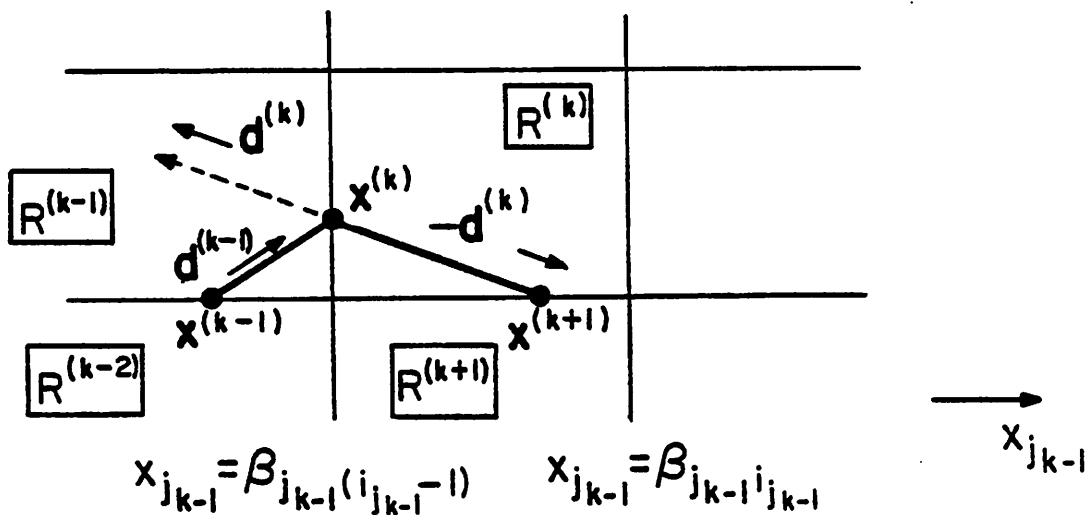


Fig.13

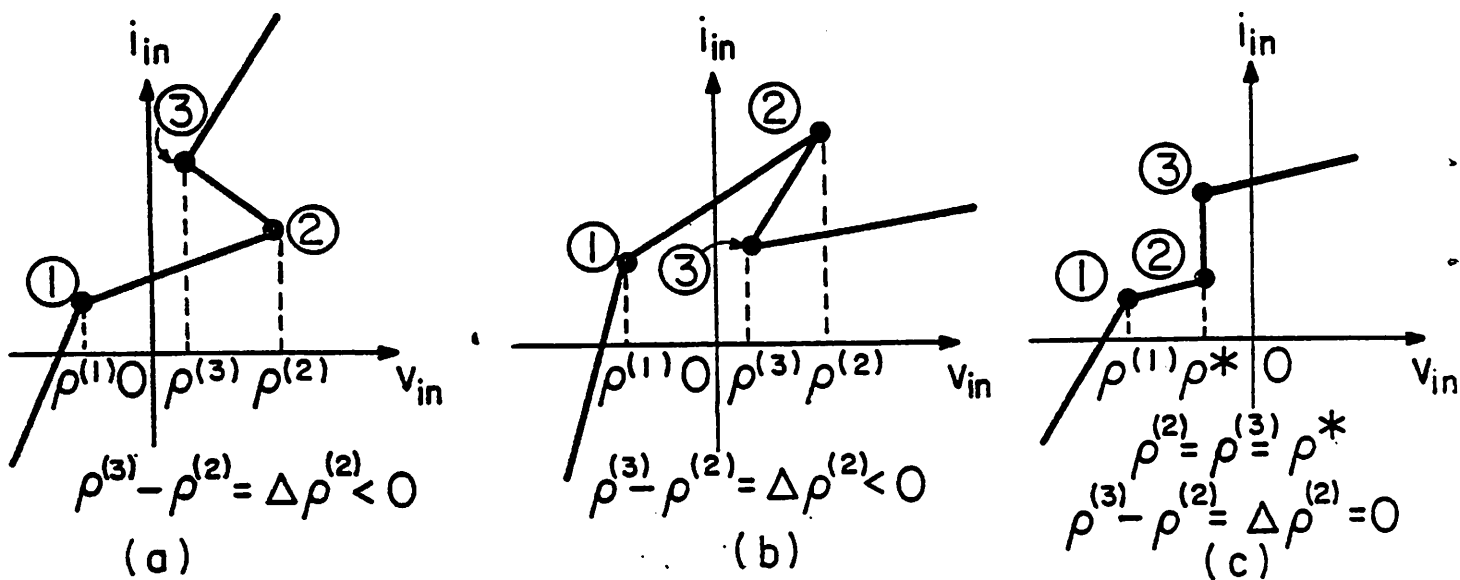
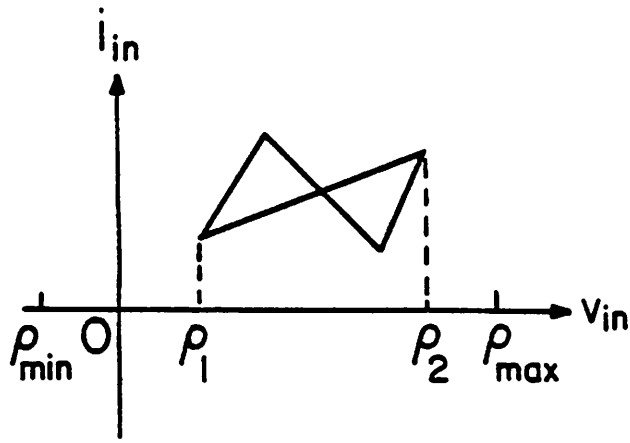
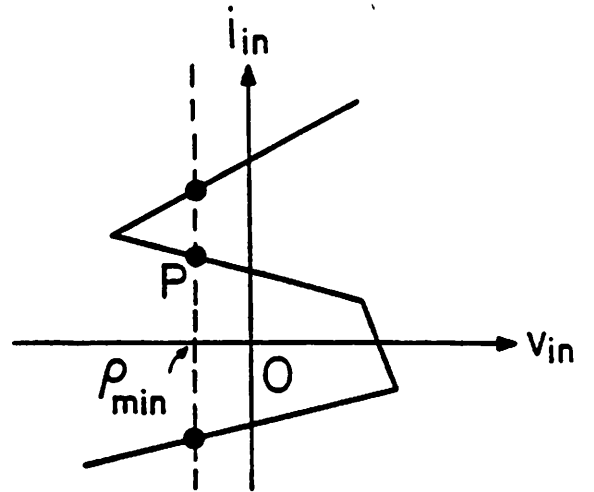


Fig.14

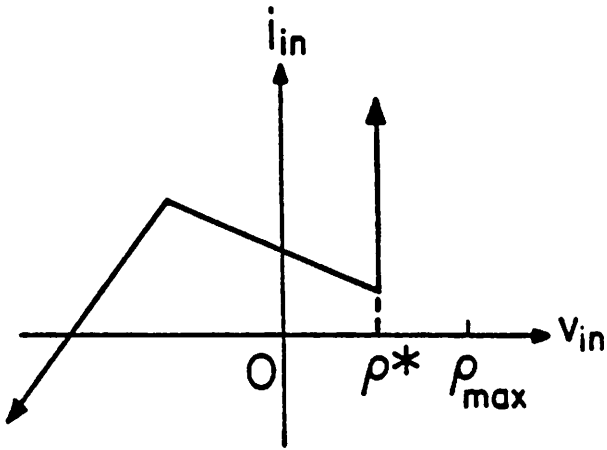


(a)

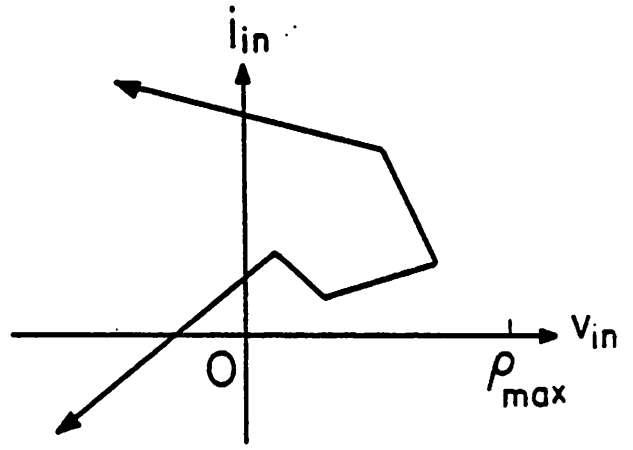


(b)

Fig.15



(a)



(b)

Fig.16

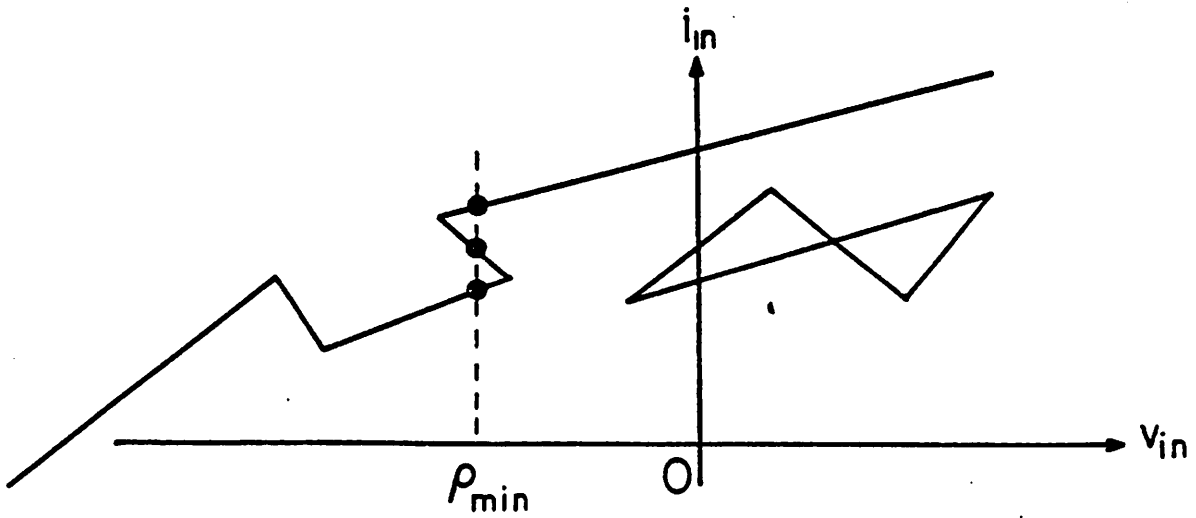


Fig.17

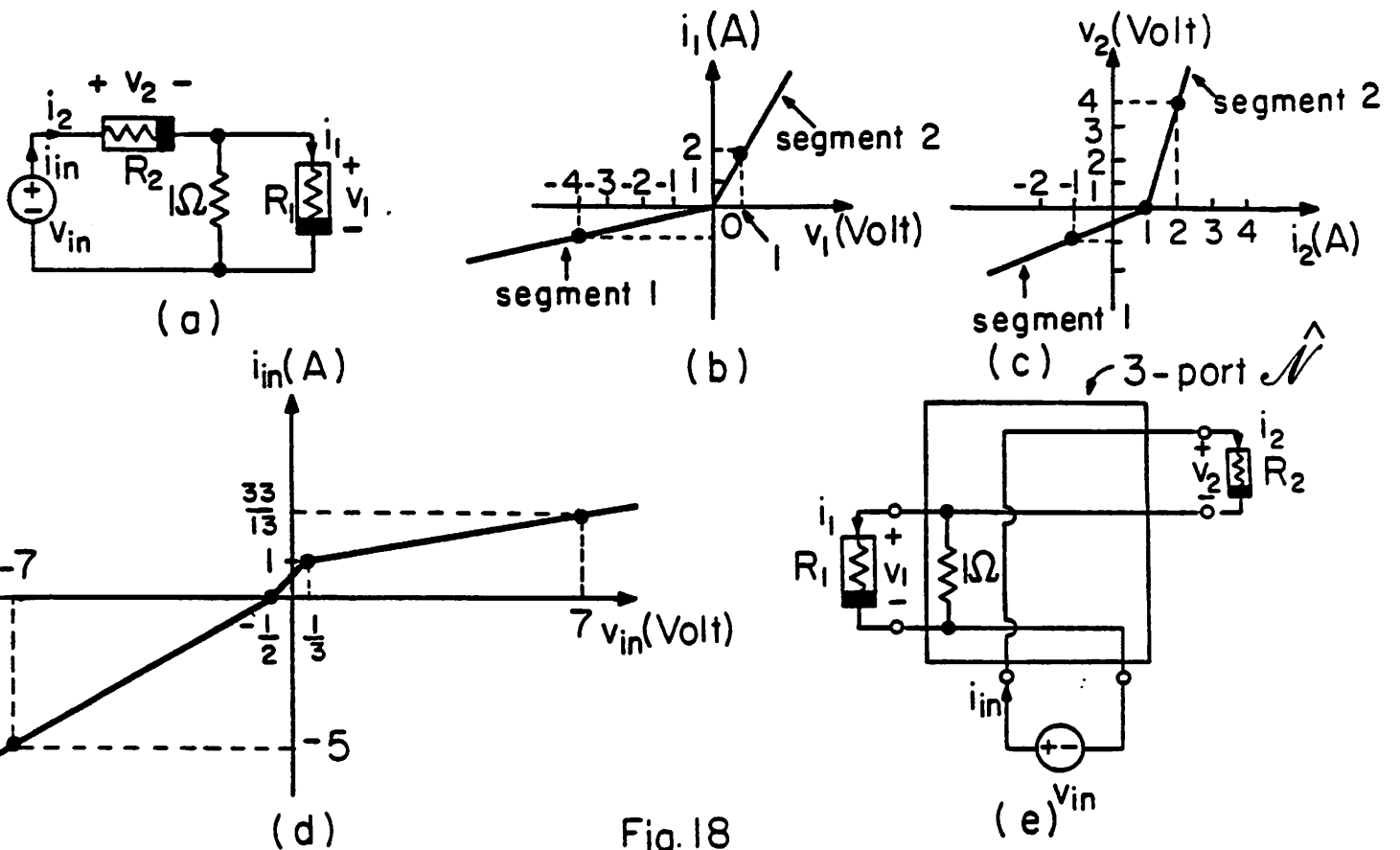


Fig. 18

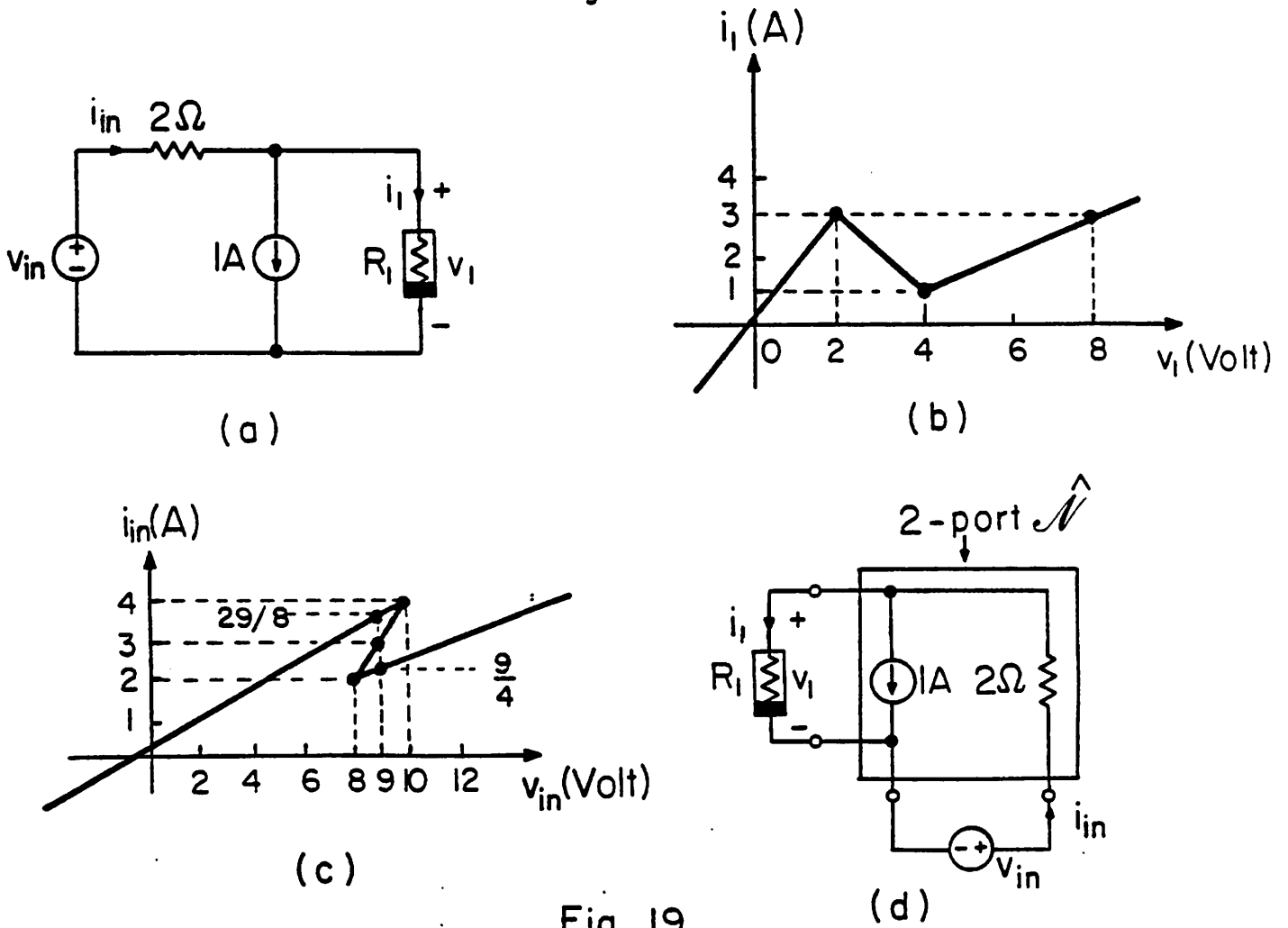


Fig. 19

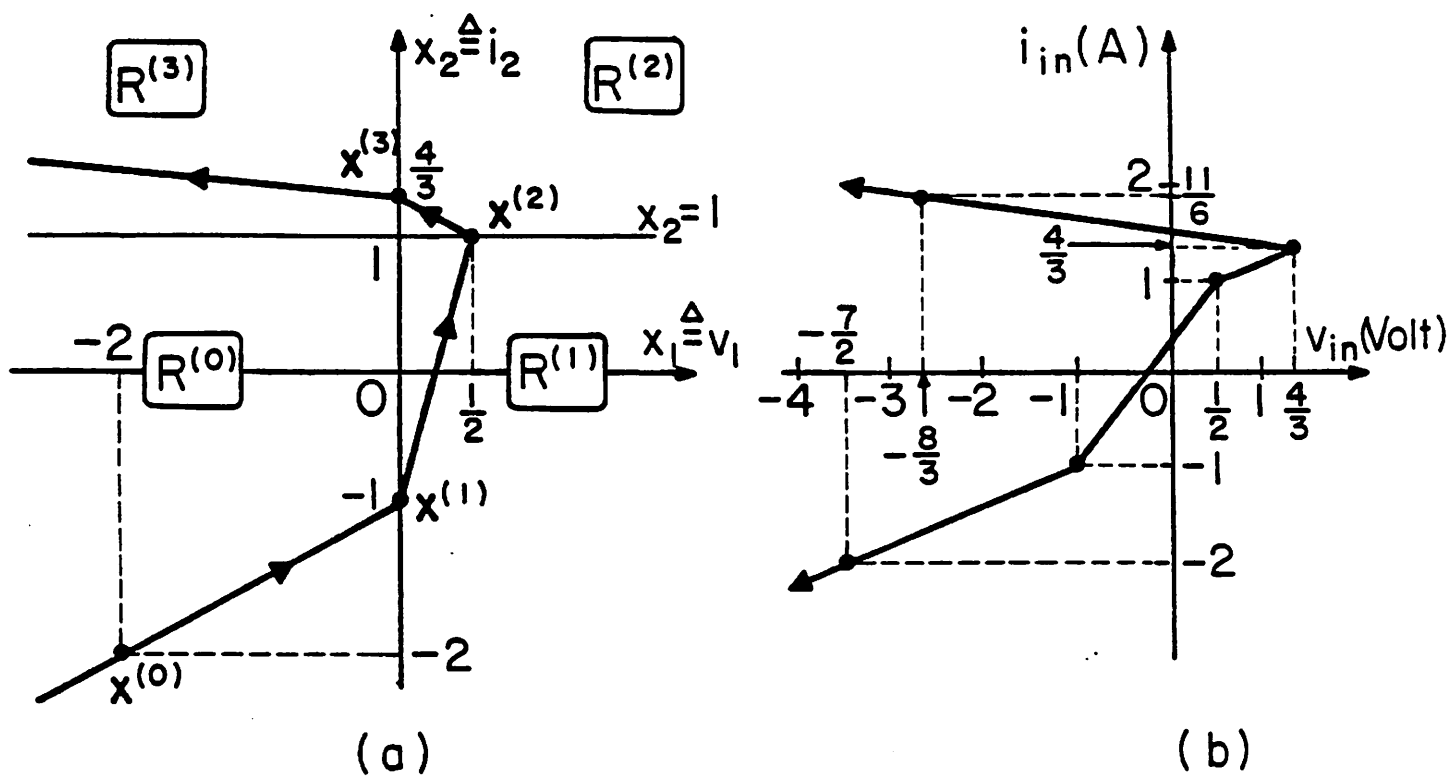


Fig. 20

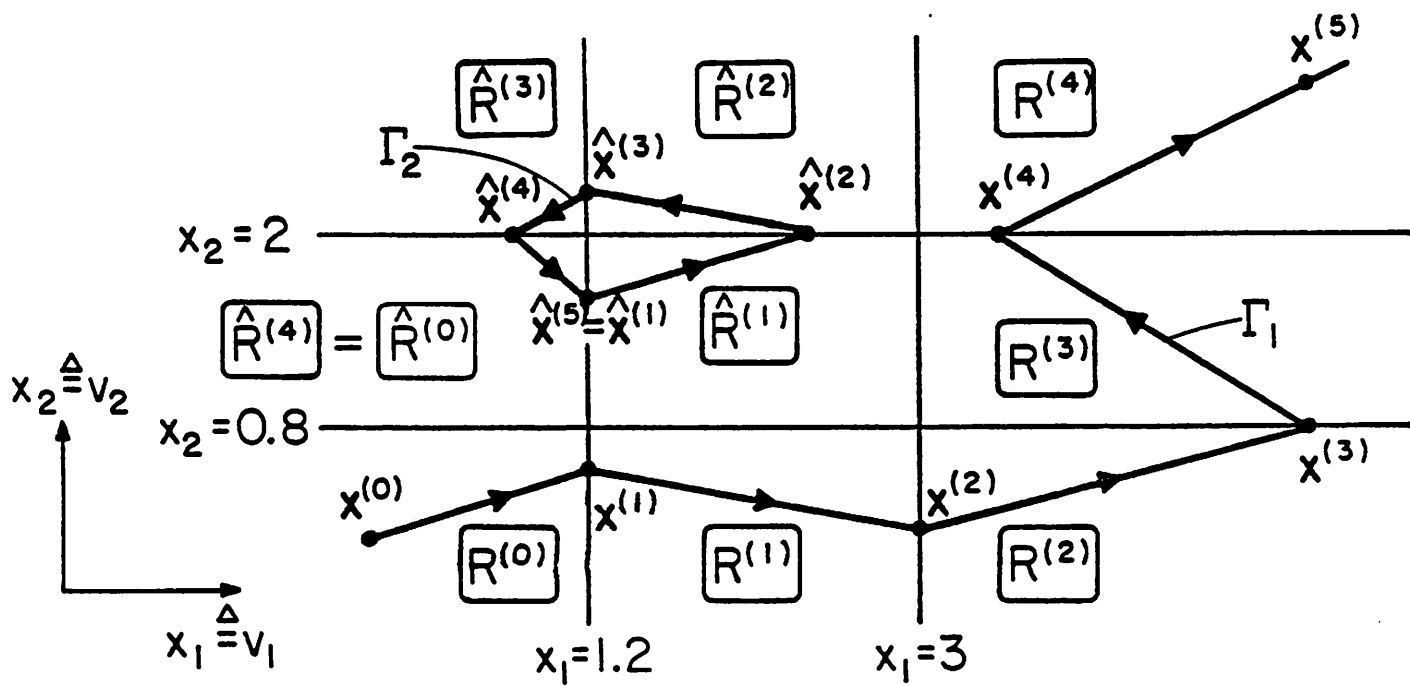


Fig. 21

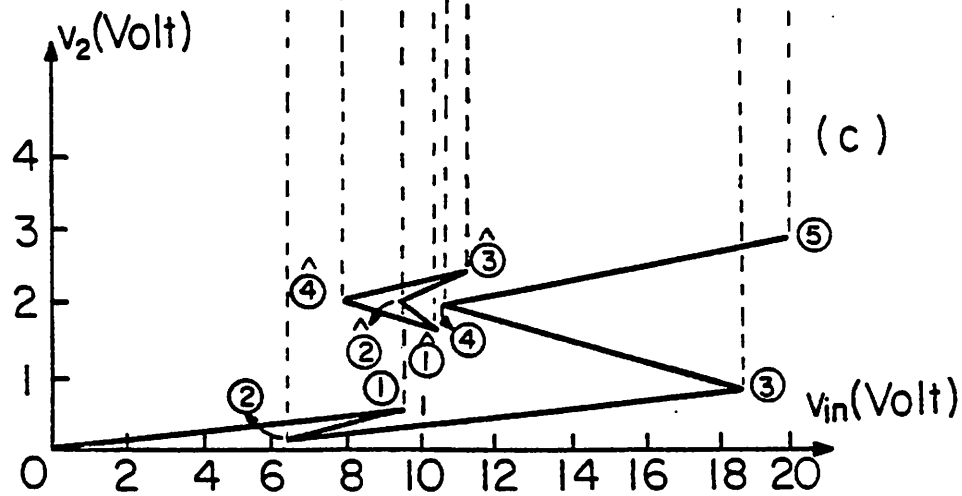
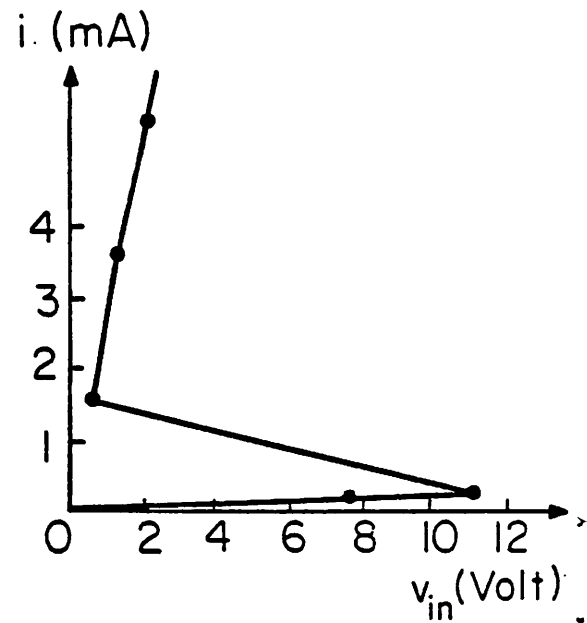
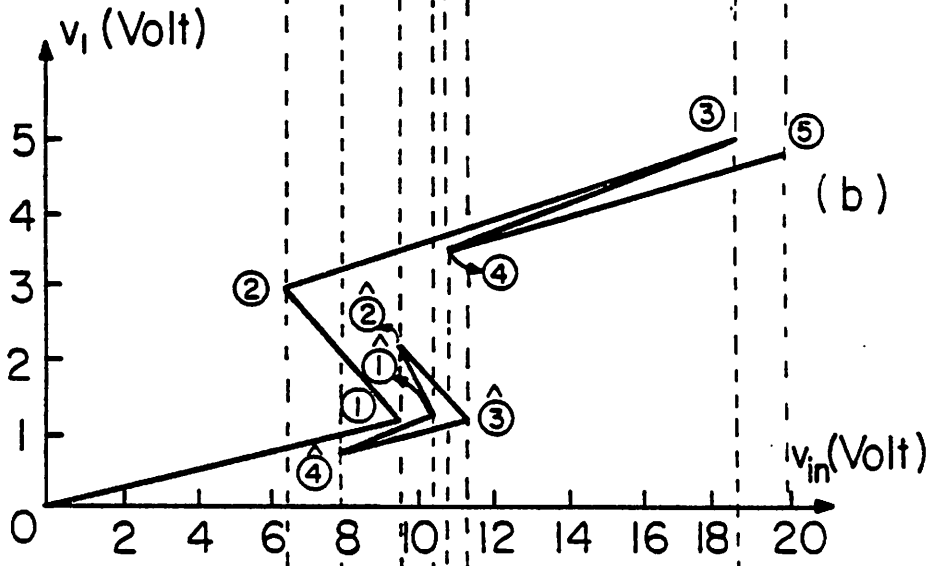
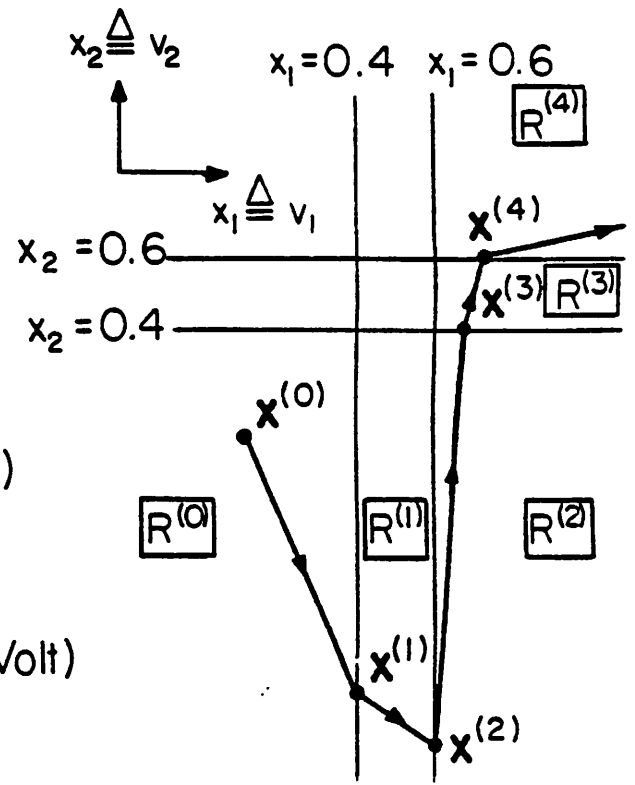
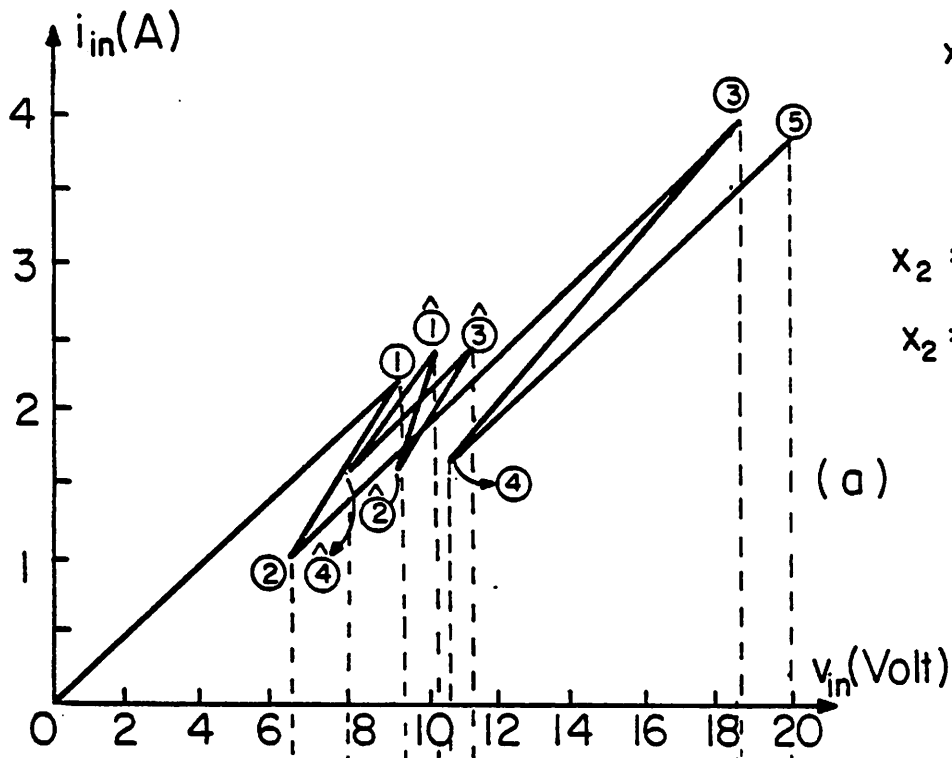


Fig. 23

Fig. 22

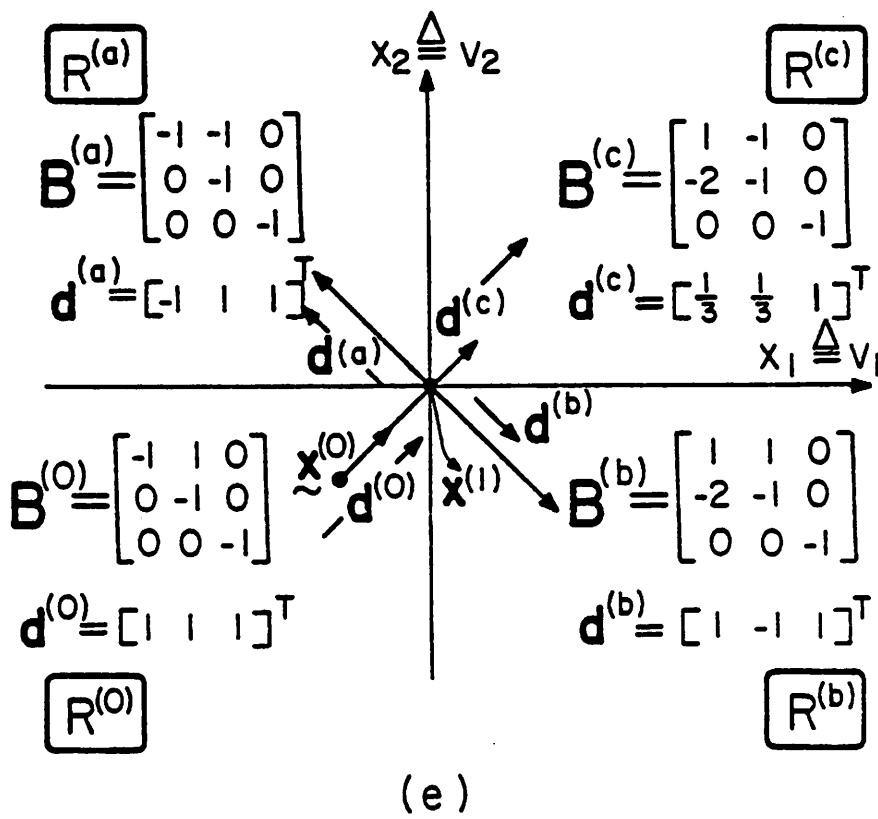
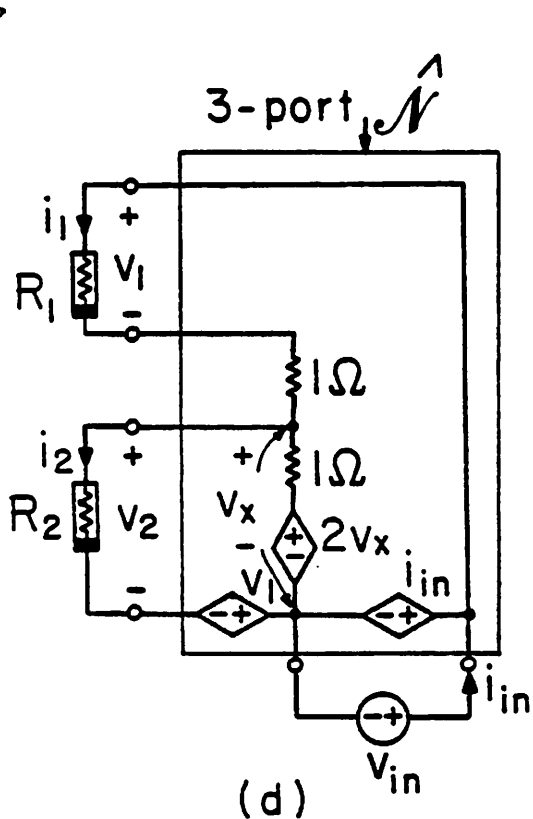
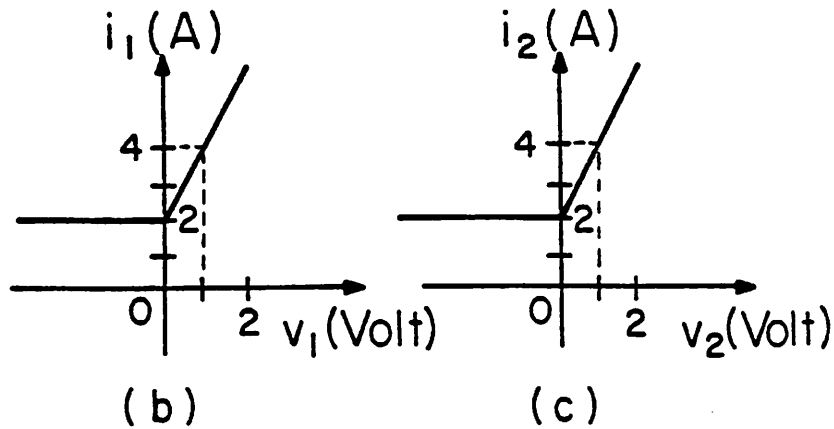
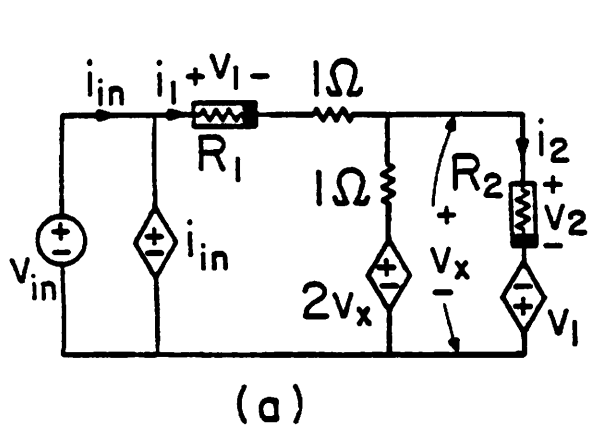


Fig. 24

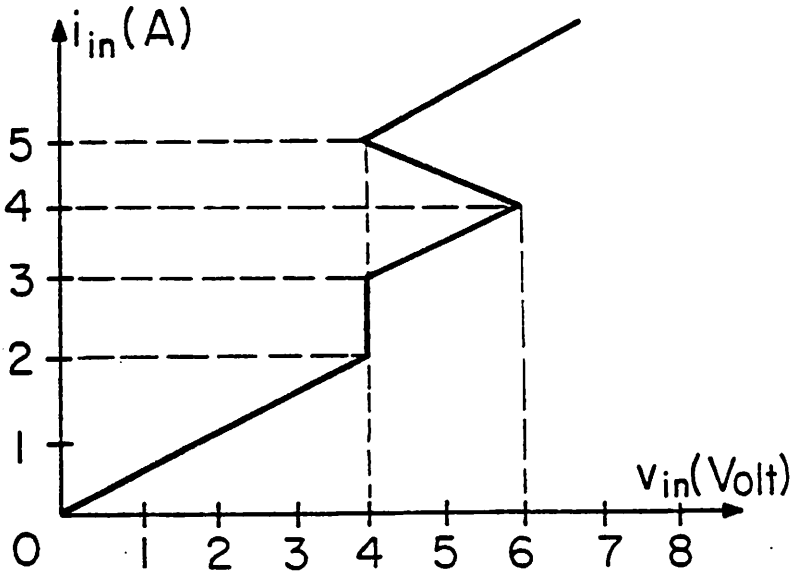
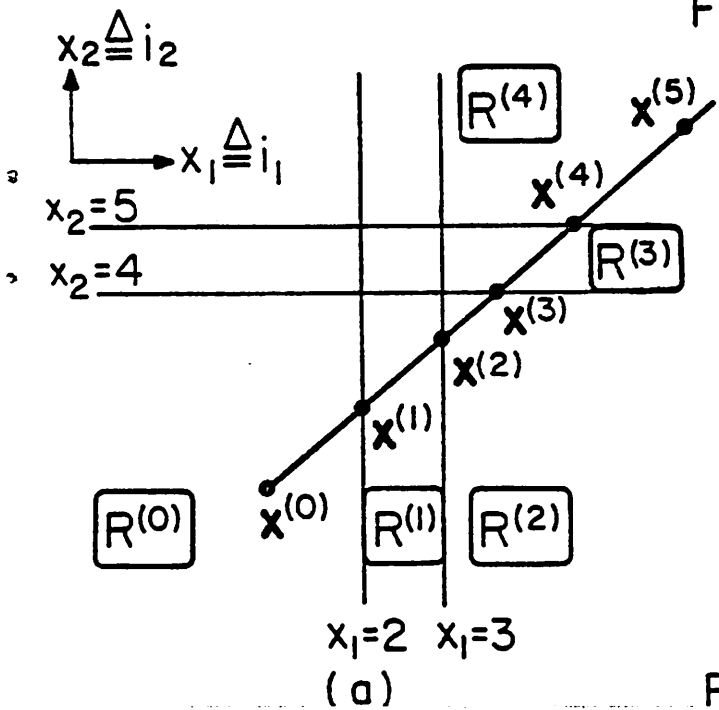
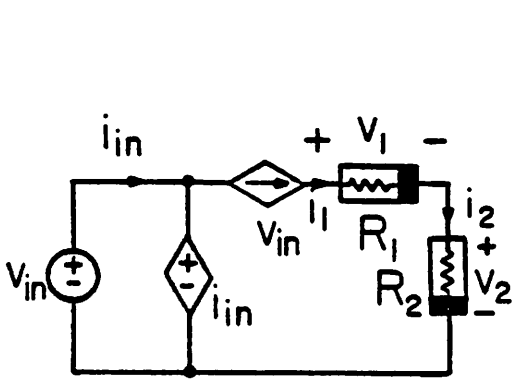
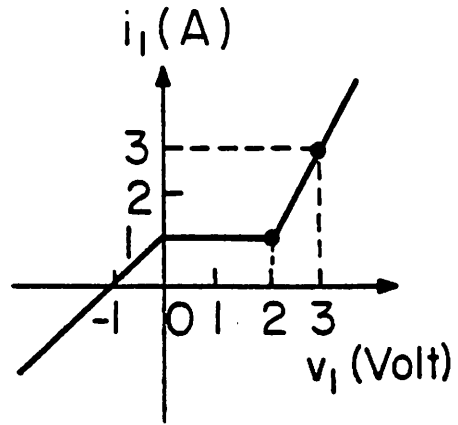


Fig. 25

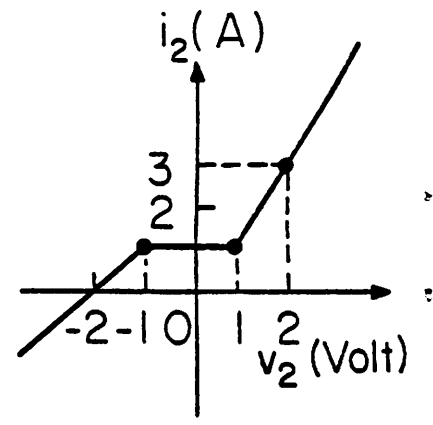
(b)



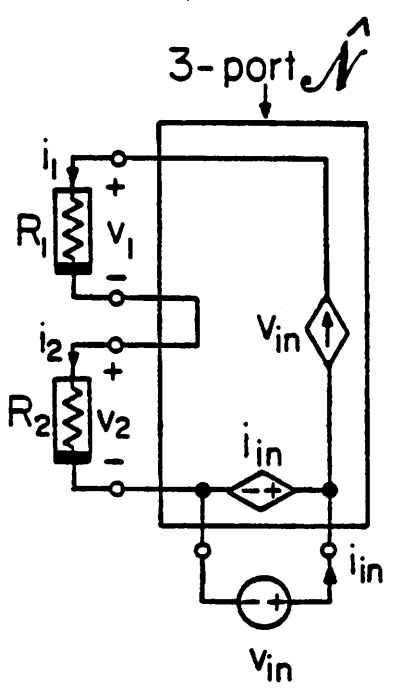
(a)



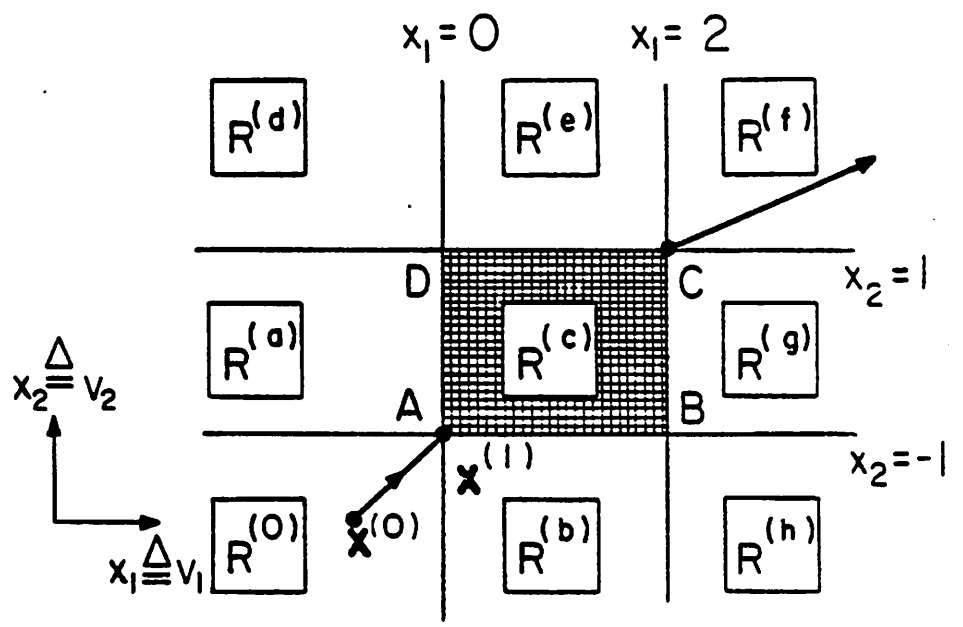
(b)



(c)



(d)



(e)

Fig. 26

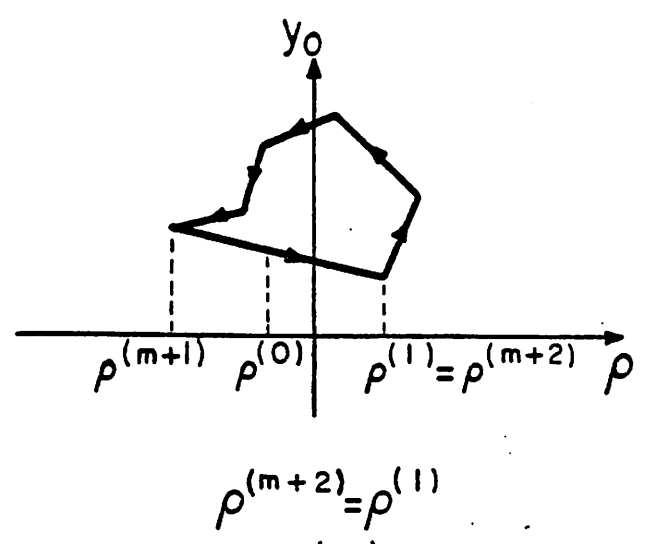
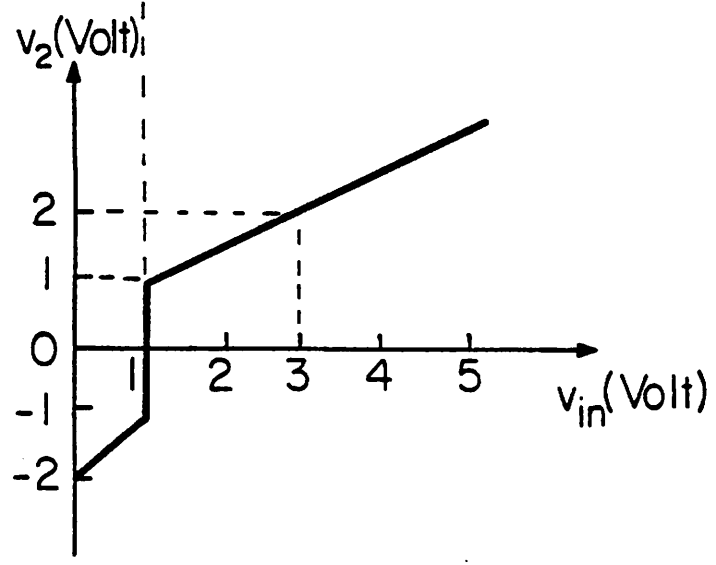
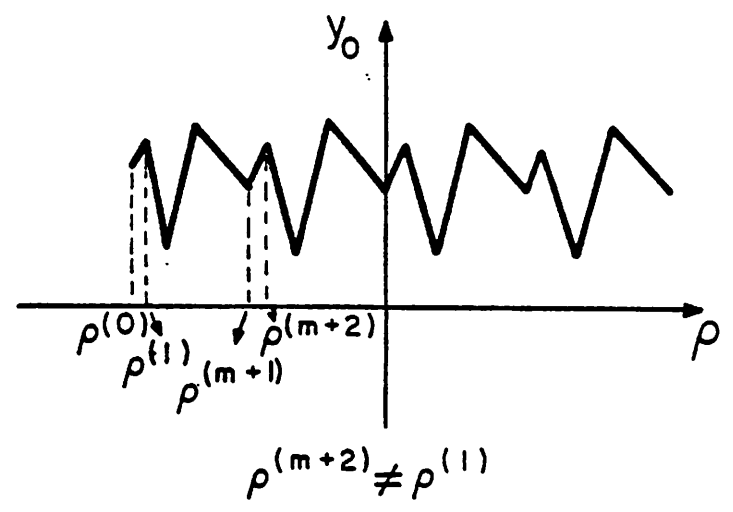
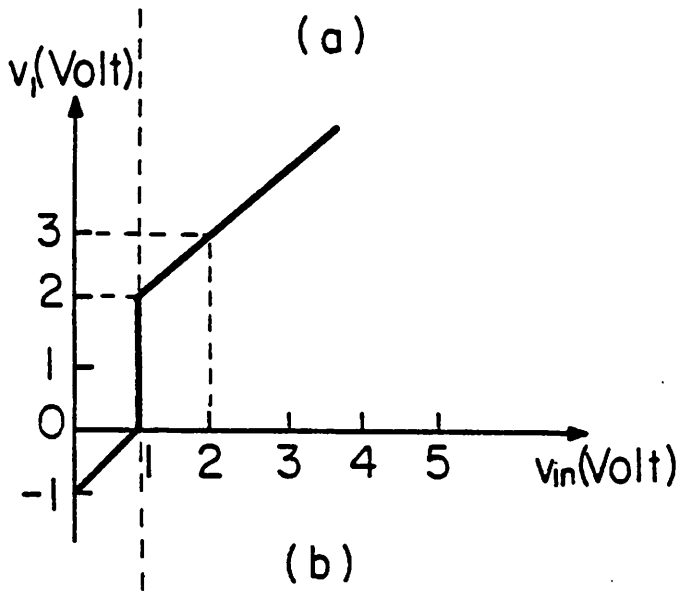
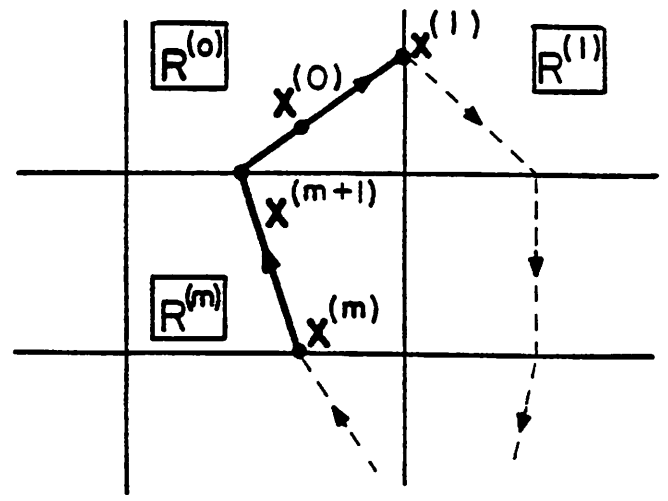
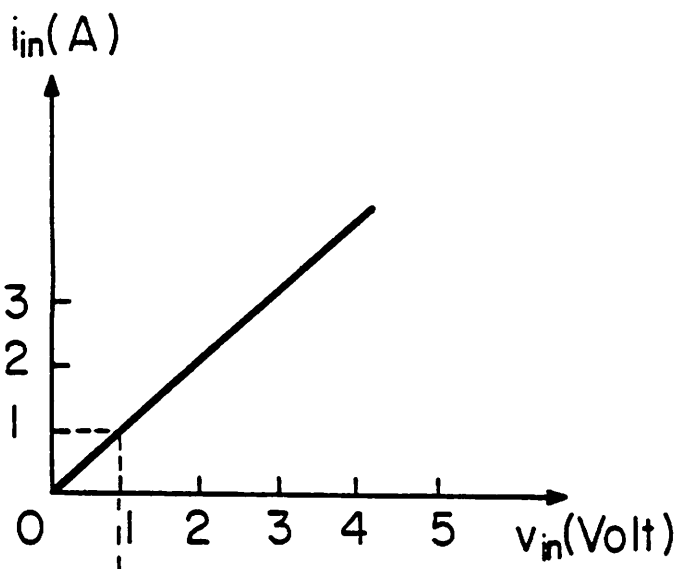


Fig.27

Fig.28